AN EXPERIMENTAL INVESTIGATION OF UNSTABLE COMBUSTION IN SOLID PROPELLANT ROCKET MOTORS

Thesis by
Captain
Wilmot Grant Brownlee
Royal Canadian Artillery

In Partial Fulfillment of the Requirements
For the Degree of
Doctor of Philosophy

California Institute of Technology
Pasadena, California
1959

To my wife,

LILLIAN

ACKNOWLEDGEMENTS

I wish to express my sincere thanks to Dr. Frank E. Marble for his continuing and considerable efforts on my behalf and for his encouragement and enthusiasm which were so instrumental in initiating and sustaining my program of studies at the California Institute of Technology.

I am deeply grateful to the Canadian Army, of which I am a member, for the opportunity extended me for advanced study and for the complete financial support they have so generously given.

The experiments were conducted at the Jet Propulsion Laboratory under ORDCIT Project Contract No. DA-04-495 Ord 18, Department of the Army, Ordnance Corps. I appreciate very much the opportunity of working at such a renowned establishment. Cooperation, in every way most complete, was given me. In particular I wish to express my gratitude to Mr. G. Robillard, Chief of the Solid Propellants Rocket Section, who extended to me full use of the facilities of his section, encouraged the program throughout and gave freely of his time in many interesting discussions. Dr. E. M. Landsbaum conducted some earlier experiments which were very useful at the outset of the program. His continued interest throughout the program was most helpful.

I am indebted to the many people who contributed to the program through their careful labours in manufacturing and firing the rocket motors; and to those in the Service Groups who participated in so many different ways.

I wish particularly to thank Dr. F. H. Wright for his encouragement and interest and for many informative and helpful discussions.

Finally, but certainly not least, I wish to thank Mrs. Ruth Toy and Mrs. Dianne Christman for their careful and expert work in preparing this manuscript.

ABSTRACT

Unstable combustion in solid propellant rocket motors is characterized by high frequency chamber pressure oscillations, often accompanied by changes in the mean burning rate. Experiments with case-bonded, cylindrically perforated motors were reproducible as a result of careful manufacturing control and extended propellant curing time. In these motors the oscillations were in the fundamental pseudo-standing tangential mode and were accompanied by increases in the average burning rate. At sufficiently high pressure levels all firings were stable. Reduction of the operating level led to mild instability. A sufficient further reduction produced a sudden change to maximum instability. Continued reduction in pressure level from this point resulted in a gradual decrease in degree of instability but it could not be experimentally verified that a low pressure stable region existed. The levels at which these events took place were frequency dependent and generally increased as the tangential frequency was reduced. At given operating level, the instability became less severe when the grain length was reduced below a critical value. Increasing the length above the critical value moved the point of maximum instability to somewhat higher levels but did not affect the level at which the motors became stable. The pressure levels for stability and for maximum instability moved to lower values with decreases in the propellant grain temperature in a manner not entirely accounted for by the effect of grain temperature on burning rate. Stable, mildly unstable and severely unstable operation was observed throughout the range -80°F to 180°F. The maximum instability decreased with grain temperature.

Slab motors with opposed-plane grain surfaces exhibited oscillations in the transverse sloshing mode but no accompanying changes in the burning rate. Tangential oscillation of equivalent amplitude strongly affected the burning rate in the cylindric motors; hence it appears that increases in the burning rate are associated with tangential velocities rather than pressure fluctuations.

TABLE OF CONTENTS

SECTION	TITLE	PAGE
	ACKNOWLEDGEMENTS	
	ABSTRACT	
	SYMBOLS	
I	INTRODUCTION	1
II	SURVEY OF ANALYTICAL INVESTIGATIONS OF THE UNSTABLE COMBUSTION PROCESS	5
III	TIME HISTORY OF A TYPICAL UNSTABLE FIRING	20
IV	EXPERIMENTAL SETUP AND INSTRUMENTATION	26
V	QUALITY CONTROL AND REPRODUCIBILITY OF RESULTS	33
	Processing Controls	34
	In-batch Reproducibility	36
	Batch-to-batch Reproducibility	38
	Motor Construction; Effect on Instability Process	40
VI	EFFECT OF CHANGING PROPELLANT OPERATING PRESSURE AND GRAIN PERFORATION DIAMETER	43
	Experiments Varying the Chamber Pressure	45
	Experiments Varying the Grain Perforation Diameter	48

	Further Experiments Varying Initial Perforation and Nozzle Diameters	52
	Speculations Concerning a Time Lag Mechanism	58
VII	EFFECT OF GRAIN LENGTH	62
VIII	EFFECT OF GRAIN TEMPERATURE	65
IX	IDENTIFICATION OF THE MODES OF GASEOUS OSCILLATION	70
X	MOTORS WITH OPPOSED PLANE GRAIN DESIGNS (SLAB TYPE MOTORS)	73
XI	INTERRUPTED FIRINGS	76
	Description of the Experiments	76
	Experimental Results	78
	Some Speculations Arising from the Results	81
XII	CONCLUSIONS AND CONCLUDING REMARKS	84
	REFERENCES	88

SYMBOLS

a	Ballistic parameter in burning rate law $r_s = a\,Pc_s^{\,n}$
Ab	Area of the burning surface of propellant grain
a_c	Speed of sound inside rocket motor
At	Area of nozzle throat
c*	Propellant characteristic exhaust velocity
Dp	Diameter of the motor port or perforation
Dp*	A particular value of Dp. See Fig. 31
dt	Diameter of the nozzle throat
f	Frequency of gaseous oscillations
H	Ratio of port area to throat area
Kn	Ratio Ab/At
Kn*	A particular value of Kn. See Fig. 31
Lp	Length of the propellant grain
n	Ballistic parameter in burning rate law $r_s = a\,Pc_s^{\,n}$
Pac	Peak-to-peak amplitude of gaseous oscillation
$\bar{P}_c$	Mean value of the unstable chamber pressure
Pc_s	Stable value of the chamber pressure
$\bar{P}c_B$	Value of $\bar{P}_c$ at the "break" in the $\bar{P}_c$ vs t curve. See Fig. 1
r_s	Stable linear burning rate of propellant
R_p	Radius of the motor port or perforation
t	Time from ignition
To	Characteristic temperature for a propellant
Tp	Prefiring temperature of the propellant grain
w {t}	Weight of propellant burned at time t

W_p	Total weight of propellant
α_{mn}	Mode number. $J'_m(\pi \alpha_{mn}) = 0$
$\bar{\gamma}$	Average value of ratio of specific heats
Γ'	Related to $\bar{\gamma}$ through $\Gamma' = \bar{\gamma}\left(\frac{2}{\bar{\gamma}+1}\right)^{\frac{\bar{\gamma}+1}{2(\bar{\gamma}-1)}}$
$\Delta \bar{P}c$	$\Delta \bar{P}c \equiv \bar{P}c_B - Pc_s$
ρ_p	Density of propellant

Subscripts:

h	Head end of motor
i	Value at ignition
n	Nozzle end of motor
p	Propellant, port, or perforation as applicable
s	Stable

I. INTRODUCTION

Although the occurrence of high frequency oscillations in solid propellant rockets, and the attendant increase of mean chamber pressure, have been recognized for nearly twenty years,[1,2,3] the basic facts underlying these phenomena are at best understood very poorly. This state of affairs certainly does not reflect any lack of enthusiasm, effort or ingenuity on the part of serious investigators but rather is a measure of the inherent experimental and theoretical difficulties of the problem. Theoretical investigations[4,5,6,7] are often severely hampered by lack of knowledge concerning key physical phenomena. It is hardly to be expected that a definitive analysis concerning the response of a burning solid propellant surface to high frequency oscillations of pressure and tangential velocity can be carried out when fundamental knowledge on the mechanism of stable solid propellant combustion is just becoming available[(8)]. Analyses of the acoustic problem and the detailed reaction of the propellant surface generally involve sufficient arbitrariness and properties of unknown magnitude that it is impossible to assess, on the basis of gross experimental results, whether the postulated mechanism is or is not operative.

Experimental investigations[9,10,11,12] present their own peculiar brand of difficult problems. From a fundamental viewpoint, one should start with a thorough investigation of the chemical kinetics and gas dynamics of the stable burning process. For until

this is well in hand, no meaningful detailed experiments concerning transient behavior can be contemplated. Experiments involving the behavior of unstable rockets are also plagued with difficulties. In the first place the preponderant portion of this work has been performed as an accessory to the development of military or commercial rockets. Naturally there is a tendency to direct this work toward the very practical aim of removing the instability rather than toward an understanding of it. Firings made under these circumstances have been very informative but invariably limited in the range of significant parameters covered and often somewhat compromised in the control exerted over experimental conditions and instrumentation. Secondly it has usually been very difficult to obtain repeatable experimental results of resonant firings; in fact decision as to whether a certain rocket type resonates or not must often be arrived at only from statistical considerations over a large number of similar firings. Although such a result may be adequate for certain manufacturing decisions, it is not quite so significant as a means for understanding the instability mechanism.

At present there appear to be two possible approaches to advance the understanding of resonant combustion beyond its present imperfect state. The first, of course, is the fundamental attack on the basic mechanism. This lengthy pursuit has the strong advantage that in the course of the work, numerous other solid propellant combustion problems will also be solved. The

second approach, and the one attempted in the present work, rests upon the hope that by study of carefully controlled rocket experiments entailing systematic variation of the significant parameters, one can arrive at some gross conditions governing resonance that rest only on facts that can be obtained from stable combustion processes and not upon detailed understanding of the propellant burning mechanism. This approach was taken successfully in connection with the high frequency oscillation in air-breathing combustion chambers. Here it was found[13] that the detailed combustion information required could be obtained simply from an elementary experiment with a stable combustion chamber and hence the unsolved problems of hydrocarbon combustion kinetics and combustion in turbulent mixing zones were, to a large extent, bypassed. The present work has not yet yielded similar success with resonant burning in solid propellant rockets. The progress, however, has been most encouraging and the results significant and very useful.

The present extensive series of rocket experiments was planned with full knowledge of the difficulties faced by previous experimenters. It was recognized that without essentially complete reproducibility of results, as to whether resonance occurred and what its pattern was, the outcome would be largely meaningless. Consequently realization of this aim was taken as the first objective and modification of quality control and curing procedures studied accordingly. The achievement of reproducibility was actually

one of the major accomplishments of the investigation. It was possible then to investigate the occurrence or non-occurrence of resonance in case-bonded, cylindrically perforated motors over wide and systematic variations of propellant grain geometry, rocket chamber pressure level, grain temperature, etc. All in all some 450 rocket firings were made under highly controlled conditions. A composite propellant was used with a polysulfide fuel and ammonium perchlorate oxidizer. Some further experiments with a slab type motor elucidated certain features of combustion instability. Although the results have not as yet led to a simple picture of unstable combustion oscillations they have illuminated some features hitherto clouded through incomplete and sometimes disjointed information.

II SURVEY OF ANALYTICAL INVESTIGATIONS OF THE UNSTABLE COMBUSTION PROCESS

In recent years a number of theoretical investigations have been made of the problem of combustion instability in solid propellant rocket motors. Because of its complex nature, a completely general solution of the problem of sound field amplification in a solid rocket motor is hardly feasible or desirable. The conservation equations would have to be solved for an irregular cavity. The boundaries of the cavity include a sonic orifice, solid walls, heat insulating materials and the burning surface of the propellant. The medium through which the sound field propagates consists of high temperature, chemically reactive gas which may or may not be in chemical equilibrium and which enters the cavity at the burning surface and leaves at the sonic orifice. Near and at the burning surface a complex combustion process transforms the receding solid propellant into hot combustion products. The details of the combustion process are not explicitly known for quasi-steady state operation, hence the unsteady features are even more obscure.

In consequence of these difficulties various investigators have all made assumptions which tend to accentuate the features of the problem in which they were interested and, of course, rendered it more tractable from a mathematical point of view. Representative of the work done to the present time are the investigations of Grad [4],

Cheng [5], Green [6] and Hart and McClure [7]. The first two analyses are concerned with the conditions under which self-excited gas oscillations within the perforation of a combustor can be amplified through their effect on the combustion process. Green's work assumes the existence of unsteady conditions at the surface of a burning propellant slab and investigates the conditions under which they can lead to an increase in the time average burning rate. The analysis of Hart and McClure, the only one that can claim to be a theory in the sense that it relates to the chemical fundamentals of the combustion process, is one dimensional also in that local conditions are considered at the surface of a slab of burning propellant without reference to combustor geometry. The conditions under which local periodic disturbances of the flow may be amplified are developed.

In the work of both Grad and Cheng, the characteristic modes of oscillation within the combustion chamber were obtained by solution of the wave equation, which assumes that isentropic flow conditions exist and that the changes in velocity, pressure and density from mean flow conditions are infinitesimals of the first order. Oscillations in the characteristic modes would ordinarily be quickly damped by the inherent losses of the system. The effect of the downstream exit of the motor is included in the theories by an impedance-type boundary condition at the nozzle end of the grain. In order for the oscillations to be amplified it is necessary that their interaction with the combustion process lead to the addition of energy in the proper phase. The phase relation will depend on any natural

time delays between the disturbance applied to the reactive zone adjacent to the solid grain and the response of this zone. In Grad's analysis this time delay τ is assumed constant and is taken to be the time required for the chemical reaction at the burning surface to reach equilibrium after a disturbance. On this basis the relation between the instantaneous burning rate $\dot{m}\{t\}$ at time t and the equilibrium value of the burning rate f(t) is given by

$$\frac{d\dot{m}}{dt} = \frac{1}{\tau}(f - \dot{m}) \qquad (1)$$

The steady state burning rate must depend on the local fluctuating values of pressure and temperature. Using this fact and equation 1, Grad determines a radial boundary condition which takes the place of the solid wall boundary condition $\frac{\partial \rho}{\partial r} = 0$ at the wall. In this way the parameter τ enters the final solution and it is the subsequent detailed relation between the period of the oscillations and τ that determines whether or not oscillations of given frequency can be amplified. The effect of the downstream boundary condition, the mean flow and the sensitivity of the burning process to changes in pressure and temperature determine, together with τ, the degree to which oscillations in particular modes will be driven. The theory indicates that a combination mode with axial, radial and tangential components is the most likely to be amplified. That is, its growth with time is largest of all unstable modes. Grad concludes that stability may be promoted by proper choice of the value of certain

operating parameters. The system should be more stable the lower the values of $\left.\frac{\partial r}{\partial p}\right|_T$ and $\left.\frac{\partial r}{\partial T}\right|_p$ where r is the dynamic burning rate and p and T are the gas pressure and temperature respectively. The use of grains with low values of length to diameter ratio should tend to stabilize the system. Again, instability is more likely to occur at stagnation points in the flow, hence, if possible the grain design should avoid such points in the inner perforation. Finally, the larger the chemical time constant τ and hence the slower the chemical reaction the more stable the system.

It is interesting to note that this pioneering work of Grad was carried out before any experimental work had indicated the oscillatory nature of resonant burning; the whole idea of the unstable combustion was largely a conjecture. Consequently, his work must be looked upon as the first demonstration, experimental or theoretical, that unstable oscillations can exist in a solid propellant rocket. As will be seen through description of the ensuing work, the theoretical advances since Grad's work have been largely changes in detail.

The essential difference between the Grad and the Cheng theories lies in the type of radial boundary condition imposed. As has been noted, Grad postulates a relaxation time for the chemical reaction which is considered to be a constant. Cheng, on the other hand, takes over bodily the variable time lag introduced by Crocco [14]

in his work on the unstable combustion of liquid propellant rockets. During combustion the solid surface undergoes a primary decomposition reaction into intermediate gases due to heat transfer and/or interaction with activated species from neighboring gas. The intermediate gases are then activated by the final combustion products during a time interval τ . Finally, the activated intermediate gases react at a high rate to become the end combustion products. Cheng assumes that this latter rate is so large that the intermediate gases generated at the rate $\dot{m}_i \{ t \}$ at time t can be considered to burn instantaneously at time $t + \tau$. Thus, from a mass balance

$$\dot{m}_b \{ t \} = (1 - \frac{d\tau}{dt}) \dot{m}_i \{ t - \tau \} \qquad (2)$$

where $\dot{m}_b \{ t \}$ is the instantaneous rate of burned gas generation at time t. The time lag τ is assumed to be affected by the gas pressure and temperature oscillations. Under isentropic conditions the temperature can be expressed in terms of the pressure, and the time lag then depends on the pressure only. The local rate at which energy is absorbed in the activation of the intermediate gases is taken to vary as $p^n \{ t \}$ at time t where $p \{ t \}$ is the instantaneous pressure of the burned gas acting on the intermediate gas. It is assumed that the total amount of activation energy required for an average combustible intermediate gas element during the time interval τ is constant. Hence

$$\int_{t-\tau}^{t} p^n \{ t' \} \, dt' = \text{const.} \qquad (3)$$

During steady state operation $\dot{m}_b$ is equal to $\dot{m}_i$ since τ is then constant. The steady state rate of burned gas generation is given by

$$\dot{m}_i \{t\} = \text{const.}\ p^n \{t\} \qquad (4)$$

when the erosive effect of drifting velocity is neglected. If equation (3) is differentiated and the result used with equation (2) and (4) there results

$$\frac{\dot{m}_b \{t\}}{\bar{m}_b} = \frac{p^m \{t\}}{\left[p\{t-\bar{\tau}\}\right]^{m-n}} \quad \frac{1}{p^n \{t\}} \qquad (5)$$

where τ has been replaced by an average value $\bar{\tau}$ and $\bar{m}_b$ is the steady state burning rate. Thus the instantaneous burning rate is assumed to depend on the pressure only. The parameter n is a measure of the rate of burning under steady conditions, larger n corresponding to higher burning rate at given pressure. The parameter m is a measure of the time taken for activation of the intermediate gases, larger m corresponding to shorter activation times. A radial boundary condition is then obtained by matching the instantaneous rate of burned gas generation, as given by equation 5, to the radial influx of mass, ρv. It is assumed that the reaction zone thickness is negligibly small compared with the perforation radius. Since the nature of the radial boundary condition is different in the Grad and Cheng theories, the predictions of the theories with respect to stability can be expected to be at variance. Cheng shows that a simplified overall pressure index of reaction $S = m - (n/2)$

must be larger than a certain minimum value S_{min} if instability to be possible. S_{min} is given by

$$S_{min} = \frac{1}{2\gamma}\left[1 + 5.15\, A_i\, A_r\, \lambda^2\, |\bar{v}_1|\right] \qquad (6)$$

where A_i and A_r are the real and imaginary parts of the nozzle admittance A, and are given as plotted functions of a reduced frequency parameter; λ is the ratio of grain length to perforation diameter and $\bar{v}_1$ is the nondimensional average radial inflow velocity at the boundary, referred to the speed of sound in the burned gas. For cylindrically perforated motors Cheng concludes that the most unstable mode is the combination mode made up of the fundamental components in the circumferential, radial and axial directions. Cheng refers to this mode form as the fundamental spiral mode. He concludes that the circumferential component will amplify the fastest and that its frequency will be equal to the acoustic value. The frequency of the radial component will be almost equal to the acoustic value but the axial component will differ significantly from the acoustic organ-pipe values. During a firing, the parameter λ decreases with time since the perforation radius is increasing. At the same time Cheng assumes that the radial velocity $\bar{v}_1$ of the burned gas is constant during the firing.* By calculating the value of S_{min} for a

---

* In an actual firing with a cylindrically perforated grain $|\bar{v}_1|$ should vary as λ rather than as indicated by Cheng since pressure increases progressively with time due to the increased burning area. However, this makes no essential change in Cheng's results since $\lambda^2\, |\bar{v}_1| \sim \lambda^3$ Hence $\lambda^2\, |\bar{v}_1|$ decreases with λ .

range of λ he finds that S_{min} rises very steeply and exceeds unity for λ greater than about 18 to 20. It is not expected that the over-all pressure index S will be this large since n must be less than unity if the motor is to be inherently stable to small disturbances during stable operation and m is expected to be on the order of unity. Since S must be greater than S_{min} for unstable operation, it appears that high values of the ratio grain length to perforation diameter, λ , tend to prohibit instability. Consequently Cheng expects a rapid destabilization of the motors as burning proceeds and λ decreases after which destabilization will occur at a lower rate. Furthermore, the axial geometry of the motor enters strongly through the dependence of S_{min} on the ratio of the distance, grain exit to nozzle throat, to the grain length which Cheng denotes by e. For given λ , the value of S_{min} decreases rapidly as e is decreased. Hence for given grain length, a short grain port to nozzle throat distance tends to destabilize the motor. In a similar manner it is shown that motors with non-erosible end seals at the nozzle end of the grain are more stable than those with erosible end seals. Cheng concludes that the externally burning rod type grain will likely burn stably, the rod-in-grain type unstably, and that the tubularly perforated type will be most unstable of all. He also concludes that insertion of an inert rod along the axis of a tubular grain should stabilize the system. It should be noted here that the coefficient m is unknown and its relation to mean propellant burning conditions is, at best, uncertain. Hence the analysis can not give an absolute result but rather a correlation method.

It has been seen that the approaches of Grad and Cheng consist, in essence, of solutions of the wave equation with a radial boundary condition which differs from the acoustic solid wall condition. In both cases the reaction zone is considered to be of negligible thickness and the interaction between the oscillations in the burned gas and the combustion process enters the solutions as a fluctuating radial mass flow boundary condition. On the other hand, Green assumes the existence of unsteady flow conditions in the burned gas and their effect on the time-average solid burning rate is calculated without reference to the problem of how the oscillations are driven. The chemical reaction and heat conduction effects in the reacting gas zone are replaced by a model which assumes convective heat transfer to the solid surface from a parallel flow of gas at flame temperature. It is assumed that the effective heat transfer coefficient is an inverse function of the propellant burning rate and that the latter depends on an Arrhenius function of the propellant surface temperature. The steady-state treatment of this model leads to correct qualitative dependence of the burning rate and propellant temperature distributions upon parameters characteristic of the propellant and of the gas flow. The non-steady situation is treated as a problem in small perturbations of the heat flux, burning rate and grain surface temperature. It is assumed that a small time interval is required for the endo thermic decomposition of the solid propellant surface layer to gaseous decomposition products which then

lie in a thin homogeneous layer next to the solid surface. Hence a time lag enters this theory also but is now related to the initial decomposition reaction. Fluctuations in the effective heat transfer coefficient due to oscillations in the burned gas can then couple with the decomposition reaction when the product of angular frequency ω and the time lag τ attains certain values. Under these conditions, the time-average burning rate can deviate widely from the steady state values and Green refers to these as resonance conditions. The value of τ can only be estimated. Results are given for the arbitrary values $\tau = 10^{-3}$, 10^{-4}, and 10^{-5} sec. and a comparison is made for $\tau = 10^{-3}$ sec. and $\tau = 7.88 \times 10^{-4}$ sec. The comparison shows that the magnitude of the resonant fluctuations in surface temperature is very sensitive to the value of τ and that large deviations in the time-average burning rate can occur only when the resonance condition is approached very closely. Green gives a single example of a true resonant peak for the time lag $\tau = 7.88 \times 10^{-4}$ secs. In this case, surface temperature fluctuations sufficient to produce significant change in the mean burning rate, extend over the range $\omega = 1.09 \times 10^{4}$ to $\omega = 1.12 \times 10^{4}$ radians per second or about 3% of the centre frequency. It appears that low amplitude surface temperature excursions are possible over a much broader range of frequencies. Green concludes that an increase in the mean burning rate is favoured by low thermal conductivity of the solid propellant, large heat of phase change, high flame temperature, low activation energy of the

solid phase decomposition reaction and a high frequency factor for this reaction. In addition, an increase of the mean burning rate appears to be favored by low initial propellant grain temperatures and possibly by high temperatures also. It is expected that a detailed analysis of the model by Nachbar and Green[15] will be published at a later date.

The introduction of an arbitrary time lag is avoided in the theory of Hart and McClure. In this theory as in Green's analysis, the details of motor geometry are omitted. However, in this case the objective is to determine under what conditions periodic perturbations of the steady state reaction process can lead to amplification of the perturbing oscillations in the burned gas. The model treated is one-dimensional and does not include the effect of gas velocities parallel to the plane surface of the grain. Time-dependent reaction rate chemistry is avoided by assuming that the reactions are so fast that the instantaneous volumetric rate of reaction equals the steady state rate under the same instantaneous local conditions. The proposed model of the combustion process consists of a solid surface at which solid phase decomposition reactions take place. Mass flows outwards through an induction region to the gas phase reaction zone. Heat is transported from the gas phase reaction to the solid phase decomposition reaction. The transfer rates of heat and mass through the induction zone are taken to be finite. The induction zone is small compared with the wavelength of the sound waves and the flow velocities are small compared with speed of sound. Hence the change in

pressure across the region is negligible. Consequently the induction region is completely defined by the equations of heat and mass transfer

$$\frac{\partial}{\partial x}\left(k\,\frac{\partial T}{\partial x} - m C_p T\right) = \frac{\partial}{\partial t}\left(C_v \rho T\right) \qquad (7)$$

and

$$\frac{\partial m}{\partial x} = -\frac{\partial \rho}{\partial t} \qquad (8)$$

where m is the instantaneous mass flow rate, k is the thermal conductivity of the gas, and T is the local gas temperature. It is assumed that the specific heats, thermal conductivity and the molecular weight of the gas remain constant and that the ideal gas law is obeyed. Equations 7 and 8 are subject to boundary conditions at the cold and hot boundaries of the induction zone. At the cold boundary the rate of conversion of solid into vapor is assumed to depend on an Arrhenius function of the temperature in a thin reaction zone. Hence the reaction rate depends on the temperature and its gradient at the gas side of the solid reaction zone. The thin surface reaction zone is treated adiabatically so that the steady state relationship between burning rate, temperature and temperature gradient is valid in the time dependent case. The heat flow equation is integrated across the surface reaction and the conditions at the cold side of the solid phase reaction are matched to the solution of the time dependent heat flow problem in the non-reacting solid. At the hot boundary of the induction zone the rapid

gas phase reaction begins. It is assumed that the reaction is so fast that the time of transit of the gases through this reaction zone is negligibly small compared with the period of the pressure fluctuations. Thus the adiabatic approximation is made that the steady state functional relationship between mass flow rate, temperature gradient and pressure at the induction zone side of gas phase reaction region is valid under unsteady conditions. By integration across the induction zone the dependence of the mass flow rate on the pressure and temperature gradient at this point is related to the dependence of the steady state burning rate on pressure and body temperature of the solid. Finally equations 7 and 8 and the boundary conditions are linearized for small perturbations and the resulting solution for the induction zone is expressed in terms of Legendre functions. This solution is coupled to a sound field in the burned gas by noting that the pressure and mass flow at the boundary between the gas phase reaction zone and the product gases are essentially the same as on the induction zone side since the gas phase reaction zone thickness is very much smaller than the wave length of sound. The specific acoustic impedance is then determined at the burning-zone-product-gas boundary. Incoming sound waves are attenuated or amplified according to whether the real part of the admittance is positive or negative, respectively. In final form, the solution contains seventeen parameters which may be grouped into eleven sets, each of which may be varied independently.

The sensitivity of the result to variations in particular parameters may depend strongly on the choice of values for others. As a result of exploratory calculations with presumably reasonable values of the parameters Hart and McClure note that amplification tends to occur over a broad range of frequencies in the neighborhood of several thousand cycles rather than being sharply peaked in a narrow frequency range. Also, the system generally becomes more unstable as the body temperature of the solid grain is reduced, although this dependence is reversed in certain cases. Stability is promoted by low values of $\left.\frac{\partial r_s}{\partial p_c}\right|_{T_p}$ and $\left.\frac{\partial r_s}{\partial T_p}\right|_{p_c}$. However a zero value of $\left.\frac{\partial r_s}{\partial p_c}\right|_{T_p}$ does not guarantee stability. The high frequency response of the system is much more sensitive to chemical and physical changes of the surface reaction, than is the steady state behavior. It appears that increasing the pressure level tends to destabilize the system response to high frequencies. Hart and McClure note that comparison of theory and experiment is made difficult by the complex dependence of the solution on the various parameters, the values of which are not all known.

The status of the theoretical work at the present time indicates that the results are limited either by lack of experimental results from which gross parameters characterized by Grad, Cheng and Green may be determined, or by lack of fundamental knowledge concerning

reaction mechanisms, rates and transport properties entering into the steady burning theory. As indicated in the introduction it was the purpose of this work to conduct experiments indicating the existence of a gross mechanism rather than to implement existing analyses with data from which empirical parameters might possibly be determined.

III TIME HISTORY OF A TYPICAL UNSTABLE FIRING

Inasmuch as this paper will describe certain features from a great number of rocket firings, it is advisable first to describe one firing in complete detail. In this manner certain points of operation, features of experimental technique will be made clear as well as the general characteristics of an unstable pressure-time curve. These items will then be taken for granted in the following chapters and the main body of the experiments will be readily understandable. In figure 1 the mean pressure ($\bar{P}c$) versus time curve is shown for a cylindrical motor with nominal 3.0 in. perforation, 5 in. ID case, grain length of 38 in. and case length 38.5 in. For brevity this will be designated a 3 x 5 x 38/38.5 in. motor. The motor was fired at a grain temperature of 160°F with a nozzle throat size of 1.70 in. It is clear from the pressure time curve that this motor was severely unstable.

If we refer to figure 1 we observe that, after ignition, a stable period of 0.38 seconds follows. At 0.38 seconds, high frequency instrumentation indicated that a gaseous oscillation was present within the grain perforation. This oscillation became observable at a level of approximately one psi peak to peak; the mean chamber pressure was 380 psia at the time. As time passed, the oscillation amplitude grew larger and the mean pressure increased. The correlation between oscillation amplitude and mean pressure increase may be clearly seen in figure 2. The

lower two traces labelled $\bar{P}c_h$ and $\bar{P}c_n$ are mean pressure traces, measured at the head and nozzle ends of the motor, respectively. The upper three traces labelled Pac, 1, 2, and 3 are indicative of the peak to peak oscillation amplitude at the head end of the cavity. Increasing oscillation amplitude is indicated by a downward deflection of these traces. It is clear that the amplitude of the oscillations correlates exactly with the mean pressure increases. As the oscillation became very large, a severe increase in mean pressure occurred. The mean pressure rose smoothly to 900 psia where an abrupt change in slope occurs in the $\bar{P}c$ vs. t trace. This point will be designated the "break" in the mean pressure trace. After the break, $\bar{P}c$ rose more slowly with time to 1050 psia. At this point (point C), the oscillations decayed rapidly and $\bar{P}c$ dropped to 470 psia (point D). A second growth in instability then occurred with a maximum amplitude at point E. This terminated at point F. Finally, a period of weak instability occurred just before and during tail-off (burnout).

Data obtained from other firings enables prediction of what the chamber pressure would be under stable operating conditions. That is, the stable chamber pressure versus area ratio Kn(Pc_s vs. Kn) relation and also the corresponding burning rate versus pressure relation (r_s vs. Pc_s) are known. Neglecting length effects, which are small for the motor under consideration, these relations are:

$$P_{c_s} = (a \rho_p c^* K_n)^{\frac{1}{1-n}} \qquad (9)$$

$$r_s = a P_{c_s}^n \qquad (10)$$

In figures 3 and 4 these relations are plotted logarithmically and the resulting straight lines are labeled. Figure 3 also shows the relation $\bar{P}_c$ vs. Kn for the unstable motor under consideration, demonstrating that during instability the usual relation is invalid. At point D we observe that when the instability decays the motor returns essentially to the stable curve. However, at point F where the second unstable period ends, the motor operation deviates from the stable prediction. This is characteristic of the firings to be described and is believed due to a grain composition change which begins at a radial distance of approximately 0.4 in. from the case wall. The final unstable period occurs just before burnout and hence in the region with changed composition. The value of Kn plotted was computed with the assumption that the grain burned uniformly during the instability. It will be seen in Chapter III. that interrupted firings substantiate the method.

The unstable and stable relations between burning rate and mean chamber pressure are shown in figure 4. During stable operation the pressure index in the burning rate law was 0.323 at 160°F. During the major instability period the mean burning rate increased very rapidly and abnormally. If the same

functional form of the burning rate law is assumed, the constants involved are changed radically, as may be seen by reference to figure 4. During the period of changed composition the burning rate is abnormally low.

Throughout the firing, the outputs of the high frequency pressure transducers were recorded on a cathode ray tube oscillograph. The portion of this record corresponding to the severe instability period is reproduced in figure 5. Here one may observe the slow growth of the oscillations and the rapid onset of severe instability. The wave form is not purely sinusoidal but contains significant harmonic components. The harmonic content produces the intensity modulation and the distorted wave form. The amplitude of the wave fluctuates rapidly. Part of this is due to phase shifting of the components and part is a real fluctuation of component amplitudes.

From the record of figure 5 a crude measure of peak-to-peak oscillation amplitude was taken. In figure 6, this information has been used to plot the ratio of peak-to-peak oscillation amplitude with mean pressure, i.e., $Pac/\overline{Pc}$, and also Pac/Pc_s where Pc_s is the corresponding stable operating pressure. It may be seen that at the break the peak amplitude is roughly equal to the corresponding stable operating pressure and about one-half of the unstable mean operating pressure.

The increase in burning rate associated with the oscillation is presented in figure 7. In this figure the increase in burning rate from the corresponding stable condition is referred to the stable condition and is plotted versus the peak-to-peak oscillation pressure. At the break in the pressure-time curve, the increment in burning rate exceeds the normal stable burning rate for that value of Kn. Hence the burning rate is over twice the normal value. A fictitious burning rate may be obtained by using the unstable mean pressure in the stable burning rate law. We may call this $r_s\{\bar{P}c\}$. Figure 8 is a plot of the unstable burning rate minus $r_s\{\bar{P}c\}$, referred to $r_s\{\bar{P}c_s\}$ and versus Pac. It is clear that the unstable burning rate greatly exceeds that which might be expected due to the increase in average pressure alone.

In both figures 7 and 8 it is interesting to note that the relation between the unstable burning rate and the oscillation amplitude differs between the onset and decay phases of the instability. For given oscillation amplitude the unstable burning rate is greater during the decay phase.

Detailed frequency analysis of the complex wave form indicates that the strong fundamental corresponds to the fundamental tangential acoustic mode within approximately one percent. The overtones present are exact multiples of the fundamental. This situation is not strongly influenced by fluctuating pressure amplitude. The frequency analysis record for this unstable firing is reproduced in figure 9. The analyzer used operates on a band pass,

heterodyne principle. The bottom channel includes frequencies from 0 to 1500 cps. The center frequencies of the higher bands are noted in the figure. The traces record the beat frequency between the input frequency and the center frequency. Whether or not the beat frequency is positive or negative must be inferred from the fact that as time passes, the frequency must decrease, due to the increased geometrical dimensions of the motor. It may be seen that the fundamental oscillation begins in the neighborhood of 6700 cps. The end of the first unstable period occurs at, roughly, 5200 cps; the final period of instability extends from 4500 cps to 4200 cps.

Finally, it should be noted that this firing was made using the type 3 headplate shown in figures 10, 11 and 12. Because of the presence of the small cavity in the headplate, and also due to the lack of rigidity of the headplate, the oscillation amplitudes quoted are not precise. Further experiments indicated that approximately 10% acceleration response is to be expected. Also, a small correction (less than 4%), due to the location of the gauges with respect to the grain's surface, has been neglected. It is intended, therefore, that the amplitudes quoted be considered accurate only within this range.

IV. EXPERIMENTAL SETUP AND INSTRUMENTATION

The unstable rocket firing described in the foregoing chapter utilized a case-bonded, end-restricted motor with cylindrical perforation. All but eight of the firings conducted employed motors of this type. A schematic drawing of the cylindric-type motor is given in figure 20. A typical setup for firing is shown in figure 13. The motors were seated in three V-blocks and restrained by chains. The head end of the motor was supported by heavy steel thrust blocks welded to the thrust bed. In practice lead sheets (not shown) were placed between the motor head plate and the thrust blocks in order to provide uniform contact.

An exploded view of the nozzle assembly is shown in figure 14. The assembly consists of a nozzle plate, nozzle insert, retainer ring, gaskets, a copper safety diaphragm and retainer. As may be seen, the components are very heavy and are designed for continual re-use under severe conditions. The nozzle inserts used were, for the most part, copper with molybdenum throat sections. Some steel-graphite nozzles were used but were generally unsatisfactory for sustained re-use due to cracking and chipping of the graphite.

The instrumented headplate of the motor is shown in figure 10. The headplate itself is shown in figures 11 and 12. In figure 12 it may be seen that there exists a shallow one quarter

inch deep cavity between the shoulder where the case-end butts and the instrumented inner face of the head plate. The cavity was designed to allow space for a wafer type igniter to be installed. From the point of view of high frequency amplitude measurements this type headplate (type 3) was not completely satisfactory. The transducers were situated flush with the ignition cavity and hence did not measure the amplitude of the gaseous oscillations within the grain cavity. Furthermore, while the type 3 headplate was one inch thick in the transducer mounting section, this did not prevent extremely large accelerations from developing. Some acceleration measurements were taken and these give indicated axial accelerations in excess of 20,000 g during severely unstable motor operation. These levels were well beyond the calibrated range of the accelerometers. The accelerations induced spurious outputs from the high frequency transducers of 10% or more of the pressure outputs, depending on the type transducer used.

Nevertheless, the type 3 headplates were used in the majority of the firings. They had the advantages of being compatible with a range of grain perforation diameters; they eased the ignition problem, kept the setup time of conditioned motors short and were available at the outset of the experimental program. Finally, in the tests run using these headplates, the over-riding purpose was to discover the limiting conditions governing the

instability process. Hence amplitude measurements were not the most essential information.

While most of the firings were made using the type 3 headplate, a sizeable number were made using the type 4 headplate shown in figures 15 and 16. In this headplate the igniter cavity was removed and a protruding disc in which the high frequency pressure transducers were mounted was inserted into the perforation cavity. The design was suitable for motors with three inch perforations. When mounted, the sensing faces of the transducers were flush with the face of the protruding disc and flush with end of the grain. The cavity around the disc was filled by the head end restrictor plug. Hence the disc acted as a flat boundary at the end of the grain perforation and the pressure transducers sensed on the surface of the boundary. The type 4 headplate was massive in design. The section in which the transducers were mounted was three inches thick. In addition, the headplate was bolted at eight places to the heavy thrust block shown in figure 17. Finally, the thrust block was bolted to the thrust stand at four points, three of which are visible in figure 13. The purpose of the massive design was to eliminate the accelerations so troublesome with the type 3 headplate. In this respect the design succeeded. This was checked in two ways. As shown in figure 15, a blind pressure transducer was mounted on the outer face of the headplate. This gauge produced only a barely detectable output even under the most severe conditions.

The second method involved the use of a special adapter which made blind one of the transducers normally used to measure pressures. This test too was very satisfactory and acceleration output did not exceed five percent of the pressure output.

Ignition. - Both wafer and tubular igniters were used in most firings. In general the motors were over-ignited. Inasmuch as motors were fired over a wide range of sizes and operating conditions it would otherwise have been necessary to develop a broad selection of igniters to produce optimum ignition in every case. Furthermore, the motors were heavily instrumented as will be seen, hence it was acceptable to over-ignite in order to avoid misfires, hangfires and incomplete ignitions.

Mean Pressure Instrumentation. - During a stable firing the pressure is quasi-steady in time. An unstable firing usually exhibits a rapidly changing average pressure upon which is superimposed high frequency pressure fluctuations. Low frequency response instrumentation tends to average out the high frequency fluctuations. Taber pressure transducers, type 176, with a 0-3000 psig range were used in all but the earliest firings. This transducer is a strain gauge type and requires a carrier voltage input. The electronic setup is shown in figure 21. The demodulated output of the Miller Carrier Amplifier Type C-3 was fed to two recorders. The first of these was a Miller model H galvanometer oscillograph. The 460 cycle galvanometers were shunt damped to be down 3 db at 100 cps. The damping was used

to suppress a spurious output of the system which consisted of a beat frequency of several hundred cycles per sec. The beat frequency arose from interaction of the high frequency combustion oscillations with the carrier frequency. Comparison tests were made with damped and undamped galvanometers. The damping did not produce significant loss of mean pressure-time information. The reproduction shown in figure 2 is that of a Miller oscillograph record. The traces labeled $\bar{P}c_n$ and $\bar{P}c_h$ correspond to the outputs of two Taber gauges, one at the head end of the motor and one at the nozzle end. These gauges may be seen in figures 10 and 13. A second recorder of less sophisticated design, the Sanborn recorder, Model 127T was used at the test cell to monitor the $\bar{P}c_h$ output of the Miller Carrier amplifier. Records from this recorder are used for illustration in this report.

The Miller records were read out digitally and this pressure-time information was programmed through a Datatron Model 202 digital computer. The computation was made with the assumption that the grain perforations remained essentially cylindrical throughout the firings. This assumption was valid as is shown in chapter XI. The computer output included perforation diameter, pressure, burning rate and area ratio Kn all as functions of time. The propellant characteristic velocity c^* was also computed.

High Frequency Instrumentation. - High frequency pressure transducers, Photocon types 345 and 355 were used throughout the experimental program. These may be seen mounted in the types 3 and 4 headplates in figures 10 and 15, respectively. The transducers are water cooled, capacity type and operate in conjunction with the Photocon Dynagage units shown in figure 18. The output of the Dynagage unit consists of a voltage with mean D.C. level proportional to the average pressure in the motor but with a rapidly fluctuating high frequency component which represents the gaseous oscillation pressure at the transducer.

In most firings, three Photocon transducers were used, all mounted in the head plate of the motor as has been described. Of the two types of Photocons, the type 355 was preferred since its response to acceleration was approximately one half that of the type 345. In addition, the type 355 proved to be more rugged. The zero readings from both types of gauges tended to shift during the severe instabilities, presumably due to increased heat transfer rates. Hence, their D.C. outputs were not particularly useful. The D.C. output of one transducer was always monitored, however, since this proved advantageous in cases where very sudden steps occurred in mean pressure such as when the propellant grain failed or where the safety diaphragm burst during a firing. The electronic setup connected with the gauge is shown in figure 22. The outputs of the three Dynagage

units were A.C. or D.C. coupled to three channels of a high speed cathode ray tube oscillograph, Hathaway Instruments Type SC 16-A. In addition, the output of one gauge was low-pass filtered and D. C. coupled to a Hathaway channel. A Hathaway record is shown reproduced in figure 5. The outputs of the Dynagage units were also A. C. coupled to three A. M. channels of a J.P.L. modified Ampex Model 306-7, 7 channel tape recorder.

Finally, the high frequency components of the gauge wave forms were filtered to varying degrees, full wave rectified and fed to damped 460 cps galvanometers in the Miller recorder system described earlier. The resultant traces gave a crude measure of the amplitudes of the high frequency components, correlated in time with the mean pressure traces ($\bar{P}c_h$, $\bar{P}c_n$) as has been described in chapter III(see figure 2). These traces allowed easy differentiation between extreme pressure peaks due to propellant grain break-up and those due to increased instability levels.

IV. QUALITY CONTROL AND REPRODUCIBILITY OF RESULTS

The experimental results are significant only insofar as they could be repeatedly obtained in a reproducible manner. By reproducible is meant the repeatability of the $\bar{P}c$ vs. t curves for firings under identical conditions and the repeatability of the onset of instability. In the illustrative firing of figure 1 the unstable increase in mean chamber pressure ($\bar{P}c$) corresponds to an increasing level of gaseous oscillations. It was characteristic of the firings that at some increased $\bar{P}c$ the smooth unstable rise ceased. (See "break" point in figures 1 and 3.) After these large deviations have occurred it should not be surprising should the character of the $\bar{P}c$ vs. t curves deviate widely from firing to firing. Actually there was a remarkable correspondence in the overall pressure time behavior of most firings made under identical conditions. Nevertheless there were many exceptional cases. Some of these deviations can be attributed to mechanical failure of the propellant grain structure. In others, the instability persisted at high levels for unusual periods of time.

On the other hand, the initial phase of the instability process (up to break in the chamber pressure versus time curve) was in general remarkably reproducible. That is, the overall delay time from ignition to the break in the $\bar{P}c$ vs. t curves did not vary greatly for similar motors and the $\bar{P}c$ values at the break, while somewhat scattered, were on the whole quite consistent.

The reproducibility of unstable firings in this work is in contrast to most of the experience in this field. It was, in fact,

not achieved easily and the means by which it was accomplished constitutes one of the major efforts of the investigation. Although much may still be desired with regard to reproducibility from one lot of raw materials to the other, the accomplishment here is of sufficient importance to merit detailed description.

Processing Controls. - The overall process of manufacturing and firing the motors involved a great many steps. In order to eliminate so far as possible the unknown effect of any variations in procedures, standard methods of operation were adopted. Most of these were normal procedures long in use at the Solid Rockets Section of the Jet Propulsion Laboratory. A partial list follows:

a. Storage of Raw Materials

(i) Fuel: Stored in sealed containers; removed for use by a dry nitrogen pressure feed.

(ii) Oxidizer: Stored in plastic bags in sealed containers with desiccant.

(iii) Additives: Stored in sealed containers.

b. Mixing-Casting Process

(i) Took place in a temperature-humidity controlled environment.

(ii) Each ingredient weighed separately.

(iii) Mixer was thoroughly cleaned with solvent on previous day and allowed to dry.

(iv) The mix was temperature controlled during the entire process.

(v) Ingredients were added to the mix in an ordered time sequence.

(vi) Mixing was done under vacuum to remove reaction gases and air.

(vii) Casting was done under vacuum and with vibration shaking to eliminate voids due to trapped gases.

c. Curing and Restricting

(i) Curing took place in temperature controlled ovens for a specified time period at a standard temperature of 160°F.

(ii) The propellant grain was then trimmed to length and weighed and the restrictor plugs applied and cured in the curing oven for a specified time period; i.e., (16 hours each).

(iii) The motors were reweighed and placed in 80°F ovens.

d. Assembly and Firing

(i) The perforation diameter was measured internally at 0°, 120° and 240° circumferentially and at intervals of approximately eight inches along the grain length.

(ii) The motors were reweighed and assembled with the top end during casting used as the nozzle end during the firing.

(iii) After assembly the motors were conditioned in temperature-controlled ovens or refrigerators for a period of approximately 24 hours.

(iv) On the firing day, each motor was removed from conditioning, instrumented and fired in a time interval of approximately 20 minutes.

(v) After firing, the motor case was reweighed with and without the eroded restrictor plugs in order to make an accurate determination of the weight loss due to propellant consumption.

e. Batch Check Motors

(i) At least one, and usually two, 2 1/2" ID x 5" OD motors with a grain length of five inches were made in each batch of propellant.

(ii) These motors were fired with low frequency response instrumentation only, to yield propellant ballistic data such as c^*, r vs. Pc_s, Pc_s vs. Kn.

Despite these precautions, early experiments indicated a need for improvement in both in-batch and batch-to-batch reproducibility. The data obtained showed that reproducibility depended on the length of time allowed for the curing process.

In-batch Reproducibility. - The effect of cure time on in-batch reproducibility is illustrated in figure 23. All batches of propellant were made from the same lots of raw ingredients. The firings are grouped in pairs of geometrically identical motors, by batches. Batches R25, R28, and R26 were cured 72 hours at 160°F with the casting mandrel in place; received

32 hrs at 160°F with the casting mandrel removed during the application of the end restrictor plugs; and received 24 hrs at 160°F while completely assembled for firing, during a pre-firing, temperature-conditioning period. It is clear that satisfactory in-batch reproducibility was not achieved.

However, an 89 hr. cure, followed by the additional processing just described, produced the results shown for R27. In this case the firings are almost identical up to the break in the unstable rise in $\bar{P}c$. A further increase of cure time to 116 hrs led to the firings of batch R24 which leave nothing to be desired insofar as in-batch reproducibility is concerned. Hence, it may be concluded that the cure time must exceed some minimum value if in-batch reproducibility is to be attained.

It is not clear in exactly what manner the additional cure time influences the instability process. Tensile specimens were cast in subsequent batches. These were cured 120 hours at 160°F in their molds, removed and aged at 160°F for periods of time ranging up to 130 additional hours. Tests indicated that the physical properties improved rapidly during the first two days of aging. For example, the ultimate tensile strength increased by a factor of two. Further aging up to a total of 130 hours produced no significant change.

The aging times involved in the tensile specimen tests cannot be carried over directly to the motors. The propellant grains of the motors are very much larger in dimension, hence

the times required to reach the same overall state of cure may be quite different. The motors probably require a longer period of time to reach a state of uniformity since the reaction products of the curing process must on the average diffuse through greater distances. Hence the tensile specimen tests probably provide a lower limit for the times involved in reaching a particular state of cure of the motor grains. After the initial cure time with the mandrel in place, it is unlikely that the propellant grain is in a more advanced state of cure than is the corresponding tensile specimen. Thus it must be expected that chemical changes will take place at a rapid rate during at least the next 48 hours of processing at 160°F.

The time required to reach a particular state of overall cure should be more uniform for motors made from the same batch of propellant than for those made from different batches since manufacturing variations can enter more easily in the latter case. Furthermore, changes in manufacturers' lots of raw ingredients with attendant variation in their chemical nature could be expected to produce further changes in the necessary overall cure time. It will be shown shortly that a cure of 120 hours with the casting mandrel in place plus 32 hours for restricting plus 48 hours additional was sufficient to produce reasonable uniformity of results in the remainder of the experimental program.

Batch-to-batch Reproducibility. - In the early part of the program batch-to-batch reproducibility was checked by firing a reference motor from each batch of propellant. The reference

motors were 3 x 5 x 31/31.5 in. with dt = 1.70 in. In all, 21 such motors with a cure of 116 hrs or more were fixed. All firings were unstable. Representative results are shown in figure 24. Each motor is from a different batch and the firings are arranged in the order in which the motors were made, which was not necessarily numerical order. Due to practical considerations it was not immediately possible to make a large number of batches from fixed manufacturer's lots of raw materials. Changes in lots of raw materials are noted. It will be seen that good batch-to-batch reproducibility was obtained until batch R37 when a new lot of curing agent A was introduced. Further difficulties developed when a new lot of fibre additive was used.

At this point it became possible to reserve large quantities of raw materials from fixed lots. The remaining firings illustrate the degree of reproducibility attained in subsequent work. The overall delay time from ignition to the break in the P_c vs. t curve is consistent. The magnitude of the unstable pressure increase is somewhat scattered. It will be seen subsequently, however, that when a larger number of firings under varying conditions are considered, the unstable pressure increase is a well defined parameter.

A standard cure of 120 hrs, plus 32 hrs for restricting, plus 48 hrs additional was settled on as being sufficient to overcome variations in the overall manufacturing process. In subsequent firings gross changes were made in many of the motor operating parameters. These resulted in very definite trends in the manner

in which the motors exhibited instability. The existence of such trends is in itself a strong argument for the existence of controlled conditions. In many cases the firings were repeated and these repetitions also offer confirmation.

Motor Construction; Effect on Instability Process. - Certain features of the motor construction remained fixed in all firings. In particular, the free volume between the nozzle end of the grain and the nozzle throat was essentially constant with only small variations due to the dependence of nozzle contour on throat diameter. The linear distance from throat to port was also constant, both factors arising from the use of nozzle plates of fixed design.

On the other hand, motors with various grain lengths and initial port diameters were fired. Hence the ratio of perforation volume to nozzle free volume varied, as did the ratio of burning surface length to throat-to-head-end length. Three motors were made from the same batch of propellant using the design shown in figure 25. It will be noted that both the nozzle free volumes and the throat-to-head end distances differed in these motors while the grain length was fixed at 30.5 in. The $\overline{P}c$ vs. t curves shown in the same figure are essentially the same in the three cases. Hence it may be concluded that the aforementioned ratios do not exert a strong influence and thus did not produce systematic changes in the main body of the experiments.

A second feature of motor construction which remained unchanged in all firings was the use of restrictor plugs, one on each end of the grain. The plugs were made from a polysulfide base with

curing additives but no oxidizer, and were cast and cured in position. During the firings, the head-end plugs remained essentially intact while the nozzle end plugs were for the most part badly eroded by the hot gas flow. To make certain that the plugs did not influence the instability process in some unknown manner, the three motors shown in figure 25 were constructed and fired. One motor was constructed in the standard manner, the second with no nozzle end plug, and the third with no head-end plug. The absence of the plugs increased the area ratio Kn by approximately 3.5% at ignition and the pressure by a corresponding small amount. It is clear from the pressure-time curves that the plugs exerted little if any influence, at least at this operating point.

As a result of the foregoing observations and rather extreme precautions taken in manufacture, assembly and firing, it is believed that the experimental trends that follow are indicative of the gross features of the instability mechanism and not of random influences in manufacture. It is true that the behavior of rockets manufactured under less well controlled conditions may, to a significant extent, be strongly affected by such influences and consequently they may not correspond strictly to the present experiments. In this regard two comments may be made:

1) The experiments reported here were conducted solely for the purpose of elucidating the instability mechanism, in the sense that the results give trends that any adequate theory must reproduce.

2) In any industrial situation where instability problems must be met in a fundamental manner, reproducibility must be

achieved by refined process control and hence the present results will apply.

At this time, however, we tend to emphasize item one, that the present experimental results are a prerequisite to a meaningful theoretical treatment.

VI. EFFECT OF CHANGING PROPELLANT OPERATING PRESSURE AND GRAIN PERFORATION DIAMETER

Several series of cylindrical motors were fired in which only the nozzle throat size was changed from firing to firing. In a particular series, the grain length, initial perforation diameter, grain temperature and propellant composition remained fixed. From series to series, the initial perforation diameter was varied. These firings were intended to investigate the effect of the chamber pressure level or propellant burning rate level on the occurrence and characteristics of the instability.

A simple time independent relationship exists between pressure or burning rate, oscillation frequency and nozzle size for the cylindric motors. This may be seen as follows. The stable operating pressure of a solid propellant motor is dependent on ballistic parameters and on the geometrical configuration of the motor. If the ballistic parameters are held constant by a particular choice of propellant and grain temperature, then the stable pressure-time history of the motor depends only on the geometry, a part of which is time dependent due to propellant consumption. Under the conditions stated in the first paragraph, the stable operating pressure and burning rate depend primarily on the ratio of burning surface area to nozzle throat area. This ratio is usually called Kn. For a cylindrical perforation with restricted ends,

$$Kn = \frac{4DpLp}{dt^2} \qquad (11)$$

where Dp is the perforation diameter, Lp is the grain length and dt is the nozzle throat diameter. Hence the pressure-time history depends on the choice of dt as well as on the value of Dp at each instant, through equations 9 and 11.

On the other hand, the local speed of sound in the motor is almost constant throughout a firing since it is relatively unaffected by changes in operating pressure. Hence the frequencies of the various modes of gaseous oscillation vary with time only through their dependence on the changing geometry. Thus, for a cylindrical motor, the frequency to be associated with the fundamental tangential mode of oscillation is, in essence, uniquely determined at every instant by the perforation diameter alone, i.e., $f = \frac{\text{constant}}{Dp}$. Therefore

$$Kn \sim \frac{1}{f\, dt^2} \quad . \tag{12}$$

That is, the functional relationship between acoustic frequency and pressure or burning rate is roughly invariant with time and depends only on the choice of nozzle size. This conclusion presupposes that the oscillations do not interact with the combustion process in such a manner as to produce changes in the ballistic parameters. In Chapter III it was shown that the oscillations cause radical departure from stable conditions. Nevertheless, the motors do not oscillate initially and the above considerations must apply during the early onset phase of the instability process.

At a given grain temperature, the initial value of Kn, Kn_i together with the initial port (perforation) diameter completely

specifies the operation of a cylindrical motor in the Kn-Dp plane. This follows from equation (11 since

$$Kn_i = 4\, Dp_i \frac{Lp}{dt^2} \qquad (13)$$

Hence

$$Kn = \frac{Kn_i}{Dp_i} Dp \qquad (14)$$

The assumption has been made that the grain perforation remains cylindrical throughout the firing.

If the motor operates in a stable manner one may use equations 9 and 10 to obtain the chamber pressure and burning rate corresponding to Kn. Finally, the initial values of Kn and Dp are well defined by pre-firing measurements and do not involve pressure measurements and associated data reduction. Thus, if the initial operating points of many firings are defined in terms of these parameters, most of the experimental scatter should be due to variations in the ballistic parameters themselves. In view of these considerations, Kn_i and Dp_i will be used to specify the operating points of all cylindrical motors.

Experiments Varying the Chamber Pressure. - Several series of motors were fired in which the initial value of Dp, Dp_i, was fixed, as were Lp and the grain temperature Tp. Two series are shown in figure 26. Five firings are shown in figure 26 in which Dp_i = 2.45 in., Lp = 31 in., and Tp = 160°F. These motors were fired with nozzle sizes ranging from 1.70 in. to 1.35 in. As a result the initial value

of Kn ranged from 109 to 174 and the initial operating pressure from approximately 180 psia to 325 psia.

Several features of the firings are immediately apparent. The most striking perhaps, is the degree of instability exhibited. As the initial value of Kn was increased by reduction of nozzle throat size in successive firings of otherwise similar motors, the degree of instability increased. However, this trend did not continue indefinitely. An increase of Kn_i from 140 to 156 in. resulted in a sharp transition from a strongly unstable motor to a weakly unstable motor. A further increase of Kn_i to 174 led to a completely stable firing. This same trend has been confirmed for motors of several different initial values of Dp. The results obtained for Dp_i = 2.8 in. are also shown in figure 26.

The break in the unstable pressure rise is usually clearly defined and should be indicative of the degree of instability the unstable process may attain before the various unknown limiting damping factors balance the driving forces. If we call the mean pressure at the break $\overline{P}c_B$ and the pressure which should have existed at this value of Dp had the run been stable Pc_s, then the ratio $(\overline{P}c_B - Pc_s)/Pc_s \equiv \Delta\overline{P}c/Pc_s$ is a measure of the degree of instability of a particular firing. In general $\overline{P}c$ and the oscillation amplitude showed the same close correlation exhibited in figure 2, hence $\Delta\overline{P}c$ is also a measure of oscillation amplitude. A plot of $\Delta\overline{P}c/Pc_s$ vs. Kn_i is given in figure 27 for firings made with values of Dp_i ranging from 2.2 in. to 3.0 in., all with Lp = 31.0 in. and Tp = 160°F. The majority of the firings showed a linear increase

of $\Delta\bar{P}c/Pc_s$ with Kn_i until $Kn_i = 150$. At $Kn_i = 150$ an abrupt transition occurred. The magnitude of $\Delta\bar{P}c/Pc_s$ decreased rapidly from 95% to roughly 2% over the range $Kn_i = 150$ to $Kn_i \approx 160$. The appropriate values of $\bar{P}c_B$ were determined by comparison of the $\bar{P}c$ traces and the detected Photocon outputs on the Miller records. In some cases the pressure peak was partially due to grain damage.

It should be noted that the foregoing observation applies to a range of Dp_i from 2.2 in. to 3.0 in. The results are characteristic of cylindrical motors outside this range, in the sense that there always existed a value of Kn_i for given initial value of port diameter, above which a particular motor was, at the most, weakly unstable. The experimental results for a much broader range of parameters are discussed later.

A second feature of the series lies in the delay period from ignition to the "break" in the initial unstable rise of the mean chamber pressure. This delay time is short in comparison with the total run time and is on the order of a few tenths of a second. However, it represents several thousand gas oscillation cycles at the frequencies characteristic of the fundamental tangential acoustic mode.

In the early part of the delay period, immediately after ignition, the motors appeared to be stable. The instrumentation employed permitted detection of oscillations with a minimum peak-to-peak amplitude of approximately one psi. This stable period was seldom less than 0.1 sec and increased as the initial operating pressure was increased. In high pressure firings where the motors

were only weakly unstable, the initial stable period has been observed to be as large as 0.77 seconds.

After the oscillations were large enough to be detected it was observed that as time passed they increased in amplitude, on the average. However, the growth was not, in general, a smooth function of time, but was subject to many rapid and, apparently random, fluctuations. Finally, the oscillations became very large in the region where the mean chamber pressure rises rapidly.

It was characteristic that the overall delay time from ignition to the "break" in the unstable rise in mean pressure increased as the initial value of Kn (pressure) was increased. The mean stable burning rate during the delay also increased with Kn_i, due to the higher pressure, hence the amount of web burned to the "break" point became larger, due to both effects, and varied roughly from 0.1 in. to 0.3 in., depending on Kn_i. This is shown in figure 28. The overall delay time is plotted in figure 29 as a function of Kn_i.

Experiments Varying the Grain Perforation Diameter. - It is informative to regroup many of the firings just discussed and to examine them from a different point of view. As a preliminary to this, consider the effect on the mean pressure vs. time traces, of firing a series of stable motors, all with fixed nozzle throat size, grain length, and fixed grain temperature, but with various values of initial port diameter. It is clear that, except for the initial starting transient, the pressure-time traces must all lie on that of the motor with smallest Dp_i. This may be shown diagrammatically as follows:

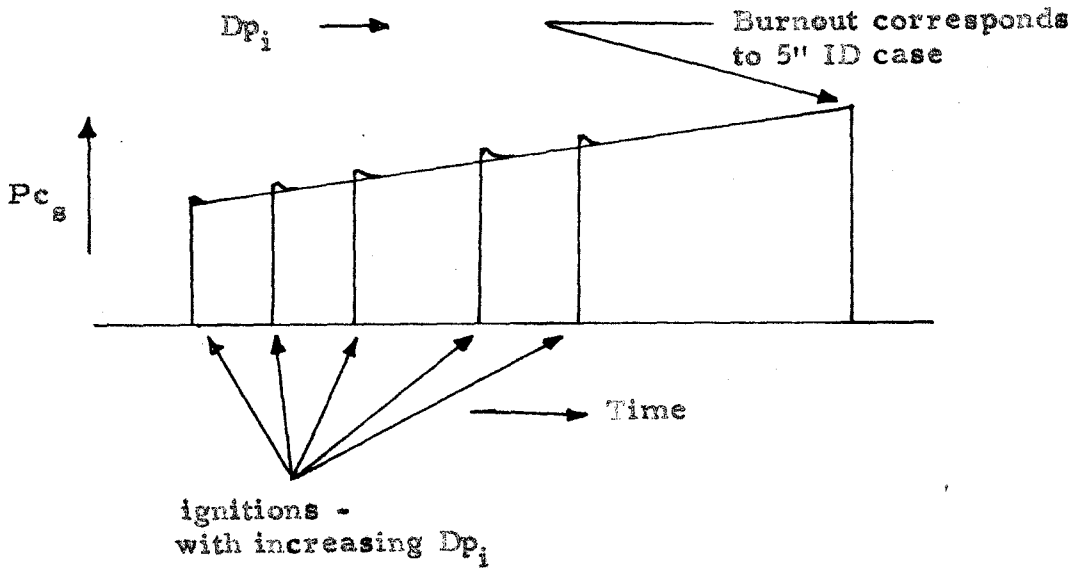

Sketch A

If we attempt this procedure with unstable firings we expect some deviations from stable conditions in the $\bar{P}c$ vs. t curve after the main part of the instability, particularly if the grain perforation has been damaged. It has been found experimentally that where large deviations occurred, the grain was indeed damaged. Pieces of propellant were found in the firing pit after such runs. These pieces were irregular in shape and of various sizes, some being so large as to have left a hole through the grain to the case wall. It is clear that such grain damage should seriously disturb the pressure-time curve for the remainder of the run. Nevertheless, it is instructive to superimpose the firing curves of such runs since we may confine our attention to the onset phase of the instability. This has been done in figure 30.

In figure 30, results are shown for five firings with dt = 1.50 in., Lp = 31 in., Tp = 160°F, and Dp_i = 2.45, 2.60, 3.0,

3.30, and 3.40 in. The firings with Dp_i = 2.45 and 2.60 in. have $Kn_i < 150$ and hence are severely unstable.

Perhaps the most important point to note is that the motor with Dp_i = 2.45 in. is severely unstable in the delay period of the 2.60 in. motor. Since both phenomena occur in the same frequency interval, it is clear that the delay period does not represent a situation in which instability is prohibited by improper relationship between frequency and any conceivable time lag. Further evidence of this is seen in figure 30 where firings are also shown in which the fixed nozzle size has been increased to dt = 1.60 in. Both the initial stable period and the overall delay period increase as the operating pressure level is increased. As has been noted earlier, in some high pressure firings the initial stable period was as large as 0.77 secs while the overall delay period to the "break" in the Pc vs. t curve has exceeded one second. No explanation of this behavior can be given at this time. The thermal diffusivity of the propellant is approximately 2.4×10^{-4} in^2/sec; hence we expect a steep temperature gradient at the burning surface which should be essentially quasi-steady space-wise since the surface is consumed at a rate on the order of 0.25 in/sec. A rough estimate indicates that the time required to reach quasi-steady temperature conditions is on the order of milliseconds. However, data reduction indicates that quasi-steady operation begins at approximately 0.1 to 0.2 seconds after ignition. Igniters were fired in a dummy cylindric motor under typical firing conditions. The total time for the

ignition pulse did not exceed a few hundredths of a second. It is recognized that during an actual ignition, the propellant grain as well as the igniter are generating gas and hence the times involved may be somewhat different. Nevertheless, it seems unlikely that the ignition process in itself is responsible for delay times as large as those observed.

On the other hand, it will be seen later that motors which were interrupted and then refired showed the typical delay period during the second firing as well as the first. Hence the delay cannot be attributed to a composition difference in the outer layer of propellant. This may also be seen from the fact that at the higher pressure levels a greater thickness of propellant is consumed during the delay period since both the delay time and burning rate have increased.

The firings of figure 30 represent only a small part of the total firings made in which the initial port diameter was varied. The 5 in. ID motor with a grain length of 31 in. has been fired with 20 different sizes of Dp_i covering the range $Dp \approx 1.5$ to 4.5 in. The nominal sizes used are tabulated below.

Initial Port Diameters of 5 in. ID, 31 in. Lp Motors

1.5 in.	2.5 in.	3.1 in.	3.35 in.
1.7	2.7	3.15	3.45
1.9	2.9	3.20	4.05
2.1	3.0	3.25	4.25
2.3	3.05	3.3	4.5

As was noted in Chapter III, a composition change is believed to occur in the 5 in ID motors when Dp reaches approximately 4.0 to 4.2 in. In this region the pressure time curves invariably changed slope towards lower than normal pressures indicating that the burning rate was abnormally low. Without exception, unstable motors became stable upon reaching this region. They remained stable until an increase in Dp of roughly 0.4 in. had occurred and then usually became unstable again. The second instability period thus occurred in a region of composition not precisely known. Furthermore, since the composition change begins at Dp $\approx$ 4.0 to 4.2 in. in motors of smaller Dp_i and with a 5 in. ID case, it is not clear where the change begins in motors with the same case ID and $Dp_i > 4.0$ in. Hence only a few motors of the latter type were fired. Motors with $Dp_i \approx$ 4.0 and 4.2 in. did not become unstable until Dp = 4.5 to 4.6 in.* However, the instability followed the same trends with pressure level as firings of smaller Dp_i and the firings are included in a later discussion for the sake of completeness.

In these and other firings instability has been observed over the frequency range corresponding to roughly Dp = 1.5 to 6.0 in. These diameters correspond to frequencies in the fundamental tangential mode ranging from approximately 14.5 Kc to 3.6 Kc.

Further Experiments Varying Initial Perforation and Nozzle Diameters . - In view of the dependence of rocket instability upon

---

* This difference is more than can be accounted for by a normal initial delay period, at least for the firings made at low pressure level.

pressure level as well as perforation size, it appeared advisable to fire a large number of motors covering various initial values of Dp and Kn. The results of these firings for Lp = 31.0 in. and Tp = 160°F are shown in figure 31. The points plotted represent initial conditions of Kn vs. Dp for the firings. Lines of constant throat diameter (dt) are indicated for Lp = 31.0 in. The change in Kn and Dp during a particular firing is obtained by following the appropriate dt line. For example, the firing with initial condition Dp = 3.05, Kn = 105 proceeds along the dt line, dt = 1.895 out to Dp = 5.0 which is the ID of the motor case.

Several features of the plot are immediately apparent. The Kn-Dp plane may be divided into two major regions: a stable region and an unstable region. The stable region is separated from the unstable region by a line (stability limit line) which, for values of Dp greater than 2.3 in., is a line of constant dt. It will be shown that this line is in general a line of constant Lp/dt^2 with the value in this case corresponding to Lp = 31 in. and dt $\simeq$ 1.37 in. For Dp less than 2.3 in. the stability limit curves upward to some extent. In this region the average axial flow velocity in the motors becomes increasingly greater as may be seen by comparing Dp to dt. But it is not known whether this accounts for the deviation.

The significance of this stability limit is emphasized by the fact that the unstable firings on the dt = 1.30 and 1.325 in. lines were unstable only in the very early part of the runs and quickly became stable as they entered the stable Kn-Dp region. All of the unstable firings with Dp $\simeq$ 2.0 in. or less were singular in

that the instability began at very low amplitude and gradually increased in intensity. This behavior was markedly different from the spiking effect observed in the firings with $Dp_i > 2.0$ in. This may be seen in figures 34 and 35 where firings along the dt = 1.30, 1.385 and 1.42 in. lines are shown for varying port diameters.

It appears that after the initial delay period the motors quickly become unstable to a limited degree. The degree of instability is not that attained at the same value of Kn and Dp if the motor starts firing at a smaller Dp_i but with the same nozzle size. This must mean that the previous pressure-time history of the grain influences the instability at a particular operating point. Although the origin of this behavior is not clear, it was certain that the degree of instability of a motor through a range of Kn-Dp values could not be determined by the firing of only one motor. Rather, a series of firings had to be made with initial conditions spaced throughout the Kn-Dp range in question.

It has been noted that for any given port diameter the instability became more severe as Kn_i was increased in successive firings until a certain critical value of Kn_i was reached. For Kn_i greater than this, the motors were only weakly unstable and became stable for sufficiently large Kn_i. If we refer to figure 31 it is now clear that the value of Kn_i for stability is that defined by the stability limit and is a function of Dp_i as just described.

Also plotted in figure 31 is the line which defines the critical value of Kn_i; below this curve the instability is strong and above it is weak. This line shall be called the transition line as opposed to

the stability limit line. The transition line intersects the stability limit at approximately $Kn_i = 150$ and $Dp_i = 2.25$ in., say $Kn^* - Dp^*$. The plot of $\Delta\bar{P}c/Pc_s$ vs Kn_i (figure 27) discussed earlier covered the range $Dp_i = 2.2$ in. to 3.0 in. and was independent of Dp_i within this range. However, points with $Dp_i < 2.2$ in. do not correlate and in general, for these $\Delta\bar{P}c/Pc_s$ is markedly too small. If we examine figure 31 we see that such points lie on the small side of Dp^* and are confined to values of $Kn_i < Kn^*$ by the stability limit curve. It seems likely that the lack of correlation is due to the proximity of the stability limit. On the other hand, for $Dp_i > 3.0$ in. the transition line rises to higher values of Kn for increasing Dp_i. The corresponding $\Delta\bar{P}c/Pc_s$ vs Kn_i plot is given in figure 36. It may be seen that very large deviations in $\bar{P}c$ occur at quite low values of Lp/Dp since for the very largest port diameters the instability occurred just prior to burnout. At this point $Lp/Dp \simeq 6.2$.

It should be noted that below the transition line shown in figure 31, the degree of instability decreased as Kn_i was reduced. Hence the firings at the lower values of Kn_i were not, strictly speaking "strongly unstable", but became so as Kn_i was increased towards the transition line. This trend has been discussed previously in connection with figure 27. Furthermore the firings for $Dp_i < 2.0$ in. did not show the pressure spikes characteristic of the firings with $Dp_i > 2.0$ in. In the former firings the magnitude of the instability increased very gradually with time,

reached a maximum value and decayed as was seen in figures 34 and 35. There is some question as to the validity of results obtained from firings with Dp_i of 4.0 in. and greater. These firings were unstable and exhibited the usual trends with operating pressure. However, when this instability occurred the burning was taking place in a region close to the casing where a change in propellant is believed to have taken place. In this region the burning rate is abnormally low as was remarked earlier in connection with figure 4.

The transition line and stability limit are shown in the $\bar{P}c$ vs. Dp plane in figure 32. The corresponding plot in the $\bar{P}c$ vs f_{100} plane is given in figure 33. Here f_{100} denotes the frequency of the fundamental tangential acoustic mode associated with Dp. The initial stable operating pressure of representative cylindrical motors versus the corresponding value of Kn is plotted in figure 41. It is clear that the burning rate remains unchanged in the operating region under discussion. This data was used to transform the Kn coordinate in figure 31 to the pressures shown in figure 32.

In addition to the 5 x 31.5 in. motors, several others with a variety of case inside diameters and lengths were fired. These motors were intended to check the instability trends already established with the 5 x 31.5 in. motors. The Kn_i vs Dp_i plots are given in figure 37. The stability limit and transition line for the 5 x 31.5 in. motors is shown in the same figure. Due to the fact

that the stability limit defines decreasing values of Kn_i with decreasing Dp_i, a difficulty was encountered in firing motors of small Dp_i in the unstable region. This difficulty lay in the low pressure or chuffing limit for the propellant. Only motors which did not chuff are shown in figure 37, since the grain shape was seriously distorted in those motors which chuffed. The small-sized motors with $Dp_i < 1.6$ in. were designed to have an initial Lp/Dp_i of at least ten, in view of results to be discussed in chapter VII. The length could not be held to 31 in. at these small port diameters due to the following considerations:

$$Kn = 4\ Dp\ \frac{Lp}{dt^2} \tag{15}$$

$$= 4\ \frac{Lp}{Dp}\ H \tag{16}$$

where H = area of port/area of throat.

If H = 1, then the port is the same size as the nozzle throat. H must be kept somewhat greater than one to avoid choking and excessive erosive burning. Hence, as Dp is reduced, Lp must also be reduced if Kn is to be made successively smaller and a reduction of H cannot be accepted. The motors with nominal Dp_i = 0.5, 1.0 and 1.2 in. were stable. Reference to figure 37 shows that they probably lie above the stability limit for the 31 in. motors.

Two successful firings were made with $D_{p_i} \approx 1.5$ in. One was stable and one unstable. In figure 37 it may be seen that the initial conditions were in good agreement with the stability limit for the 31 in. motors. This agreement was obtained in spite of the fact that the two types of motors differ in grain length, case inside diameter and web thickness. Several firings were made with 3 x 5 x 38/38.5 in. and 3 x 5 x 44.5/45 in. motors. These are also shown in figure 37. The same trends were observed as for the 31 in. motors and the stability limit is in good agreement. The 44.5 in. motors have a 44% increase in grain length as compared to the 31 in. motors. Finally, several motors were fired with 6 in. inside diameter cases. Once again agreement was obtained both in trends and with respect to the stability limit. The firing with highest Kn lies on the 31 in. limit. This motor was very weakly unstable.

Speculations Concerning a Time Lag Mechanism. - The experimental results strongly indicate that the stability limit depends only on the perforation diameter and the Kn ratio at the operating point. This may be restated as follows: The acoustic frequencies characteristic of the perforation cavity depend primarily on the cavity diameter. The quasisteady chamber pressure and burning rate depend primarily on Kn. Hence, the stability limit is believed to be determined by the interrelation

between the active acoustic mode and the combustion mechanism, without regard to such factors as web thickness, case diameter, and grain length.

In particular, in figures 31 and 37, if the slight curvature in the stability limit at small values of Dp is ignored, then this limit is roughly defined by a line of constant Lp/dt^2, say $\left[Lp/dt^2\right]_s$. Then along this line

$$Kn = 4Dp \left[\frac{Lp}{dt^2}\right]_s \tag{17}$$

But

$$Pc_s \approx (a\ \rho_p\ c^*Kn)^{1/1-n} \tag{18}$$

and

$$f = \frac{a_c\ \alpha_{10}}{Dp} \tag{19}$$

whence

$$f > \frac{a}{Pc_s^{1-n}}\ c^{*2}\ (4\ \rho_p\ \alpha_{10})\ \Gamma'\left[\frac{Lp}{dt^2}\right]_s \quad \text{for stability.} \tag{20}$$

$$> \frac{r_s}{Pc_s}\ c^{*2}\ (4\ \rho_p\ \alpha_{10})\ \Gamma'\left[\frac{Lp}{dt^2}\right]_s \quad \text{for stability.} \tag{21}$$

Since this defines the inverse of a time, it would be particularly convenient from the point of view of time lag theory should the equation be obeyed for changes in grain temperature without having to adjust geometrical factors. A discussion of the effect of grain temperature on the stability limit is given in chapter VIII.

There it will be seen that some adjustment had to be made in the factor $\left[Lp/dt^2\right]_s$ in order to determine the stability limit. The limit changed as a function of grain temperature but the change in the limit was not simply related to changes in 'a' and 'n'. This result, of course, does not prevent the assumption that a time lag is operational but states only that the time lag (if any) is probably not simply related to the ballistic parameters.

However, the trend in the stability limit with decreasing grain temperature is to lower pressures; that is, the same trend as for the burning rate. If we ignore the fact that the geometry had to be changed somewhat and assume that equations 20 and 21 hold rigidly, then we may speculate as to the effect of c* and r_s vs Pc_s. It is clear that the greater r_s is for given Pc_s, the more difficult it is to stabilize the system. Furthermore, the characteristic velocity c* enters as c^{*2}, hence an increase in c* should tend rather strongly to destabilize the system. It is interesting to note that these speculative results are in general agreement with the well-known observation that higher energy propellants are more prone to instability.

Again, we may note that as the perforation diameter is increased in size, f is decreased, hence a motor tends to become destabilized as its scale is increased, provided the

scaling is done linearly so as to leave the right-hand side of the equation unaffected. (Note that the R.H.S. of equation 20 is dimensionally free of length).

It must be emphasized that these results were obtained using cylindrical motors. There is reason to believe that the particular type of active acoustic mode influences the stability limit and the degree of mean pressure deviation for given oscillation magnitude. This is discussed in chapter X. Nevertheless, it is probably true that similar trends would be noted in motors of different internal perforation design if sufficient firings were made to determine them.

Finally, the effect of changing the propellant composition has not yet been investigated. It would be of considerable interest to discover whether or not minor changes in propellant composition, of such a nature as not to affect the basic combustion mechanism, would produce the speculated changes in the stability limit.

VII. EFFECT OF GRAIN LENGTH

A number of experiments were performed to investigate the effect of grain length on the instability process. The motors used had 3.0 in. initial port diameters. A series of firings was made with grain lengths of 17, 31, 38 and 44.5 in. and with $Kn_i \approx 130$. A plot of $\frac{\Delta \overline{P}c}{\overline{P}c_s}$ vs Lp for these firings is shown in figure 40. Representative pressure time curves are shown in figure 42. It is clear that the degree of instability at fixed Kn_i was independent of grain length for grain length greater than approximately 30 in. On the other hand, the instability became markedly weaker as the grain length was reduced from 31 in. to 24 in.; the 17 in. motors were only weakly unstable. Hence a critical grain length of approximately 30 in. existed, below which the instability decreased rapidly with decreasing grain length. Further experiments were performed with the 17 and 24. in. motors in which the operating pressure level was decreased (i.e. $Kn_i < 130$) in successive firings. For both lengths the motors became less unstable indicating that the firings at $Kn_i \approx 130$ were below the transition level. However, a firing at $Kn_i \approx 147$ with the 24 in. motor was stable indicating that the stability limit was exceeded in this case. Since the stability limit is at approximately $Kn_i = 200$ for the 3 x 5 x 31/31.5 motor (see figure 31) it would appear that the stability limit has changed as a function of grain length. However it has been shown earlier in connection with figure 37 that this is in general, not the case and that it is probably true that the stability

limit depends only on the interaction between the tangential frequencies and the burning mechanism of the propellant. A more likely explanation for the behavior of the 17 and 24 in. motor appears to be in an unfavorable increase in the losses of the system, as compared to the driving energy input. That is, it is assumed that the losses were so great as to reduce the instability below detection level at values of Kn_1 less than those corresponding to the true stability limit.

Alternatively, it may be postulated that a certain coupling must exist between the tangential mode and the longitudinal mode associated with the axial dimension of the motor. The available evidence argues against this. One may cite the experiments discussed in chapter V in which the length of the motor was changed without significant effect while the grain length was maintained constant. Thus if an axial dimension is important frequency-wise it is probably the grain length. But in fact, no high amplitude driving in axial modes was ever noted. Reference to figure 9 shows that only the high frequency oscillations are driven to large amplitude. Thus it is assumed that increased damping is the more likely explanation of the two. This argument receives further weight if we consider the firings with 3 x 5 x 38/38.5 in, and 3 x 5 x 44.5/45 in. motors, shown earlier in figure 37. The results obtained with these motors indicate that the transition level increases somewhat with grain length. This may be seen by

comparing figures 27, 38 and 39 in which $\frac{\Delta \bar{P}c}{\bar{P}c_s}$ vs Kn_i is plotted for the 31, 38 and 44.5 in. motors, respectively. The transition value of Kn is shown to be 150 for Lp = 31.0 in., 161 for Lp = 38.0 in. and probably somewhat greater than 161 for Lp = 44.5 in. In view of the foregoing discussion, this result suggests that for the longer motors large amplitude driving was possible at higher operating levels due to a more favorable ratio of energy input to losses.

Finally, it should be noted that experiments intended to investigate the stability limit must involve motors with grain lengths exceeding the critical value for the particular design, otherwise erroneous conclusions may result.

VIII. EFFECT OF GRAIN TEMPERATURE

A series of 42 cylindrical motors with Dp_i = 3.0 in. and Lp = 31 in. was fired to investigate the effect of initial grain temperature. Motors were fired over the temperature range -80°F to 180°F.

Figure 43 depicts the $\bar{P}c$ vs t curves for ten such motors spaced throughout the temperature range and all fired with a nozzle size of dt = 1.60 in. and hence with constant initial area ratio Kn_i. This series of firings illustrates an effect which has become reasonably well known. The instability is more pronounced at the high and low temperature extremes. In this case, the firings at -40, -20, and 20°F are stable. However, the remaining firings in figure 43 show that if Kn_i is lowered by increasing the nozzle throat size to dt = 1.80 in. these latter motors become unstable. This might have been anticipated on the basis of the dependence on Kn_i already described for motors fired with grain temperature Tp = 160°F.

From the firings made it was possible to determine the manner in which the upper stability limit and the point of maximum instability varied with temperature. These results were most conveniently represented in a plot of initial chamber pressure versus initial grain temperature as shown in figure 45. During and immediately after ignition, the motors were not operating in a quasi-steady state, hence the pressure during this interval was

subject to large deviations from normal. Inspection of reduced data led to the conclusion that by the time Dp = 3.15 in., the motors were in quasi-steady operation and at the same time had not entered instability. Since it was desirable to compare the operation at a condition of fixed geometry, the operating pressure at Dp = 3.15 in. was chosen for the initial pressure reference condition. The limiting curves are shown in figure 45 along with the data that determined them. For propellant temperatures below -40°F, the curves were difficult to determine accurately and consequently are shown as broken lines.

Curves of constant throat diameter or, what is the same, of constant Kn_i, are shown also in figure 45. From them, it is a simple matter to interpret the series of firings at various grain temperatures discussed earlier. In figure 43 the motors were fired over a range of grain temperature from -80°F to 180°F, with a fixed nozzle throat diameter dt = 1.60 in. and hence Kn_i = 149. From figure 45 it is seen that the Kn_i = 149 line begins in the weak instability region at Tp = -80°F, passes into the stable region at Tp = -40°F, reenters the weak region at Tp = + 30°F, and finally enters the strong instability region at 155°F. The series with dt = 1.80 in., Kn_i = 118, also shown in figure 43, lies entirely in the strongly unstable region. The two stability curves have been replotted from the data of figure 45, in terms of the initial value of Kn, as shown in figure 44. This data gives some indication of how the results of figure 31 will change when different grain temperatures are selected.

In searching for the origin of the behavior shown in figures 44 and 45 it is natural to investigate the propellant burning rate since this is a property strongly affected by grain temperature. The manner in which the grain temperature influences the burning rate and operating pressure for a particular geometry is given by

$$Pc_s \approx (a \rho_p c^* Kn)^{\frac{1}{1-n}} \tag{22}$$

$$\approx (\rho_p c^* Kn)^{\frac{1}{1-n}} a^{\frac{1}{1-n}} \tag{23}$$

The parameter n is, at the most, only weakly dependent on grain temperature. It has been determined from batch check motors made from the same batches of propellant as the unstable motors of the temperature series. A plot of n versus Tp is given in figure 46. The parameter 'a' is often taken to vary as

$$a = \frac{\text{constant}}{To - Tp} \tag{24}$$

where To is a temperature characteristic of the particular propellant. Thus, if equation 24 holds, $\frac{1}{a}$ should vary linearly with Tp. This result was not obtained with the present propellant as is shown clearly in figures 47 and 48. With the information now available on the burning rate of the propellant, it was possible to construct a plot showing the stability curves as a function of initial burning rate and propellant temperature. These are shown in figure 49. The burning rates for both limit lines increase steadily with increasing grain temperatures. The

difference in burning rate between the two curves does not differ greatly over the entire temperature range. Because the temperature effect is strong, the burning rate stability limit and transition line do not show a minimum value as do the corresponding Kn_i (figure 44) and Pc_{si} (figure 45) plots. In chapter VI a discussion of the experimental results was given for all firings at 160°F. There it was seen that the stability limit was dependent on the oscillation frequency and on the basic combustion process. In the present case the initial unstable frequency is relatively fixed since the instability begins close to ignition and the initial perforation diameter is fixed. Furthermore, the speed of sound is at the most very weakly dependent on grain temperature and chamber pressure. Hence in this series of experiments we expect that changes in the location of the stability limit must reflect the influence of grain temperature on the ability of the combustion mechanism to interact successfully with a narrow range of frequencies.

The maximum excitation that is obtained at a given grain temperature increases with increasing grain temperature as shown in figure 50, where a plot of the maximum observed $\Delta\bar{P}c/Pcs$ is given versus Tp. The firings in question are those represented by the solid symbols of figure 45.

Finally, several firings were made at grain temperatures of 160°F and -60°F with a different propellant (propellant B). The pressure-time curves are shown in figure 62. All firings were stable. Propellant B was composed of the same type fuel and oxidizer as propellant A. The additives employed were somewhat different. The physical properties and ballistic parameters for the two propellants are not greatly different. However, the differences were sufficient to produce complete stability in propellant B motors fired in the same region of the Kn - Dp plane as severely unstable propellant A motors.

IX. IDENTIFICATION OF THE MODES OF GASEOUS OSCILLATION

It has been stated previously that gaseous oscillations occur within the motor, and, that in the case of the cylindrical motor, the growth of these oscillations is always accompanied by an abnormal increase in average chamber pressure. Through the use of the instrumentation and data reduction methods described in chapters III and IV, a fairly complete description of frequency versus time and/or perforation diameter has been obtained. In figure 51 the results are plotted for a typical firing.

The firing began at zero time with an average perforation diameter of approximately 3.05 in. As the firing proceeded, the perforation diameter increased due to the consumption of propellant. The earliest detectable oscillation began with a frequency of 6.7 Kcs. The frequency then decreased smoothly with time as the perforation diameter increased. The oscillation diminished below a detectable level at 5.3 Kcs, reappeared at 4.6 Kcs and persisted through a portion of tail-off. Using the methods described in chapter III, the full low frequency data reduction for the firing provided a calculated value of perforation radius as a function of time. The product of frequency and radius is a constant independent of time with an average value of 10875 ± 1% in/sec.

On the basis of acoustic theory it would be expected that the frequency would be related to the instantaneous perforation diameter by

$$f = (\text{const})\ \frac{a_c}{Rp} \quad \text{where } a_c = \text{local speed of sound}$$

Rp = instantaneous perforation radius (25)

$$\text{Hence } f.\,Rp = (\text{const})\ a_c \tag{26}$$

which is constant provided the speed of sound or mode of oscillation does not change with time. In particular, acoustic theory predicts that tangential, radial and combination modes of oscillation in a cylindrical cavity will have frequencies such that

$$f_{mn} = \frac{a_c \alpha_{mn}}{2\,Rp} \quad \text{where } \alpha_{mn} \text{ is a mode number} \tag{27}$$

The fundamental tangential mode of operation may exist in either a standing or travelling configuration. The frequency for both cases is given by

$$f_{100} = \frac{(a_c)\ (.586)}{2\,Rp} \tag{28}$$

Thus $a_c = \frac{f_{100}\,Rp}{(.2930)12}$ ft/sec provided that the oscillation corresponds to the fundamental tangential mode. This leads to $a_c = \frac{10875}{(.2930)12} = 3085 \pm 1\%$ ft/sec. One may also obtain a_c from the relation

$$a_c = \Gamma' c^* \tag{29}$$

The overall average value of c* obtained from all firings was 4236 ft/sec. If the average ratio of specific heats, $\bar{\gamma}$, is chosen to have the value $\bar{\gamma} = 1.24$, then we obtain an identical speed of sound by the latter method.

The next higher mode of oscillation involves the mode number $\alpha_{200} = .9722$. Also, Γ' is a very slow function of $\bar{\gamma}$. Hence for reasonable values of $\bar{\gamma}$ it is possible to obtain agreement for only one mode of operation and it is clear that this is the fundamental tangential mode.

If we refer once again to figure 51, we may also note that during the most severe part of the instability, the frequency of oscillation does not deviate appreciably from the acoustic value. During this period, the oscillations are very large in amplitude and the linearizations involved in acoustic theory are likely to be invalid.

K. MOTORS WITH OPPOSED-PLANE GRAIN DESIGNS (SLAB TYPE MOTORS)

In addition to the cylindrical type motors, two designs of slab-type motors were fabricated and fired. These designs are shown in figures 52 and 53 and will be designated type 1 and type 2, respectively.

Two firings were made with the type 1 motor. The pressure-time curves are shown in figure 54. Due to the grain configuration, the operating pressure remains essentially constant for a period of time and then begins a slow tail-off. The firing at the higher initial pressure was stable. The firing at the lower operating pressure was unstable in the sense that gaseous oscillations occurred. However, no deviations in the mean operating pressure were noted as would have been the case had the motor been of the cylindrical type. The frequency of oscillation decreased with time and agreed within 2% with the acoustic value for the transverse fundamental sloshing mode. In this mode the gas moves only in a direction perpendicular to the burning surfaces; no motion of the gas tangential to the burning surfaces takes place.

The type 2 slab motors were based on trends observed in concurrent firings with the cylindrical motors. The grain length was increased from the type 1 length of 23.5 in. to approximately 38.5 in. in the type 2 motors. The steel inserts used in the type 1 motor were omitted, hence the type 2 motors burn with a regressive

pressure-time curve from ignition onward. This, together with an increase in the spacing between the grain surfaces to 1.8 in. permitted the longer motors to be fired at lower pressures without choking of the flow in the grain port. A series of six firings with the type 2 slab motor is shown in figure 54.

The firings using type 2 slab motors covered a range of Kn_i, the initial value of Kn, from 84 to 219 by choice of a suitable range of nozzle throat diameters. Only the firing with the highest value of Kn_i was stable. The remaining firings at lower Kn_i all exhibited gaseous oscillations in the fundamental transverse mode similar to those found in the type 1 slab motor. The peak to peak magnitude of these oscillations was as large as 20% of the average chamber pressure. No changes of mean pressure were observed. It is quite certain on the other that tangential pressure oscillations of these magnitudes would have produced easily detectable changes in the average burning rate of the propellant.

It is of interest to note that, in a resonating cavity, a solid boundary is subjected to pressure oscillation whether the gas motion be normal or tangential to the surface. In a local region of grain surface the two modes of oscillation should be indistinguishable insofar as pressure effects are concerned. On the other hand, at the solid surface the gas velocity is zero for the normal oscillations but definitely non-zero for the tangential mode. These tangential velocity components may

become of considerable magnitude and it appears that they may be a significant influence in affecting the propellant burning rate. The conclusion may possibly be made that while the pressure fluctuations themselves are responsible for their own excitation, it is the corresponding tangential velocities induced by them that augment the propellant burning rate. The contrast between results obtained in cylindrical motors and slab motors certainly supports such a conjecture.

XI. INTERRUPTED FIRINGS

One factor of particular importance in correlating the occurrence of instability with our meagre knowledge of the steady burning mechanism is the nature of the propellant surface during instability. No attempt was made to examine the surface while combustion was in progress, but a number of firings were interrupted during conditions of unstable burning and the grains were examined. It also appears possible that the propellant surface could become locally distorted during unstable combustion because of increases in the local burning rate associated with particular modes of gaseous oscillation. The interrupted firings to be described were carried out to permit examination of the propellant surface to determine the extent of asymmetric burning in the cylindrically perforated motors.

Description of the Experiments. - The motors fired and interrupted were case-bonded, cylindrically perforated, five-inch motors of the type discussed throughout this report. In order to interrupt the firings use was made of techniques that had been developed previously at J.P.L. A new headplate for interrupted firings, compatible with the five-inch motors and internally similar to the type 3 headplate, was fabricated. The design is shown in figure 55.

The details of the interrupt system are shown in figure 56. On an electrical command, squibs were fired in both the nozzle and head end assemblies. Gas pressure generated by the nozzle end charge sheared the two main diaphragms, and hence provided an additional nozzle exit of diameter 1.5 in. The head end charge sheared one main diaphragm. This action allowed water to be injected obliquely into the grain perforation. The water was driven by a 2000 psi dry Nitrogen gas source.

The system operated very rapidly. The time delay from the interrupt command to the cessation of combustion was on the order of a few milliseconds. The command either could be given manually or could be generated by an electronic instability shut-off circuit. This unit, shown in figure 61, was developed by the Instrument Services Section at The Jet Propulsion Laboratory. The latter method involved the use of a Photocon gauge and its associated electronic equipment. This gauge sensed the gaseous pressure oscillations at the head end of the motor. When these reached a preset level the instability shut-off circuit triggered. After a further preset time delay, the circuit generated an electric interrupt command which activated the squibs.

The automatic interrupt system was necessary because of the short times involved in the instability process. For the most part, the motors became severely unstable and returned to

weakly unstable operation within one second after ignition. Attempts by the operator to observe the progress of the firing and issue a manual command during severe instability were singularly unsuccessful. On the other hand, the automatic system, while functioning perfectly, failed to give the desired results for another reason. At the time these firings were made, the proper propellant processing techniques required to give reproducible firings had not been determined. As a consequence, the trigger levels chosen on the basis of previous firings were for the most part unsatisfactory. Nevertheless, useful information was obtained from a few successful interrupted firings and from one motor which interrupted itself by blowing off the nozzle plate during severe instability.

Experimental Results. - The pressure time traces for a 3 x 5 x 31/31.4 cylindrical motor fired at 160°F are shown in figures 57 and 58. This motor was interrupted and examined. It was then allowed to dry out, temperature conditioned once again to 160°F, refired, and interrupted again.

Before and after the first firing, measurements of the diameter were made at 0°, 120°, and 240° around the circumference and at one-inch intervals along the grain length. The change in diameter due to the first firing is plotted versus axial position in figure 57. It is essentially constant throughout the length of the motor and independent of angular location. A visual inspection of

the grain's surface revealed no abnormalities. The surface texture showed the same fine grain roughness characteristic of propellant which has burned stably. No grooves or ridges could be seen.

The $\bar{P}c$ vs t trace for the second firing is shown in figure 58. It will be seen that in this case also, a delay occurs after ignition before the instability becomes pronounced. The ΔDp vs L plot for this firing is also shown in figure 58. The average burning rate was approximately four per cent higher at the center than at the two ends of the charge. It is possible that this small differential is due to the combined effect of chamber pressure and erosive burning on the local burning rate. Both parameters are functions of length. The chamber pressure decreases from head end to nozzle end due to momentum pressure losses while the erosive factor increases due to increasing axial velocity. With respect to the grain surface condition, the same remarks apply to the second firing as to the first, even though the duration of the instability is much greater.

A third interrupted firing is shown in figure 59. In this case severe instability persisted for approximately 0.70 sec. in a total run time of 1.2 sec. The corresponding ΔDp vs L plot is given in figure 59. The surface of the grain was broken in several places by holes which were attributed to voids not removed during

processing.* No evidence was found in the firing pit to indicate that propellant had been ejected through the nozzle. Otherwise, the preceding remarks regarding grain condition apply.

Up to this point it had been uncertain whether or not the water injected to quench combustion was seriously changing the gross character of the grains' surface. This doubt was removed by chance in the firing shown in figure 60. In this case, severe instability was entered approximately one-half second after ignition and endured for approximately one second. Combustion was quenched, presumably by a gaseous expansion wave, when the nozzle assembly blew off the motor during the period of instability. The foregoing remarks regarding the surface of the grain are applicable except that more detail was evident and the surface was somewhat rougher. No organized system of grooves and ridges was seen. The ΔDp vs L plot is given in figure 60. The same tendency for the average burning rate to be higher in the center of the charge is evident. It was, of course, not possible to compare this result with a stable firing under the same conditions, since all such firings have been unstable.

---

* This condition was corrected in later motors by a more prolonged period of casting under vacuum and vibration.

Some Speculations Arising From The Results. - The primary gaseous oscillation present has been identified as the fundamental tangential mode as is discussed in chapter IX. The interaction mechanism between the main gas phase oscillation and the region of combustion must be dependent on either the local unsteady pressure or the local unsteady particle velocities, or both, either directly or indirectly. The interrupted firings indicate that there are no preferred regions of the circumference of the grain perforation insofar as increases in the burning rate are concerned. On the basis of this fact alone it might be inferred that the fundamental tangential travelling (so-called spinning) mode is the active one. For this mode the maximum amplitudes of both the pressure and velocity fluctuation are constant around the circumference of the perforation, and the waves vary only in phase angle. The high frequency instrumentation suggests, however, that the active mode is of pseudo-standing wave form wherein the orientation of the pressure nodal line fluctuates rapidly and somewhat randomly with time. It is clear that this latter mode form can produce uniform changes in mean burning rate. The tests conducted so far do not differentiate conclusively between the spinning mode and the statistically fluctuating standing mode, but favor the latter.

It would be expected that if serious changes in grain structure occurred during severe instability, some evidence of

this should remain after the motor ceases firing. This should be so, since the motor cannot operate below a certain low value of pressure. Hence, if asymmetry exists, the motor will stop operating when most but not all of the propellant is consumed. A continuing visual inspection was made of all motor casings immediately after firing. No evidence of circumferential asymmetry was found. Occasionally, it could be seen that a few voids had been present in the grain, since at these locations the case wall had been exposed to the hot combustion products for a large fraction of the run time. Also, whenever severe instability caused the ejection of pieces of propellant through the nozzle, the net effect was the same as for production voids. The locations of the damaged areas were randomly located in the circumferential direction and somewhat centrally located in the axial direction. No well-defined damage pattern was evident.

The interrupt tests were useful from another point of view. The normal data reduction methods predict a mean diameter as a function of time based on

$$w\{t\} = \frac{\int_0^t \bar{P}c\ dt}{\int_0^\infty \bar{P}c\ dt}\ (Wp) \qquad (30)$$

where

$w\{t\}$ = weight of propellant consumed at time t

Wp = total weight of propellant burned

Pc = mean total chamber pressure

and isentropic flow conditions are assumed to exist. A comparison of the predicted and measured changes in mean diameter during five firings, gave agreement within two per cent in all cases. Hence it is likely that predicted diameters used elsewhere are reliable to this extent. Furthermore, since the firings varied in degree of instability, as has been seen, with uniformly good prediction, it is likely that the low frequency pressure sensing and recording system was producing reasonable mean pressure data.

XII. CONCLUSIONS AND CONCLUDING REMARKS

By extremely careful control of the propellant manufacturing procedure and by extending the cure time to nearly twice its normal length, it has been possible to secure results of rocket firings that are almost completely reproducible with regard to the occurrence of unstable burning and early phases of variation of mean chamber pressure with oscillation amplitude. A total of over 250 research firings using case-bonded, cylindrically perforated motors were made under these conditions along with about 150 additional check firings. The following results are based upon these firings. All firings were made with a given ammonium perchlorate polysulfide propellant the composition of which was carefully controlled during the research period.

Detailed measurement of oscillatory frequencies confirmed the fact that the first tangential mode was providing the excitation and was associated with the instability. The variation of frequency with grain perforation diameter was within 4% of that to be expected from acoustic theory in spite of the fact that at times the peak oscillating pressure reached half of the mean chamber pressure. Axial oscillations were present but were weak and obviously not contributing to the excitation even though the length was varied by a factor of more than two and one-half.

At given grain temperature, stable firings with the cylindrical motors exhibit a progressive pressure-time curve. The chamber pressure increases with Kn, the ratio of burning

surface area to nozzle throat area, as the perforation diameter Dp becomes greater due to burning. In the Kn - Dp plane there existed regions of stable, mildly unstable and severely unstable combustion as defined by firings of motors with 31 in. grain length. For sufficiently high values of Kn, the combustion was stable regardless of Dp. At lower values of Kn the motors were weakly unstable. The dividing line between these regions in the Kn-Dp plane increased essentially linearly with Dp and was very nearly a line of constant nozzle size. As Kn was reduced further the instability became very gradually stronger until at a critical value of Kn the motors suddenly became severely unstable. The line of maximum instability intersected the upper stability line at a low value of Dp and gradually increased in Kn level as Dp was increased from this point. The region below the line of maximum instability was characterized by a gradual decrease in the severity of the instability as Kn was reduced from the critical value.

A reduction of grain length below 31 in. to 17 in. successively reduced the severity of the instability at given operating pressure level. An increase of grain length from 31 in. to 44.5 in. did not affect the degree of instability at given operating level; nor did the upper stability line change. However, the line of maximum instability moved to somewhat higher Kn with increasing grain length.

The effect on the upper stability line and the line of maximum instability of changing the initial grain temperature was determined for motors of 3 in. initial perforation diameter and 31 in. grain length, fired over the temperature range -80°F to 180°F. Both lines moved to lower pressure levels as the grain temperature was decreased but the reduction was not the same as that due to grain temperature effects on the burning rate. The results are in agreement with the observation that motors with fixed geometry fired over a range of grain temperatures can exhibit instability at the temperature extremes and yet operate stably at medium temperatures. Furthermore, the three instability regions described earlier existed at all grain temperatures.

Slab motors with opposed-plane grain surfaces exhibited oscillations in the fundamental and higher transverse sloshing modes. The peak magnitude of these oscillations were as large as 10% of the chamber pressure, yet no effect on the mean burning rate was observed. In the cylindric motor, pressure oscillations of this magnitude showed a strong effect on the burning rate. Hence it is concluded that the tangential velocities associated with the tangential mode were largely responsible for modification of the burning rate.

Measurement of the fluctuating pressures in the cylindric motors and grain inspection after interrupted firings suggested that the mode of oscillation was the fundamental

tangential mode. The orientation of the pressure mode line appeared to change in a random manner and did not spin at the frequency of oscillation as in the travelling tangential mode.

While these results were obtained through the use of a particular propellant and grain design it seems reasonable to suppose that the trends noted are qualitatively applicable to other motors with similar acoustic properties, provided such motors operate in an unstable manner. The latter qualification is made since the propellant composition may be such as to produce complete stability in a particular design.

REFERENCES

1. Boys, S. F., and Schofield, A., Studies Accessory to the Development of Classified Rockets, Woolwich Arsenal, England, (1942)

2. Wimpress, R. N., "Internal Ballistics of Solid-Fuel Rockets", McGraw-Hill, N. Y., (1950)

3. Smith, R. P., and Sprenger, D. F., "Combustion Instability in Solid Propellant Rockets", Proceedings of the Fourth Symposium (International) in Combustion, Williams and Wilkins, Baltimore, (1953) pp. 893-906

4. Grad, H., "Resonance Burning in Rocket Motors", Communications on Pure and Applied Mathematics, (1949), Vol. 2, No. 1

5. Cheng, S. I., "High Frequency Combustion Instability in Solid Propellant Rockets", Parts I and II, Jet Propulsion (1954), Vol. 24, pp. 27-32, pp. 102-109

6. Green, Leon Jr., "Some Properties of a Simplified Model of Solid-Propellant Burning", Jet Propulsion, (1958) Vol. 28, pp. 386-392

7. Hart, R. W., and McClure, F. T., "Combustion Instability: Acoustic Interaction with a Burning Propellant Surface", The Johns Hopkins University Applied Physics Laboratory Report TG-309, (October 1958)

8. Schultz, R., Green, L. Jr., and Penner, S. S., "Studies of the Decomposition Mechanism, Erosive Burning, Sonance and Resonance for Solid Composite Propellants", Proceedings of the Third AGARD Combustion and Propulsion Colloquium, Pergamon Press, N. Y., (1958) pp. 367-420

9. Green, Leon Jr., "Observations on the Irregular Reaction of Solid Propellant Charges", Jet Propulsion, (1956) Vol. 26, pp. 655-659

10. Price, E. W., and Sofferis, J. W., "Combustion Instability in Solid Propellant Rocket Motors", Jet Propulsion, (1958) Vol. 28, pp. 190-192

11. Green, Leon Jr., "Some Effects of Oxidizer Concentration and Particle Size on Resonance Burning of Composite Solid Propellants", Jet Propulsion, (1958), Vol. 28, pp. 159-164

12. Green, Leon Jr., "Some Effects of Charge Configuration in Solid Propellant Combustion", Jet Propulsion, (1958), Vol. 28, pp. 482-485

13. Rogers, D. E., and Marble, F. E., "A Mechanism for High-Frequency Oscillation in Ramjet Combustors and Afterburners", Jet Propulsion, (1956) Vol. 26, pp. 456-462

14. Crocco, L., "Aspects of Combustion Stability in Liquid Propellant Rocket Motors, Part I", Journal of the American Rocket Society, (1951) Vol. 21, pp. 163-178

15. Nachbar, W., and Green, L. Jr., "Analysis of a Simplified Model of Solid Propellant Resonant Burning", to be submitted for publication.

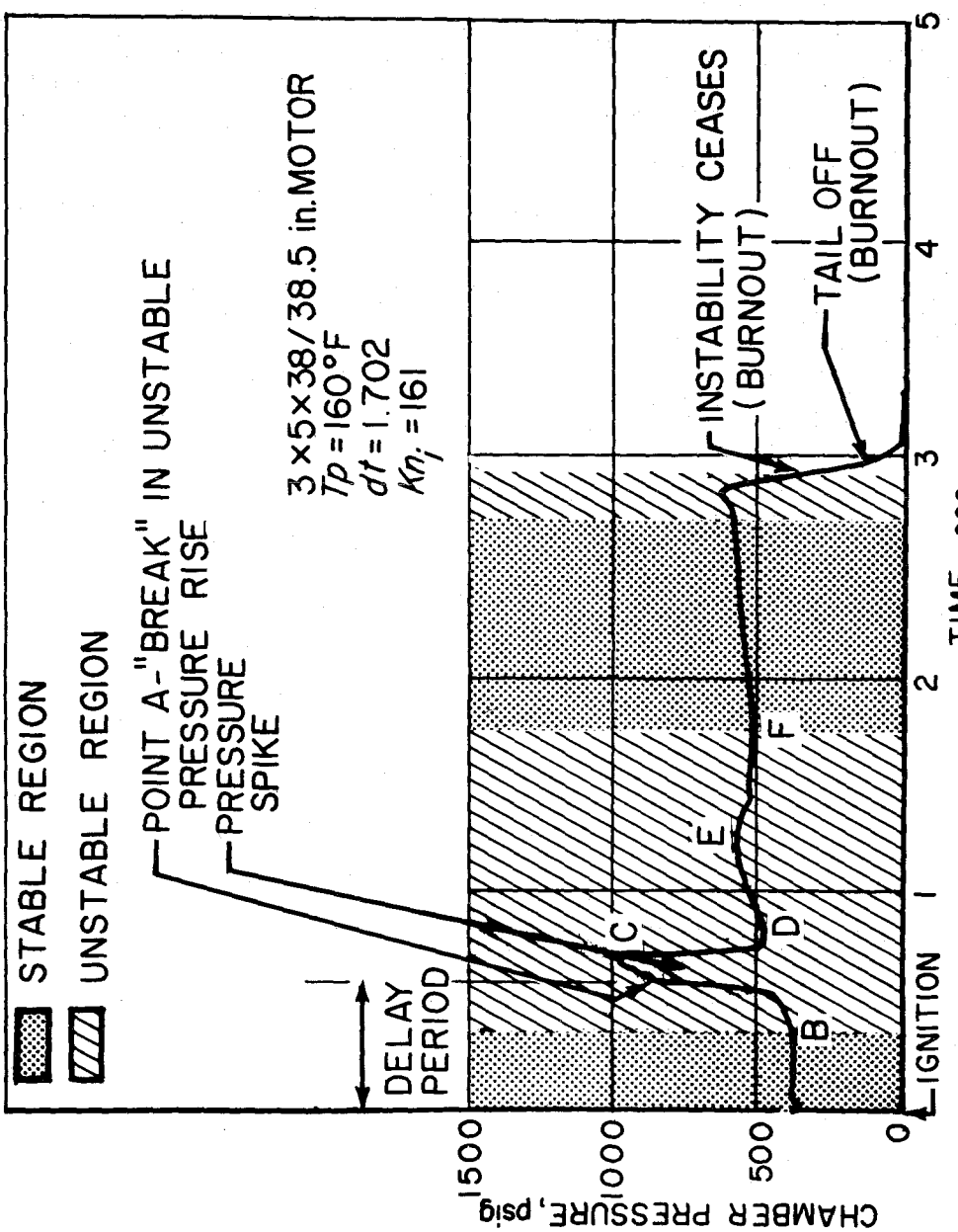

Figure 1. Mean Chamber Pressure, Time History of Typical Unstable Firing.

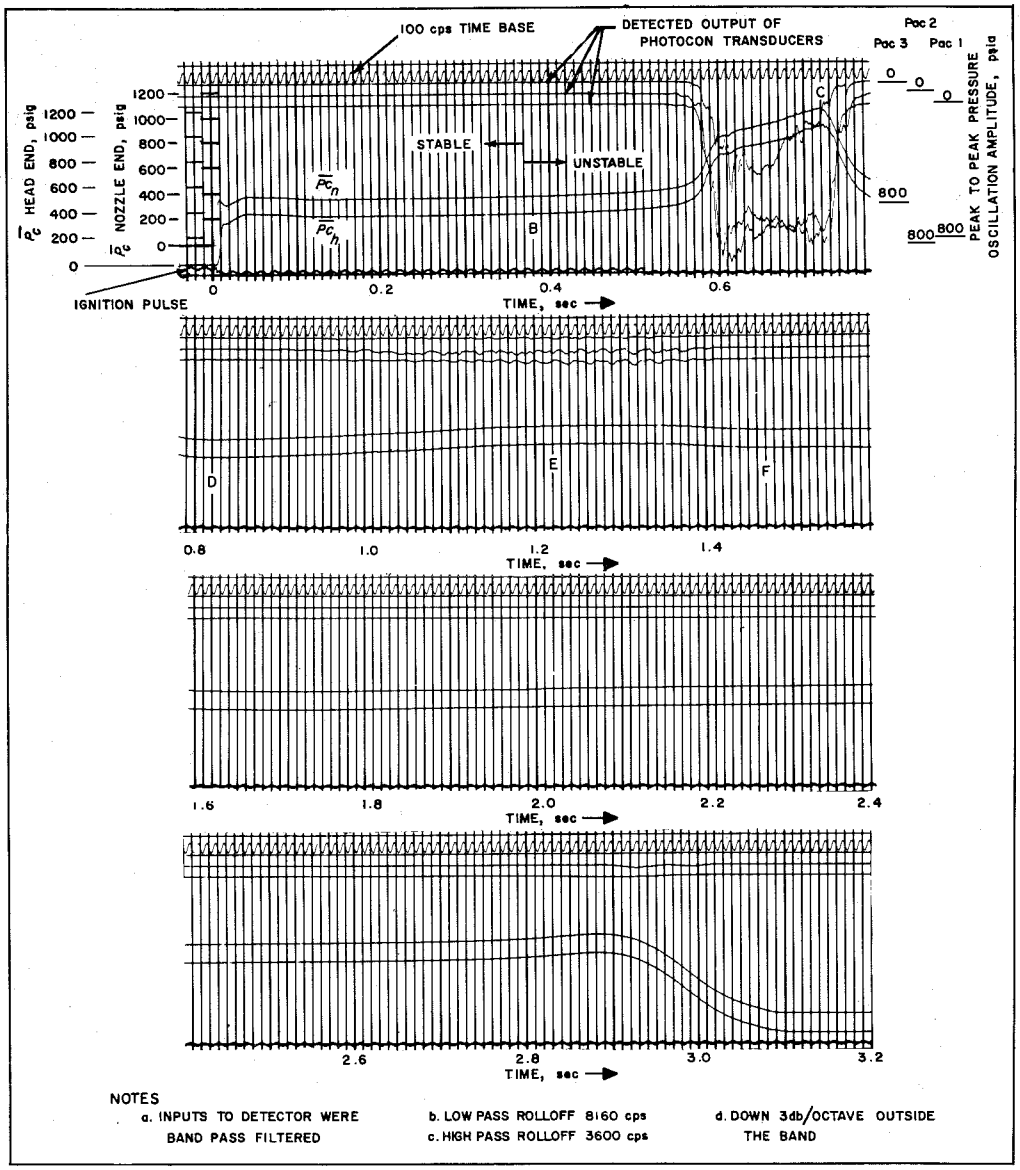

Figure 2. Miller Record, Typical Unstable Firing.

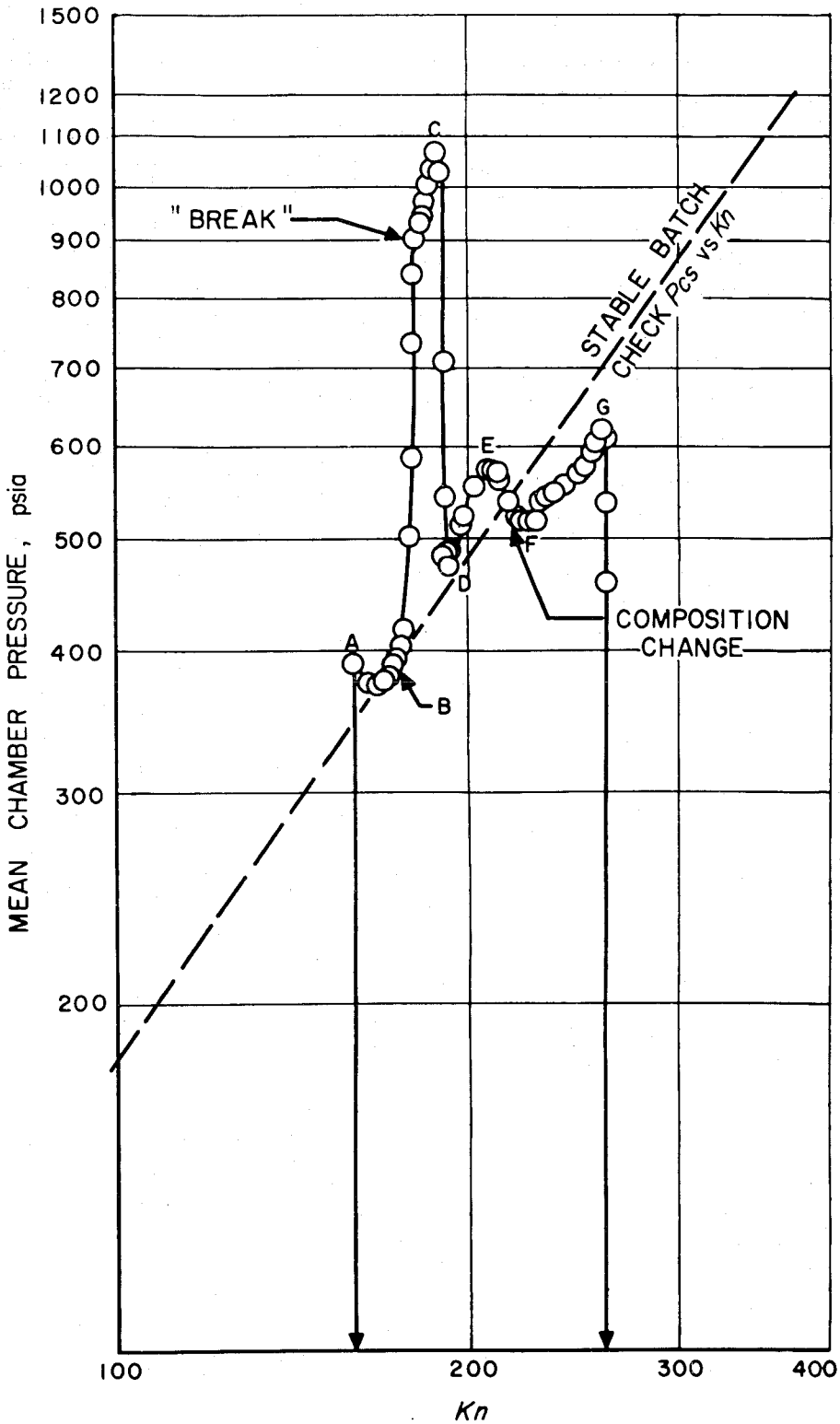

Figure 3. Mean Chamber Pressure Versus Area Ratio Kn, Typical Unstable Firing.

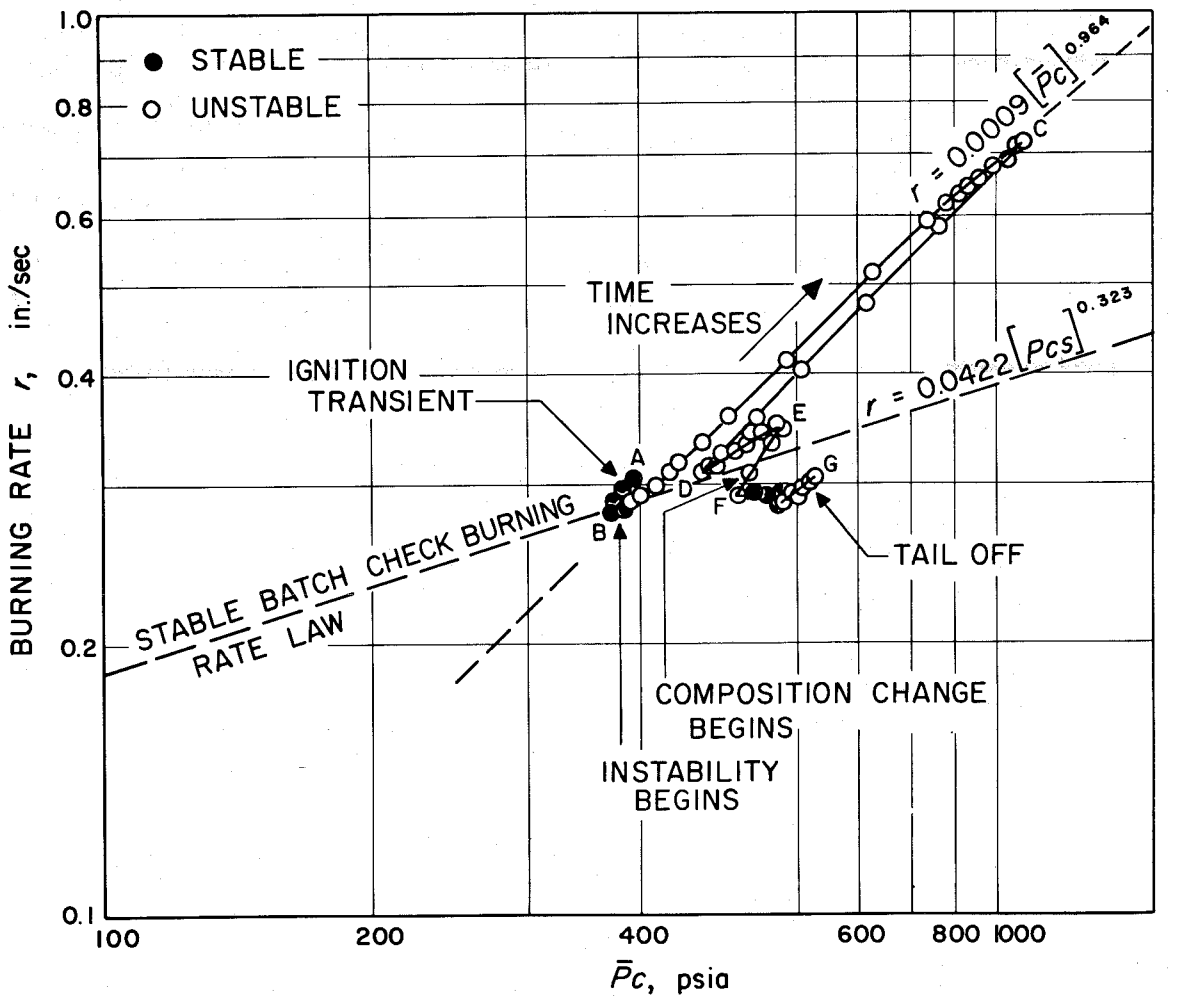

Figure 4. Mean Burning Rate Versus Mean Chamber Pressure, Typical Unstable Firing.

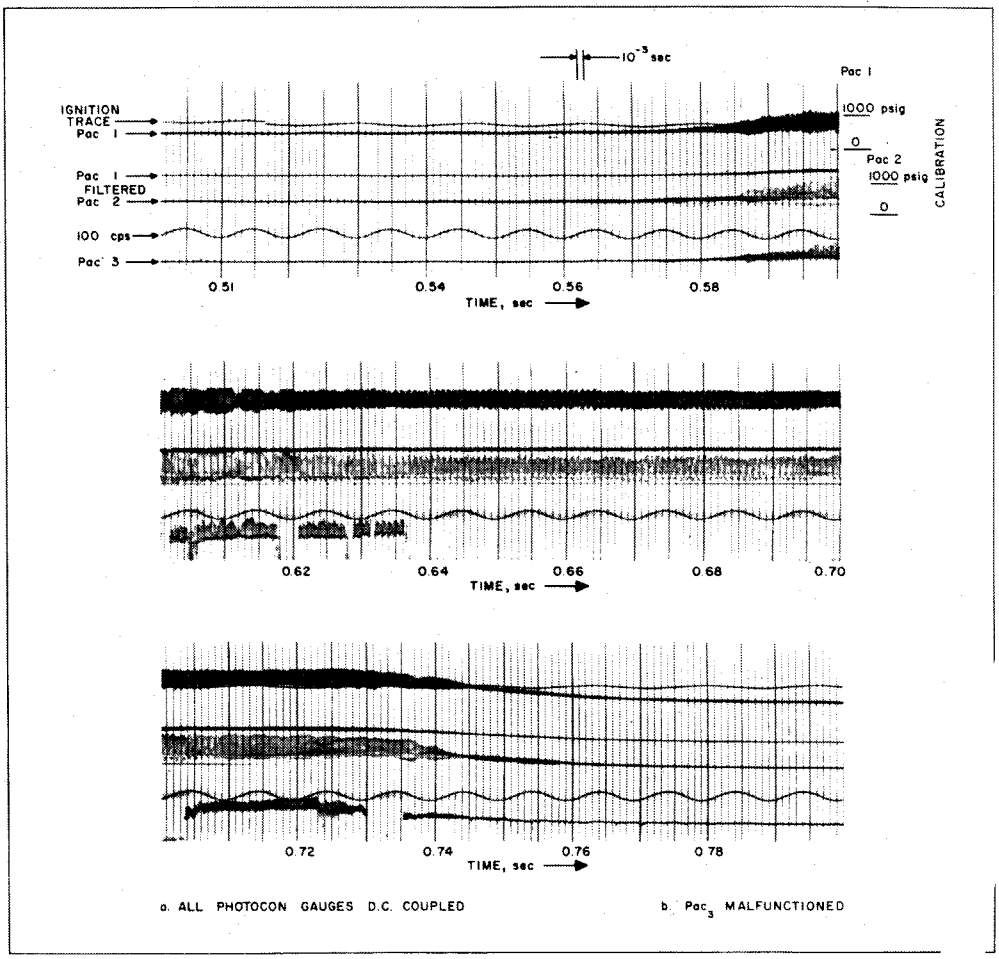

Figure 5. Hathaway Record, Typical Unstable Firing.

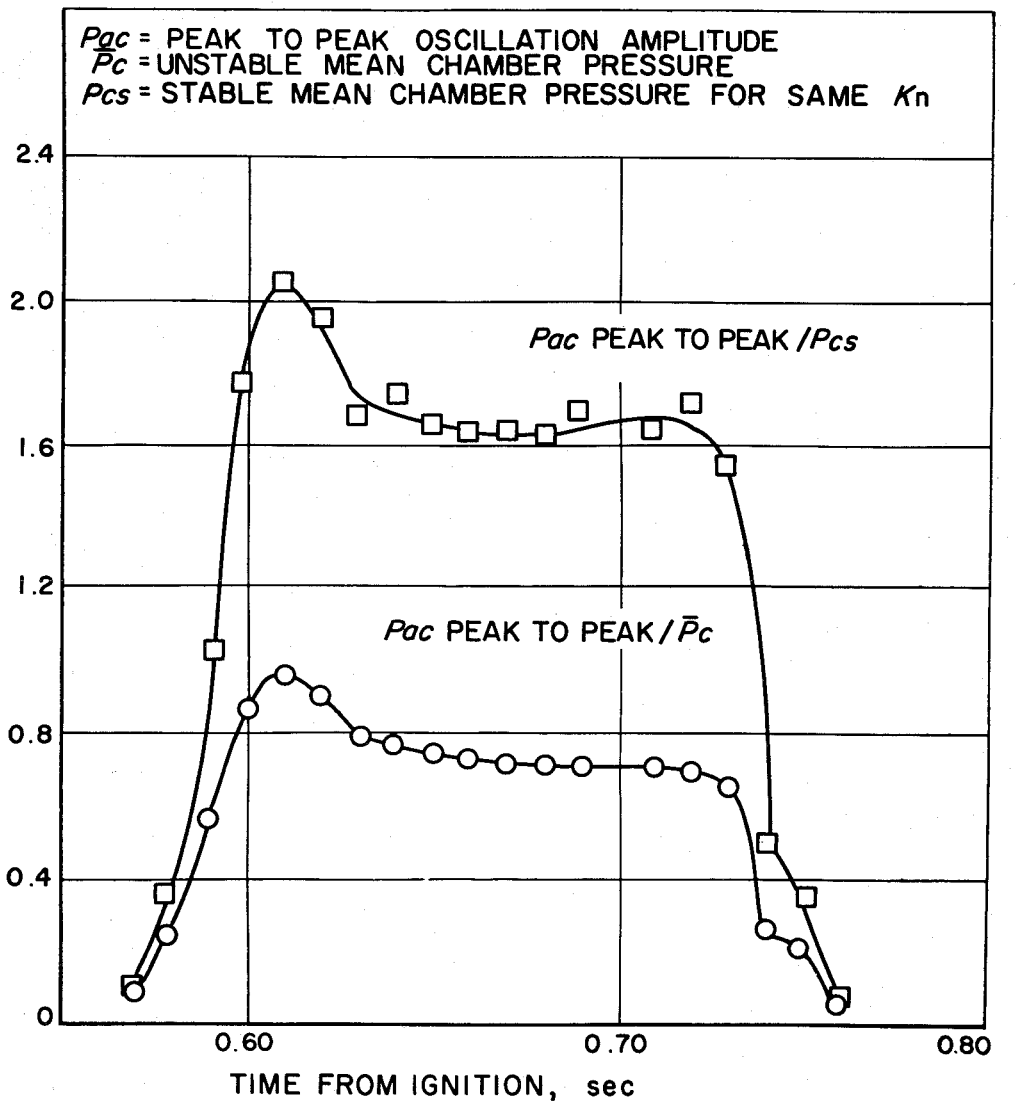

Figure 6. Gaseous Oscillation Amplitude Versus Time, Typical Unstable Firing.

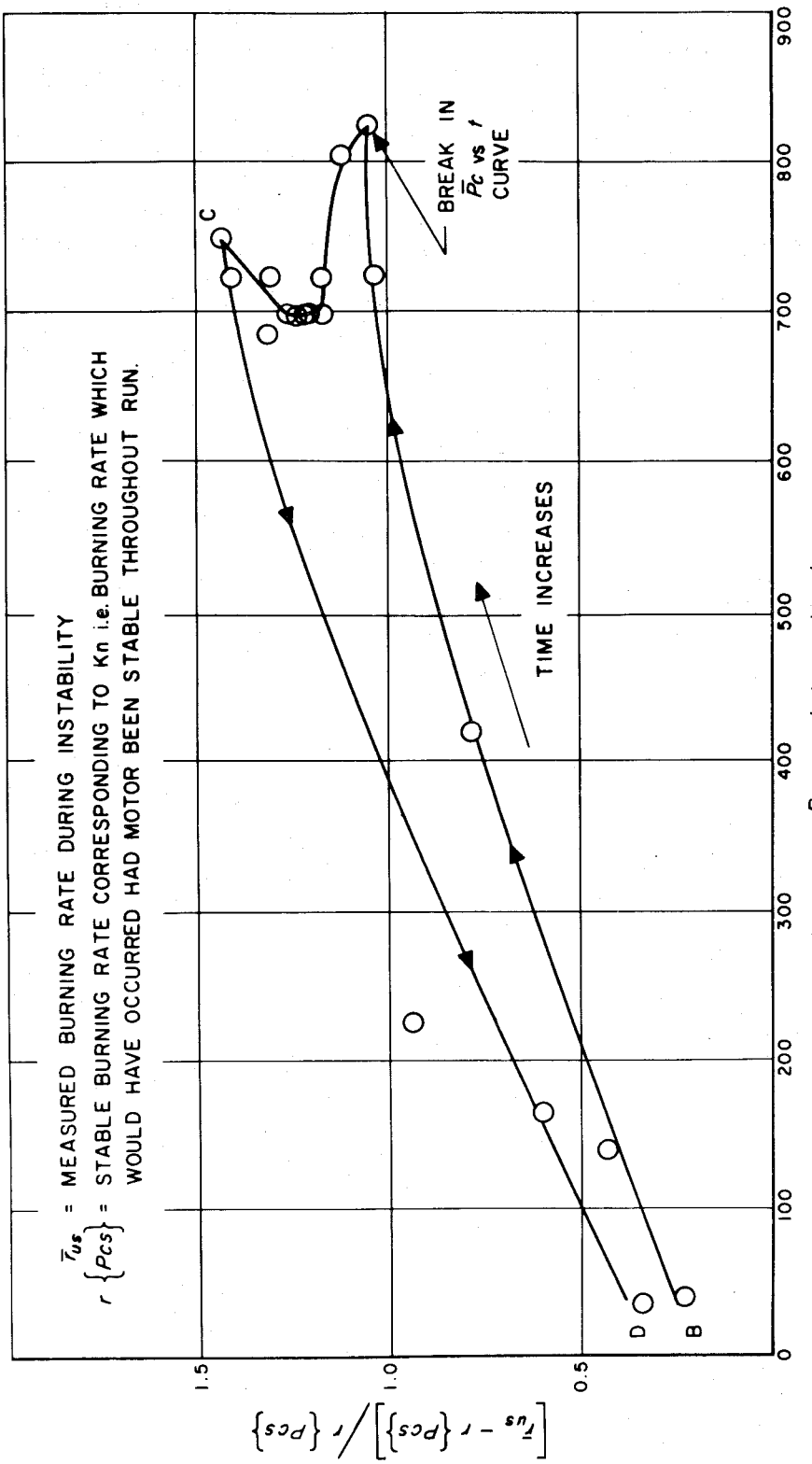

Figure 7. Increment in Burning Rate From Stable Condition Versus Oscillation Amplitude, Typical Unstable Firing.

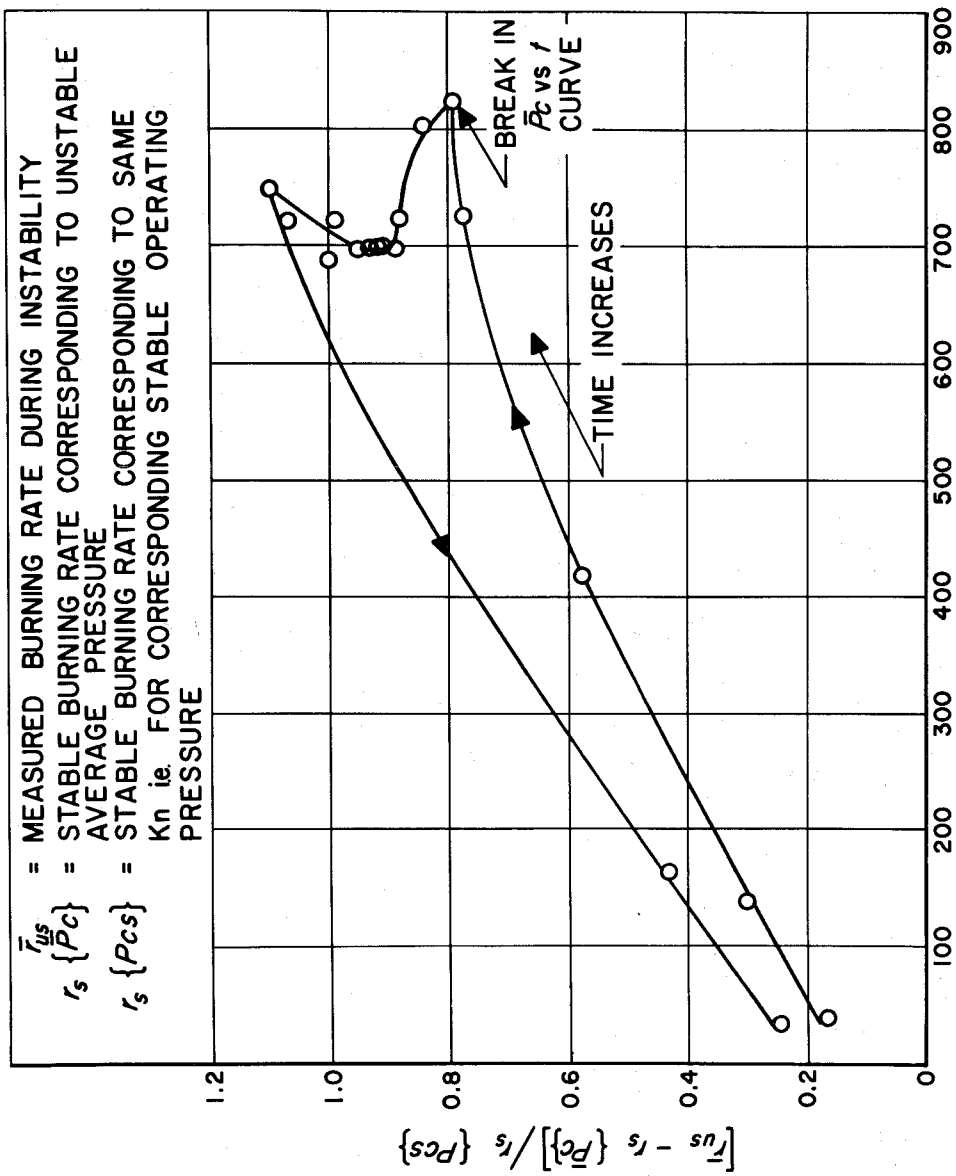

Figure 8. Increment in Burning Rate From Pseudo-Stable Condition Corresponding to Mean Chamber Pressure, Versus Oscillation Amplitude, Typical Unstable Firing.

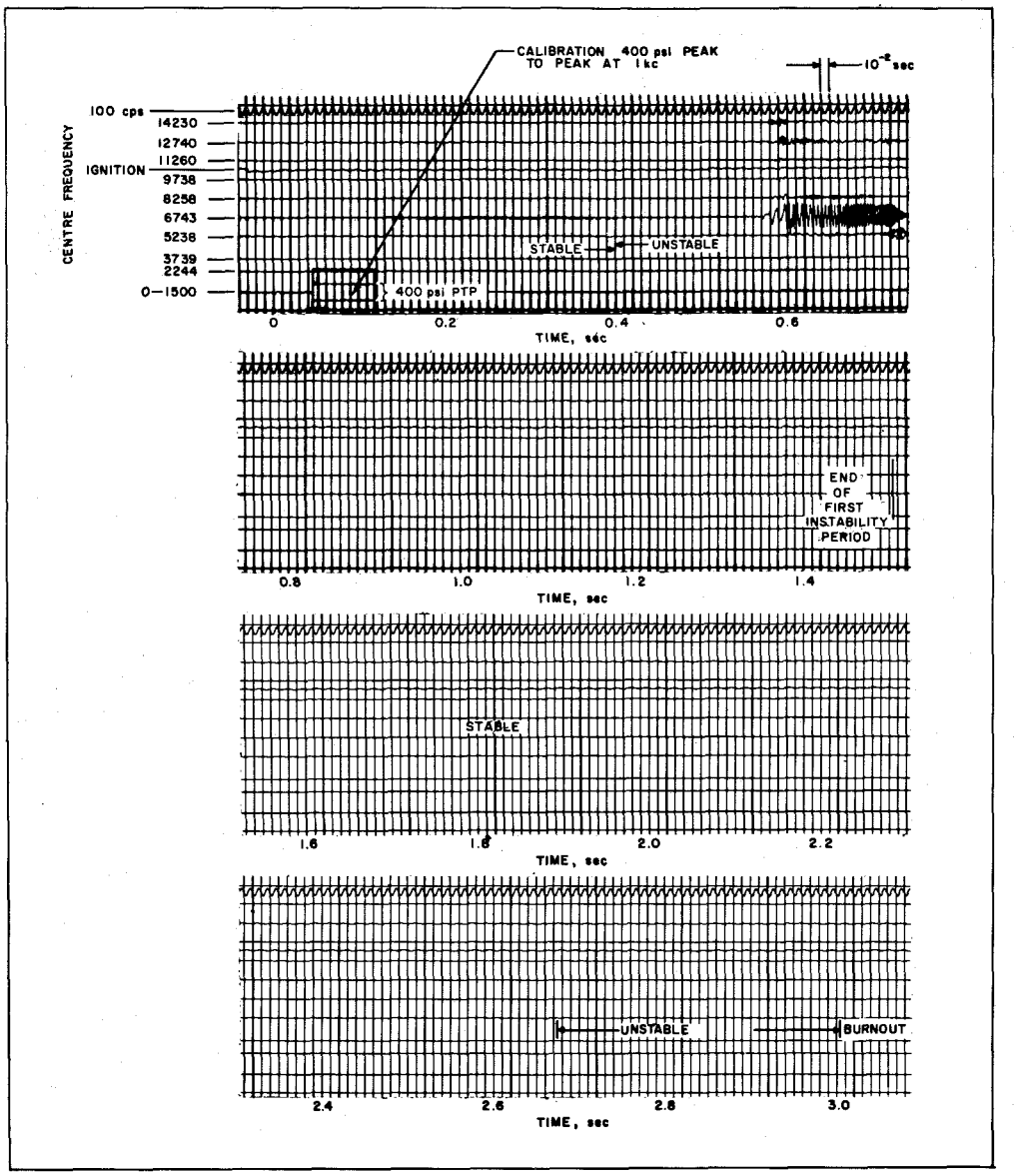

Figure 9. High Frequency Analyzer Record, Typical Unstable Firing.

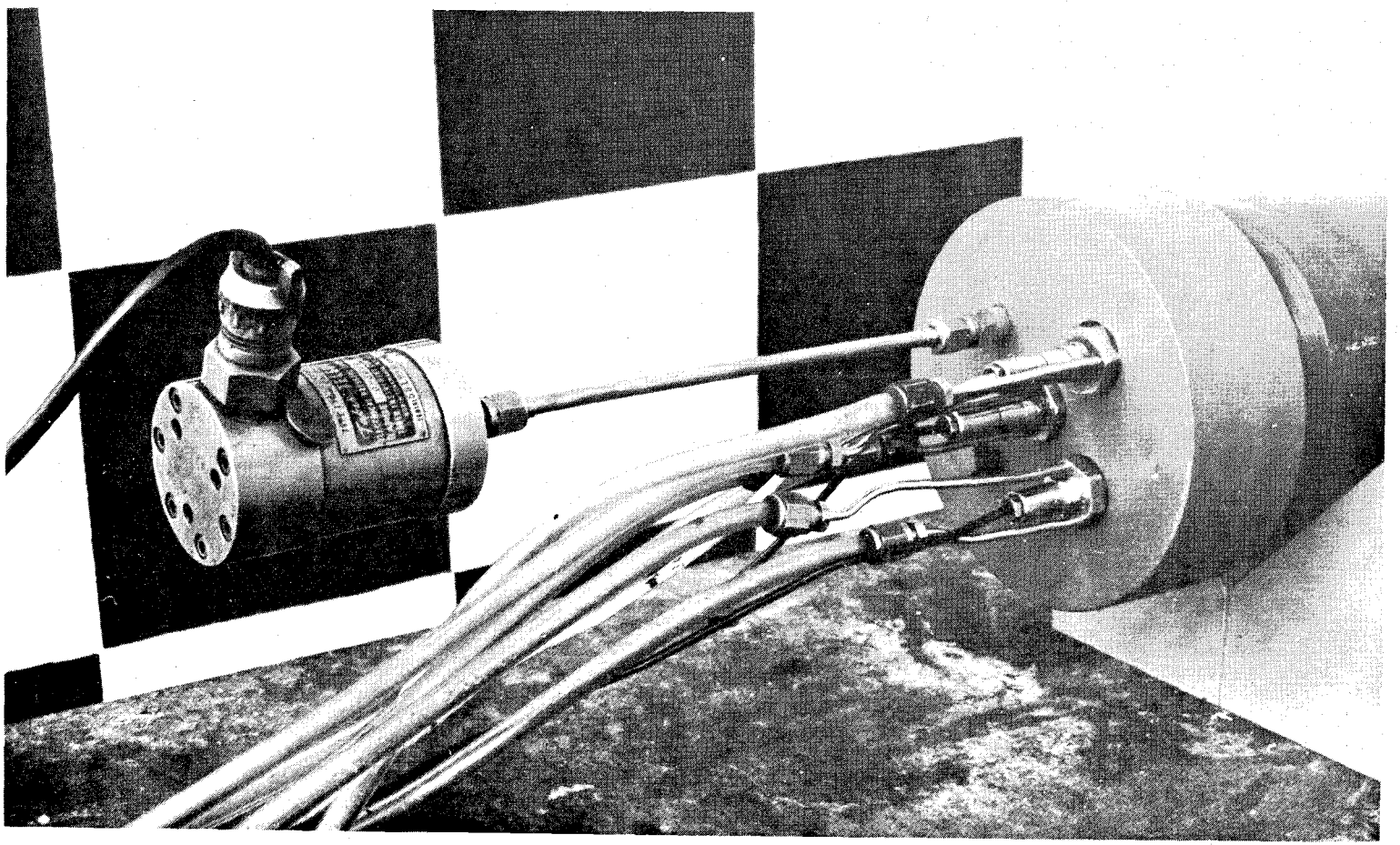

Figure 10. Instrumented Type 3 Headplate.

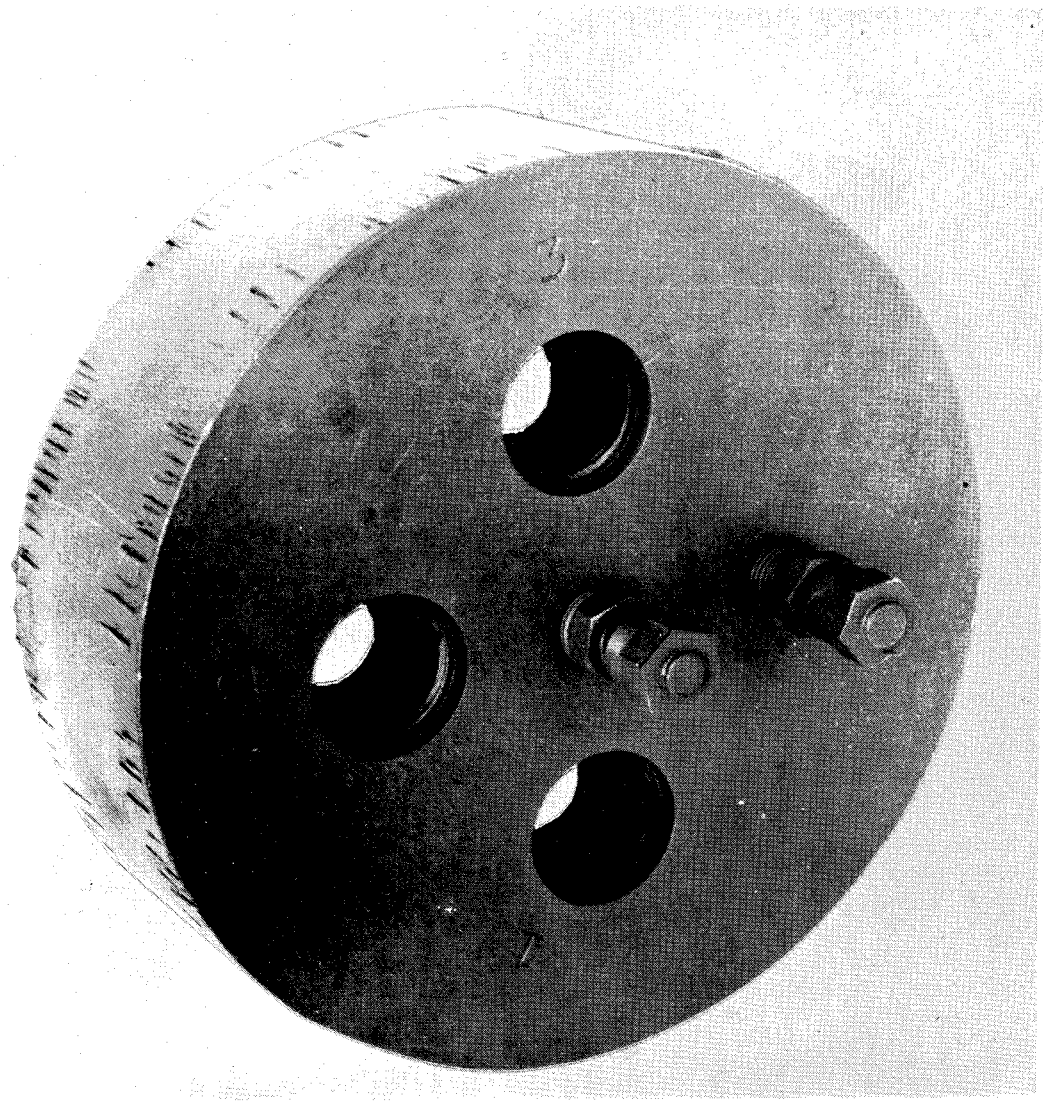

Figure 11. External View, Type 3 Headplate.

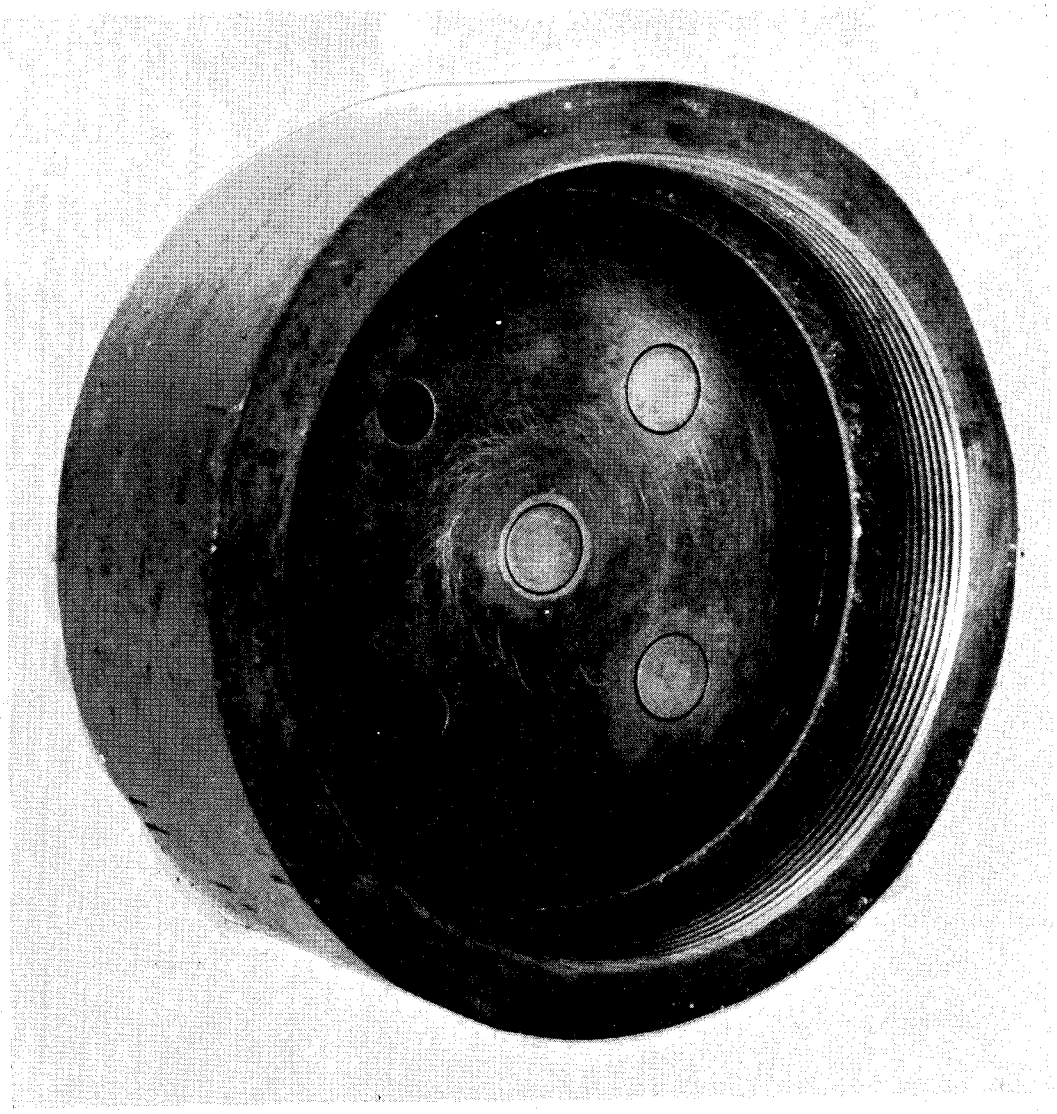

Figure 12. Internal View, Type 3 Headplate.

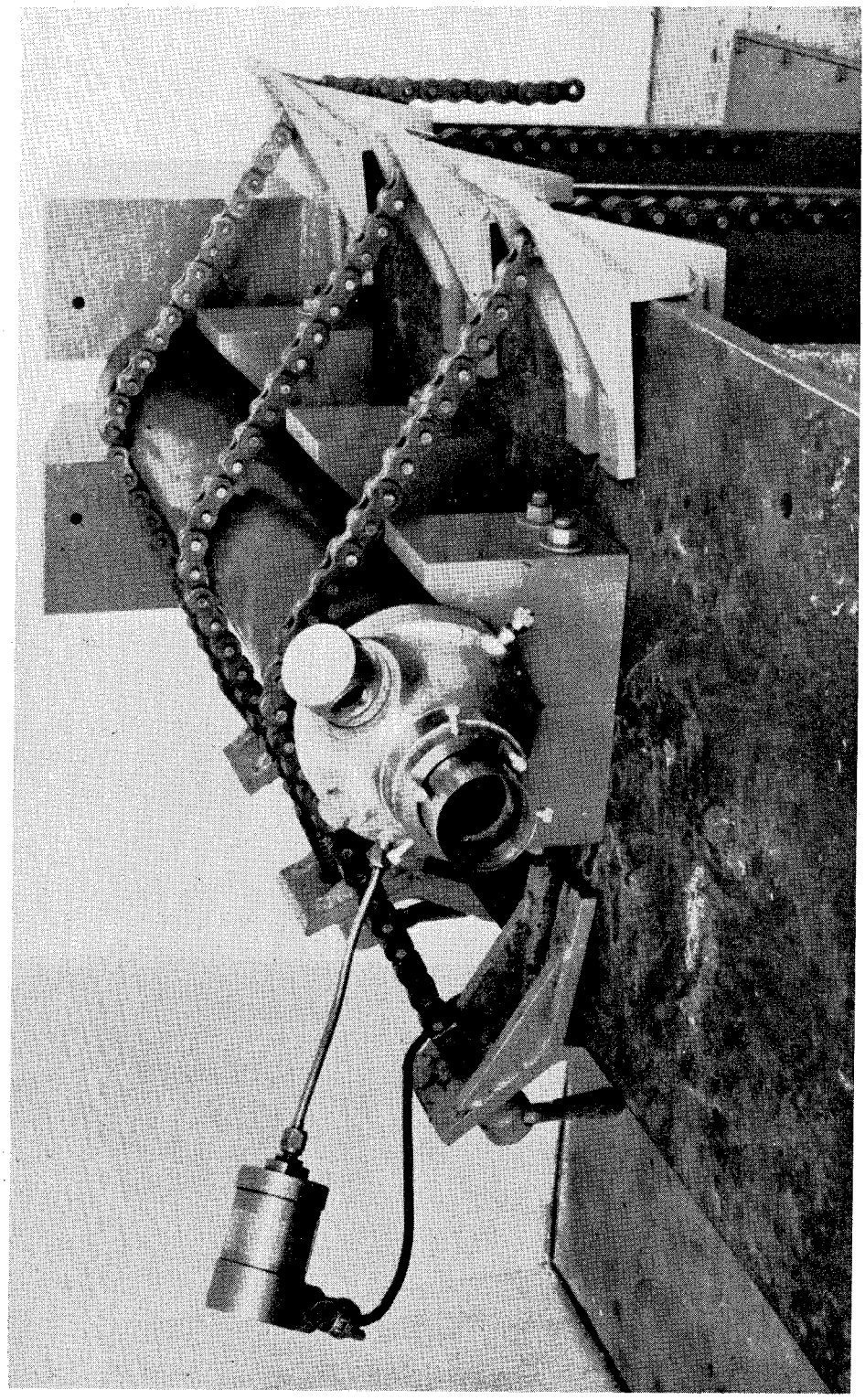

Figure 13. Instrumented Motor on Test Stand.

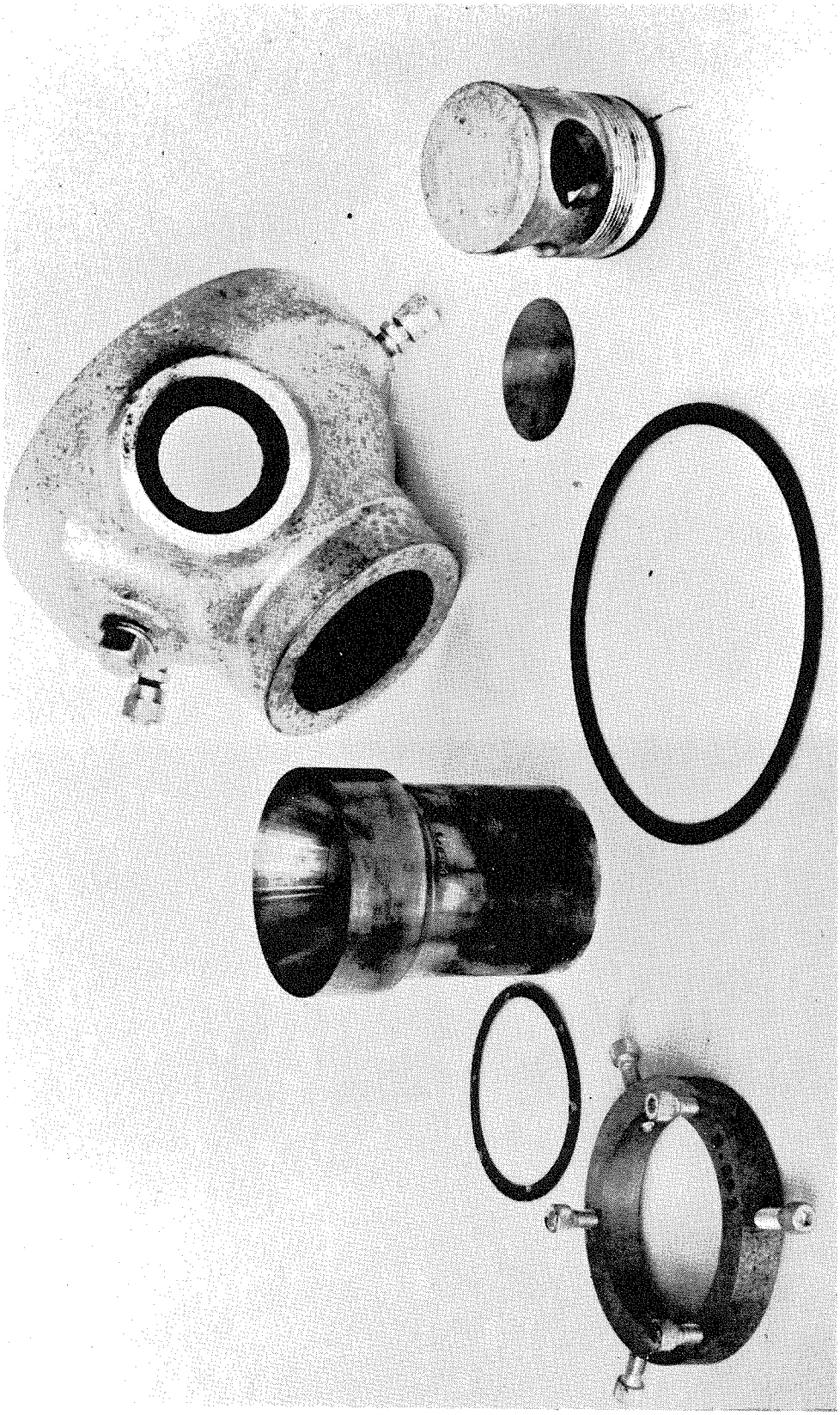

Figure 14. Exploded View of Nozzle Assembly.

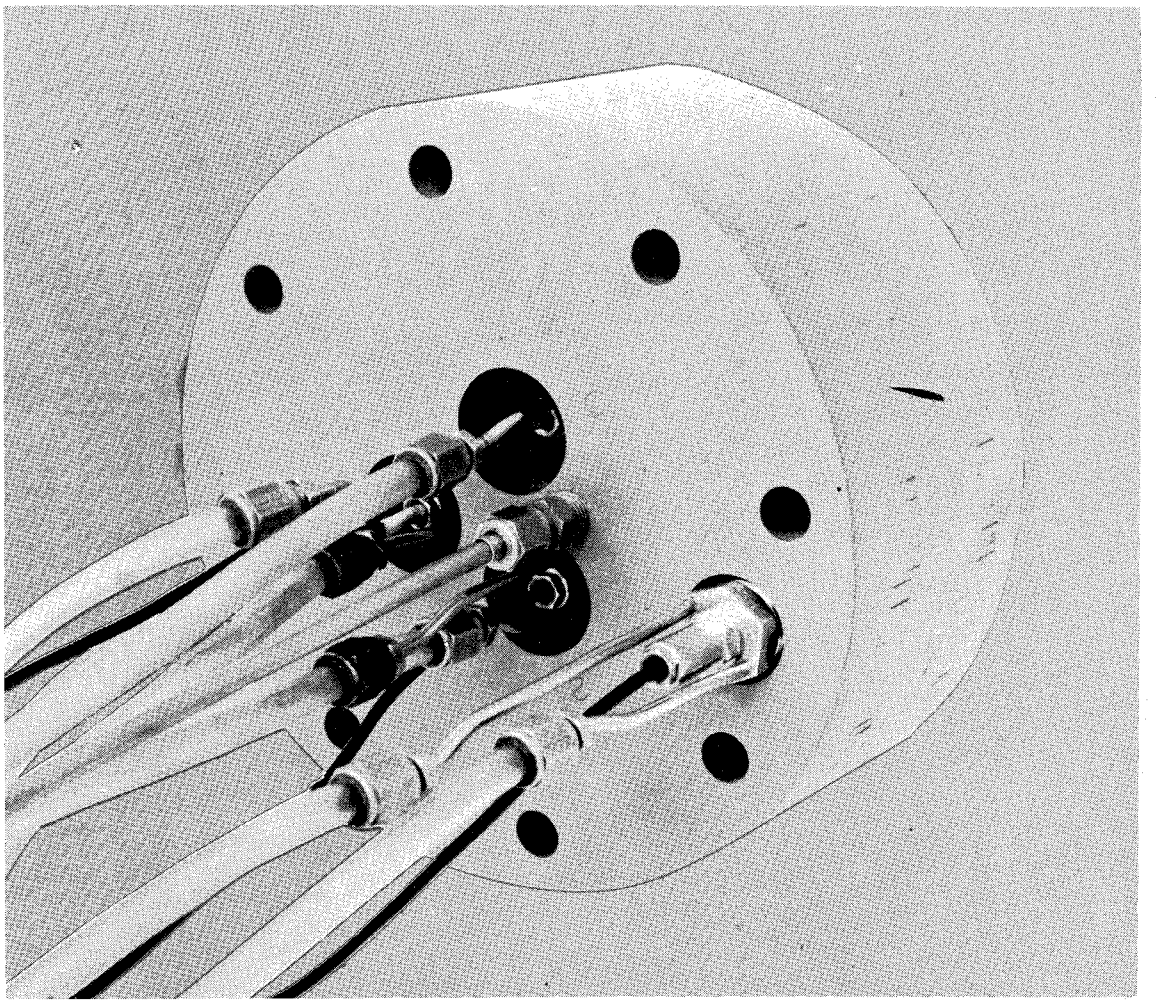

Figure 15. Instrumented Type 4 Headplate.

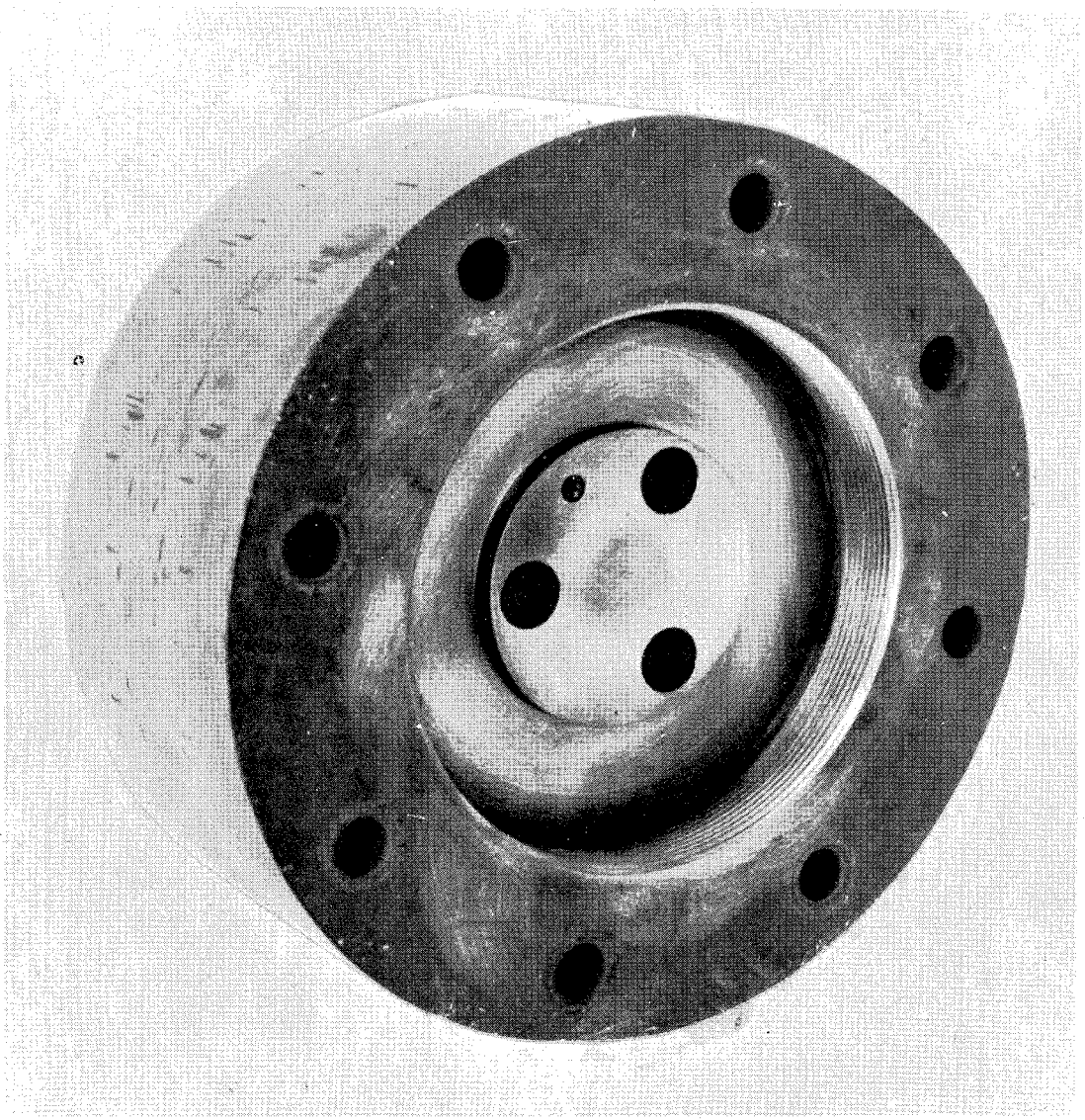

Figure 16. Internal View of Type 4 Headplate.

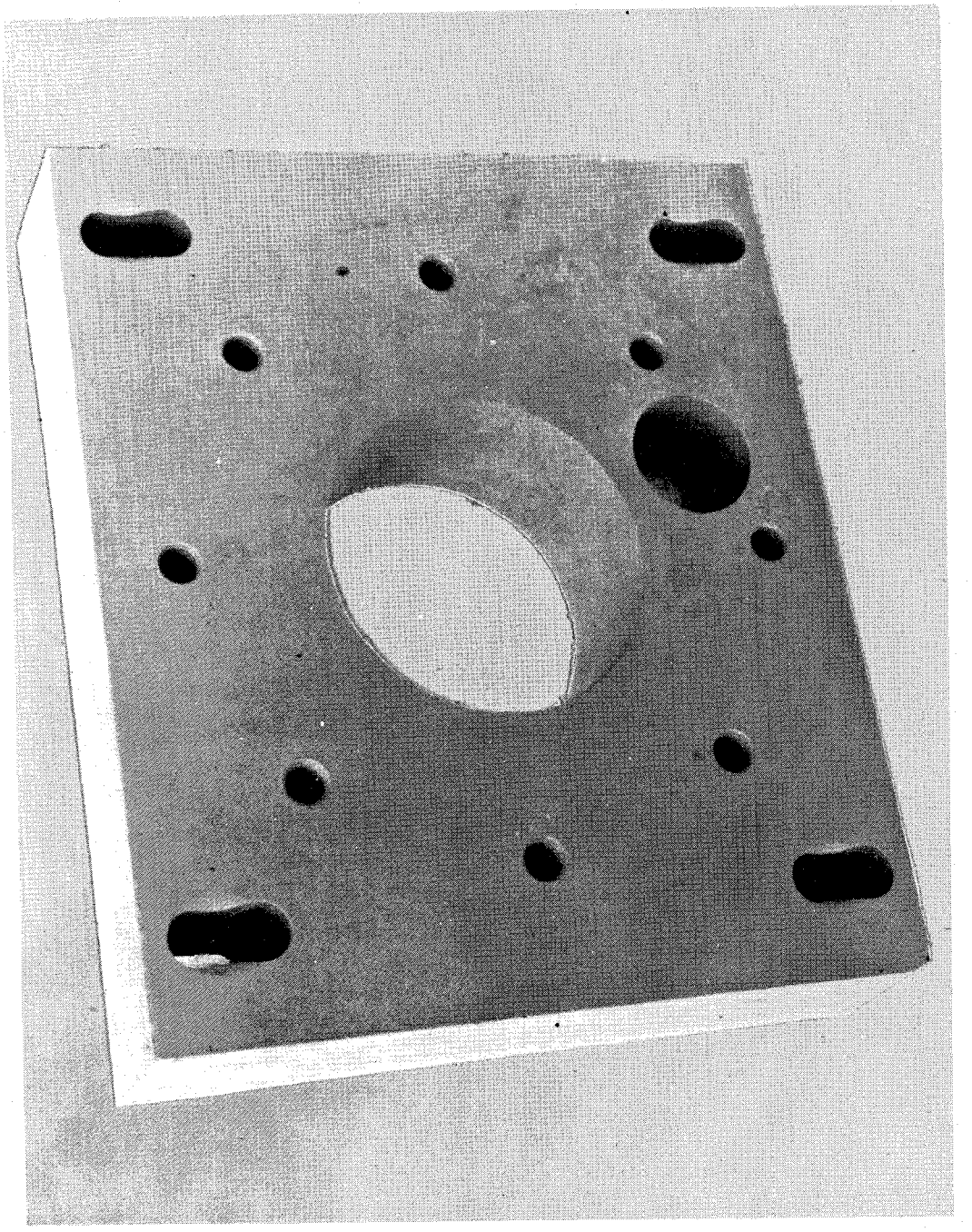

Figure 17. Thrust Block for Type 4 Headplate.

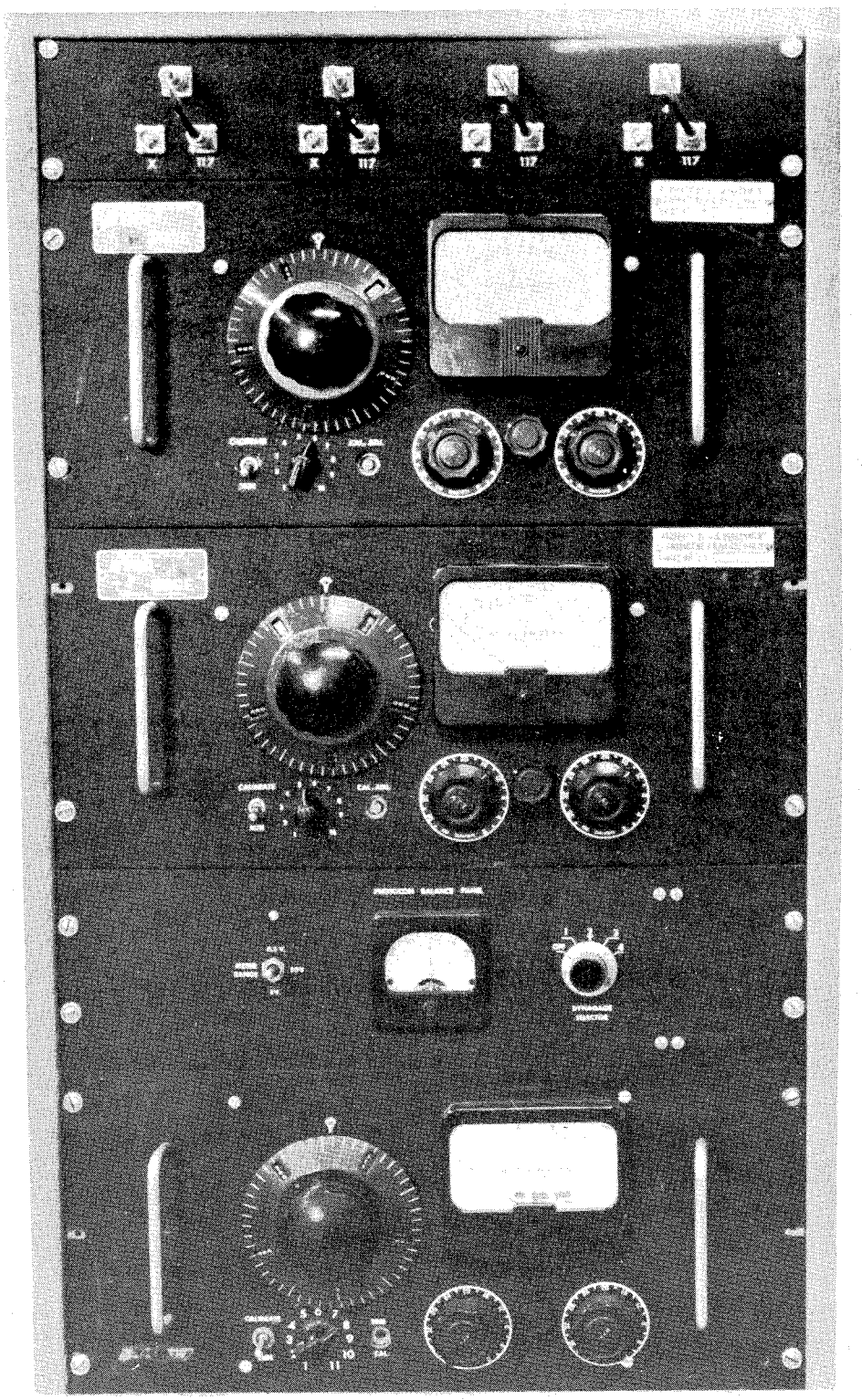

Figure 18. Photocon Dyna-Gage Units.

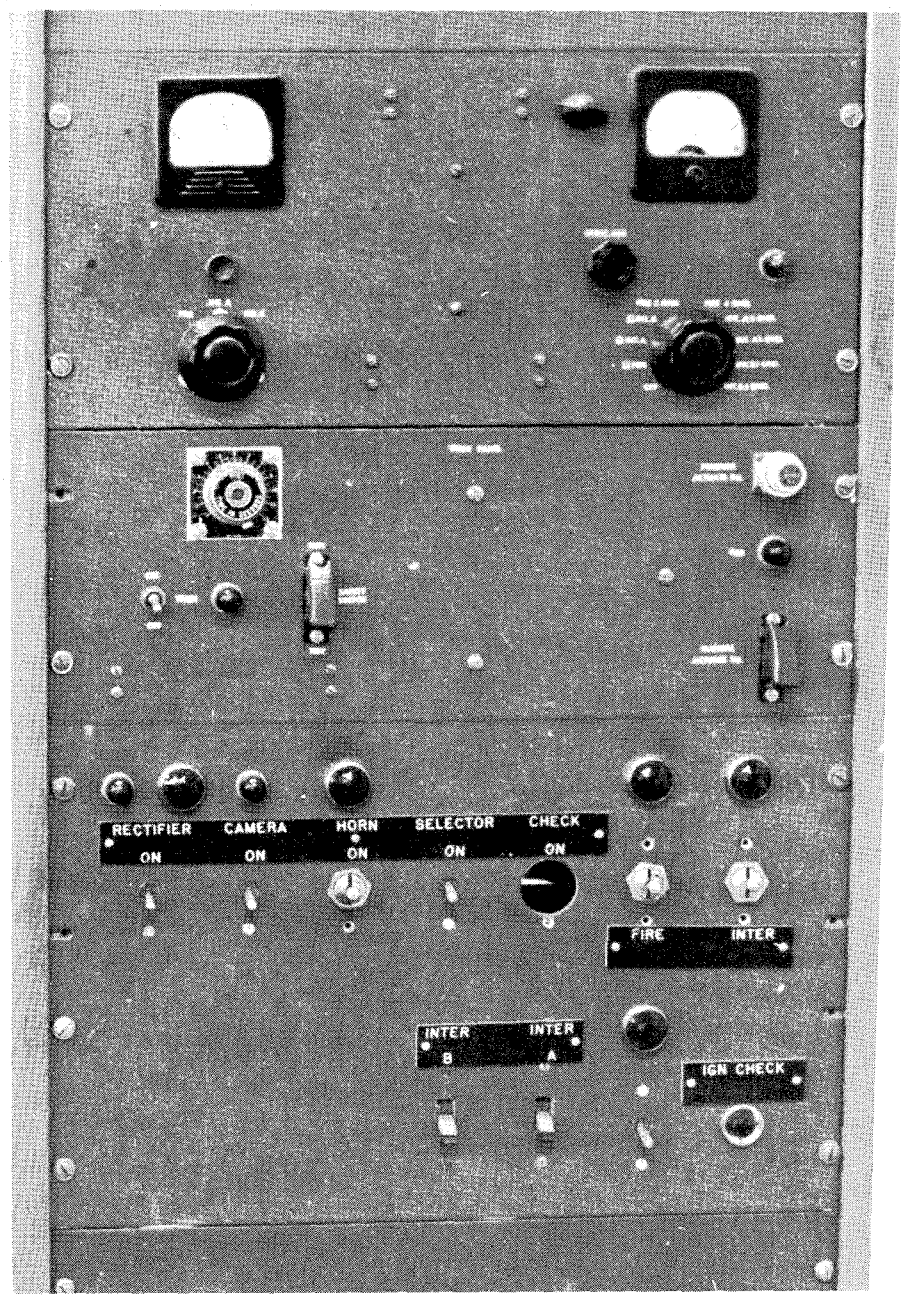

Figure 19. Firing Panel.

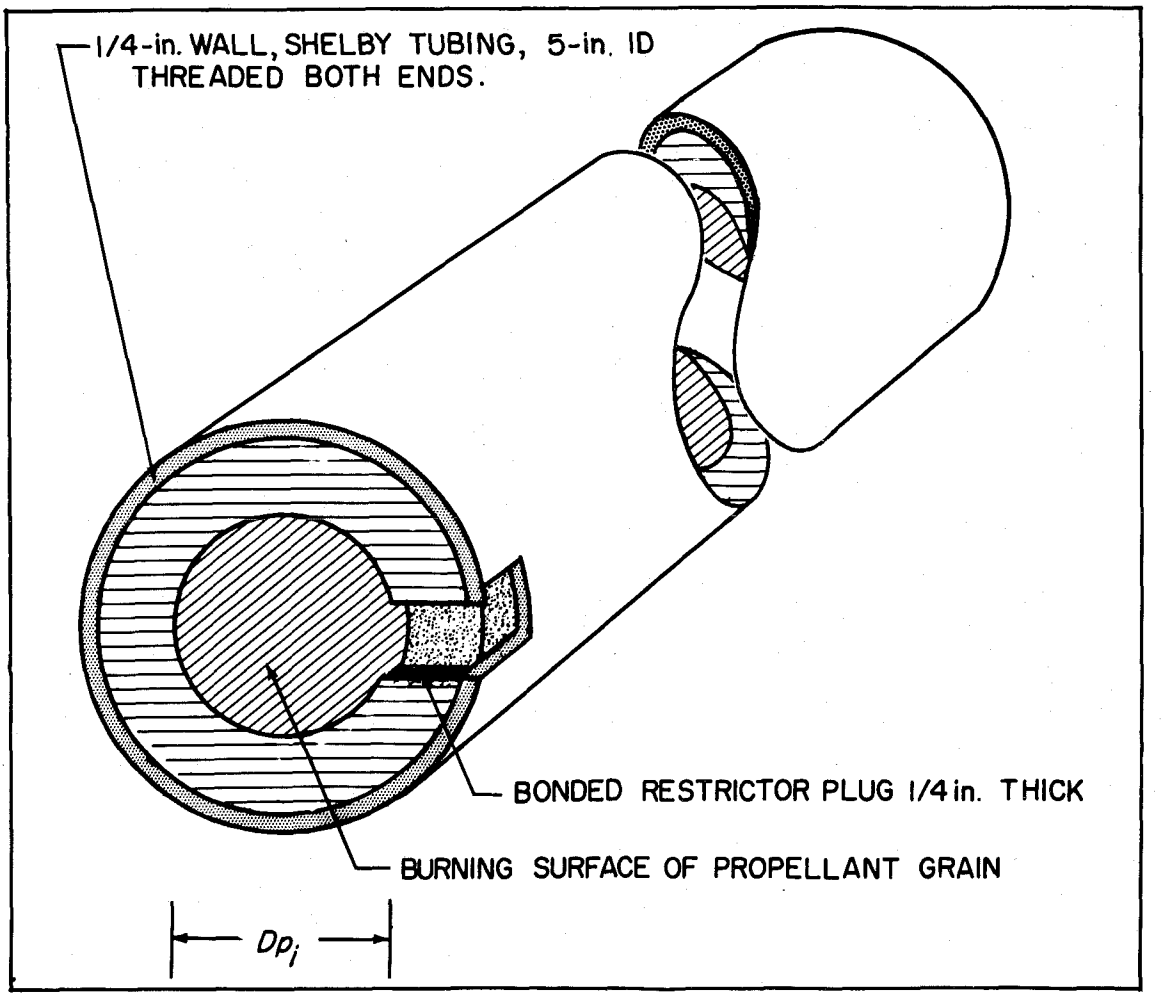

Figure 20. Cylindrical Motor Configuration.

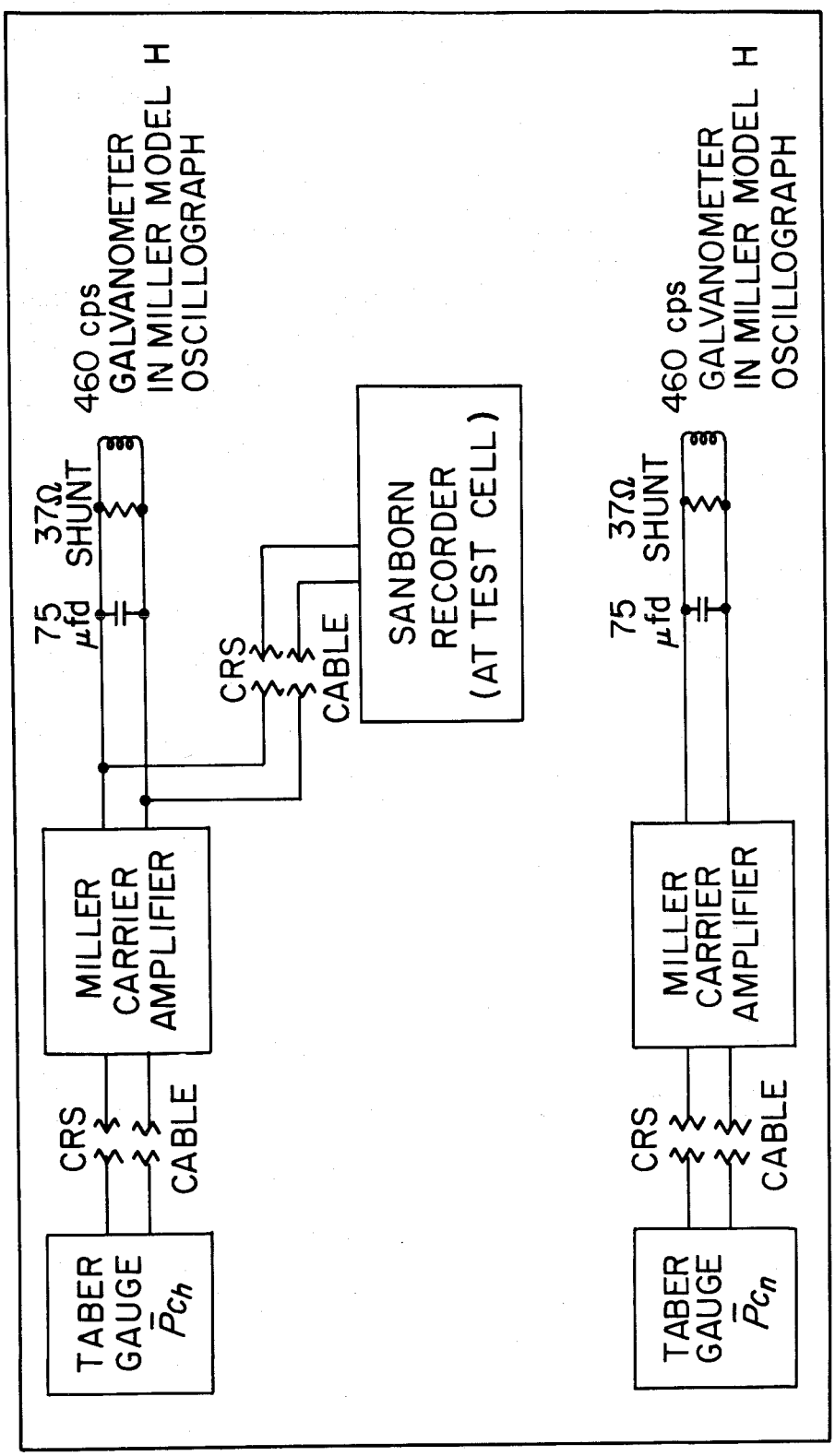

Figure 21. Low Frequency Response Instrumentation Set-Up.

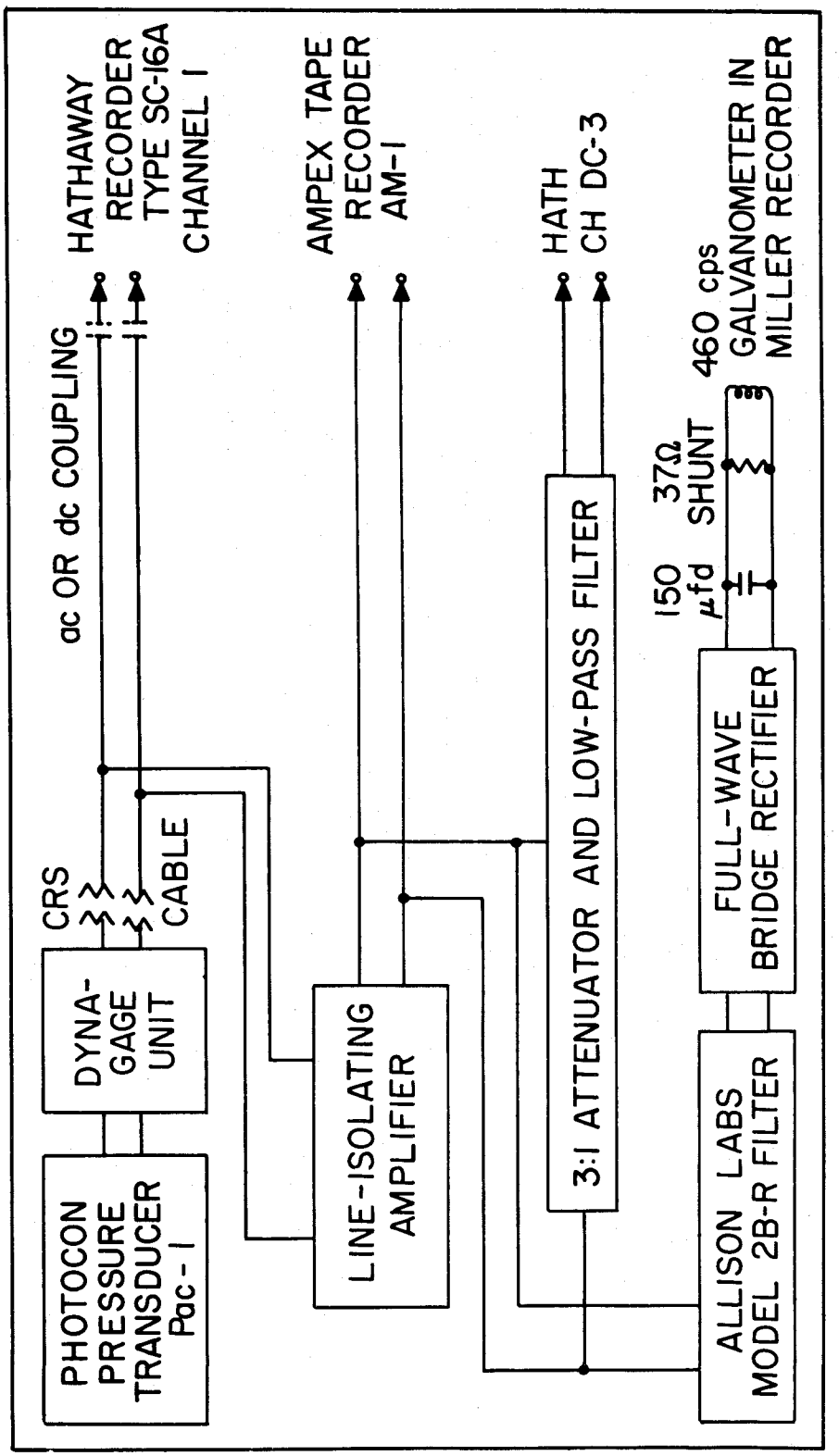

Figure 22. High Frequency Response Instrumentation Set-Up.

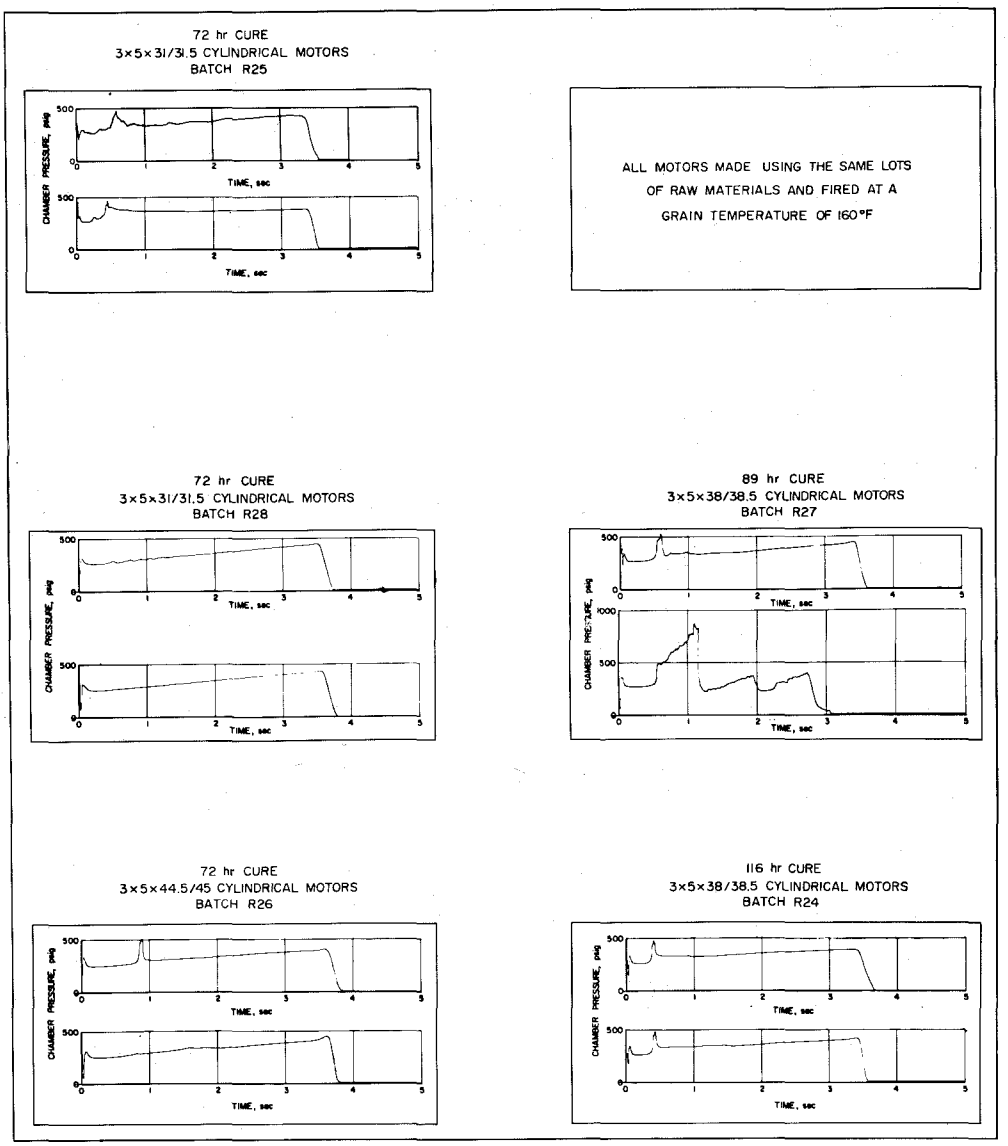

Figure 23. Effect of Cure Time on In-Batch Reproducibility.

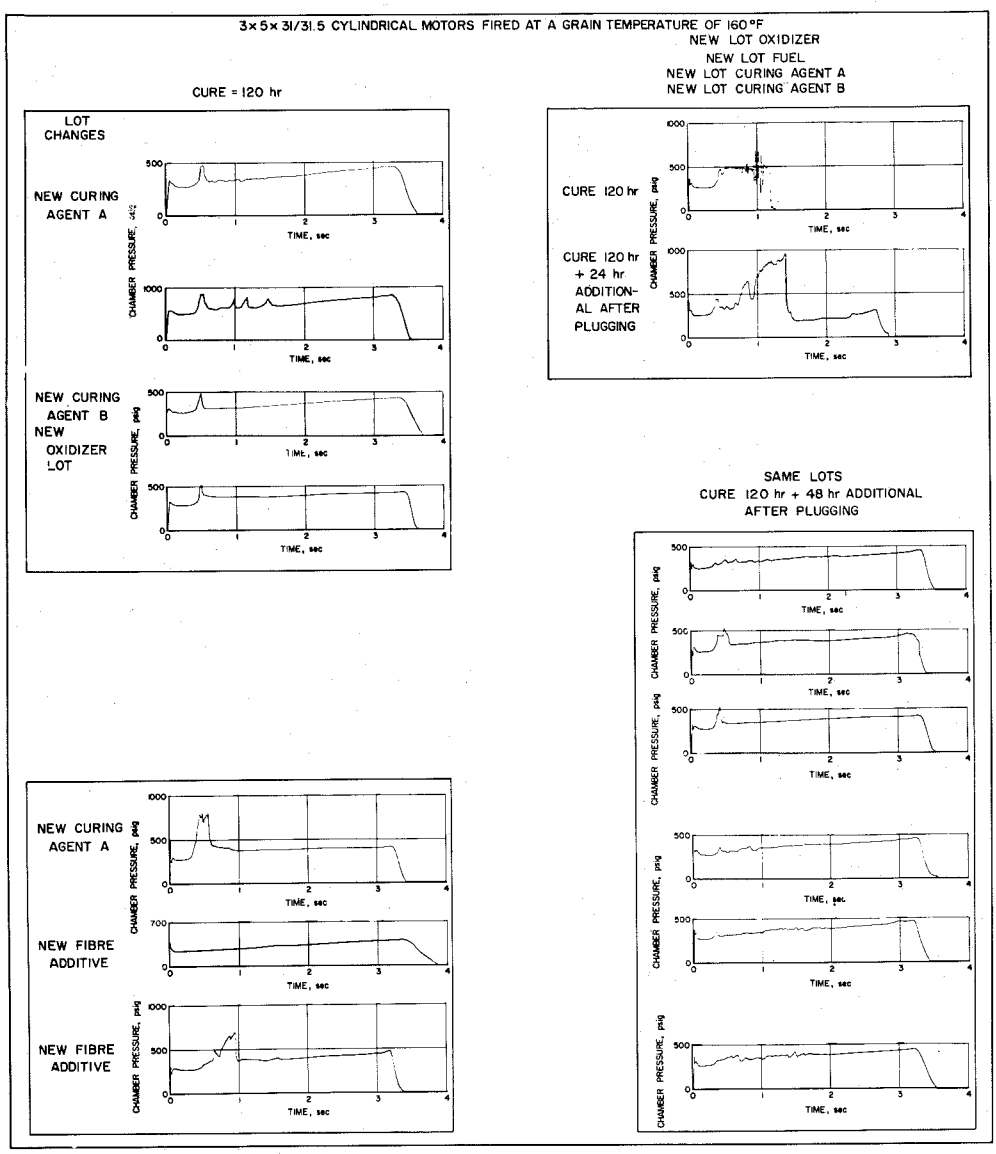

Figure 24. Effect of Changes in Lots of Raw Materials on Batch-to-Batch Reproducibility.

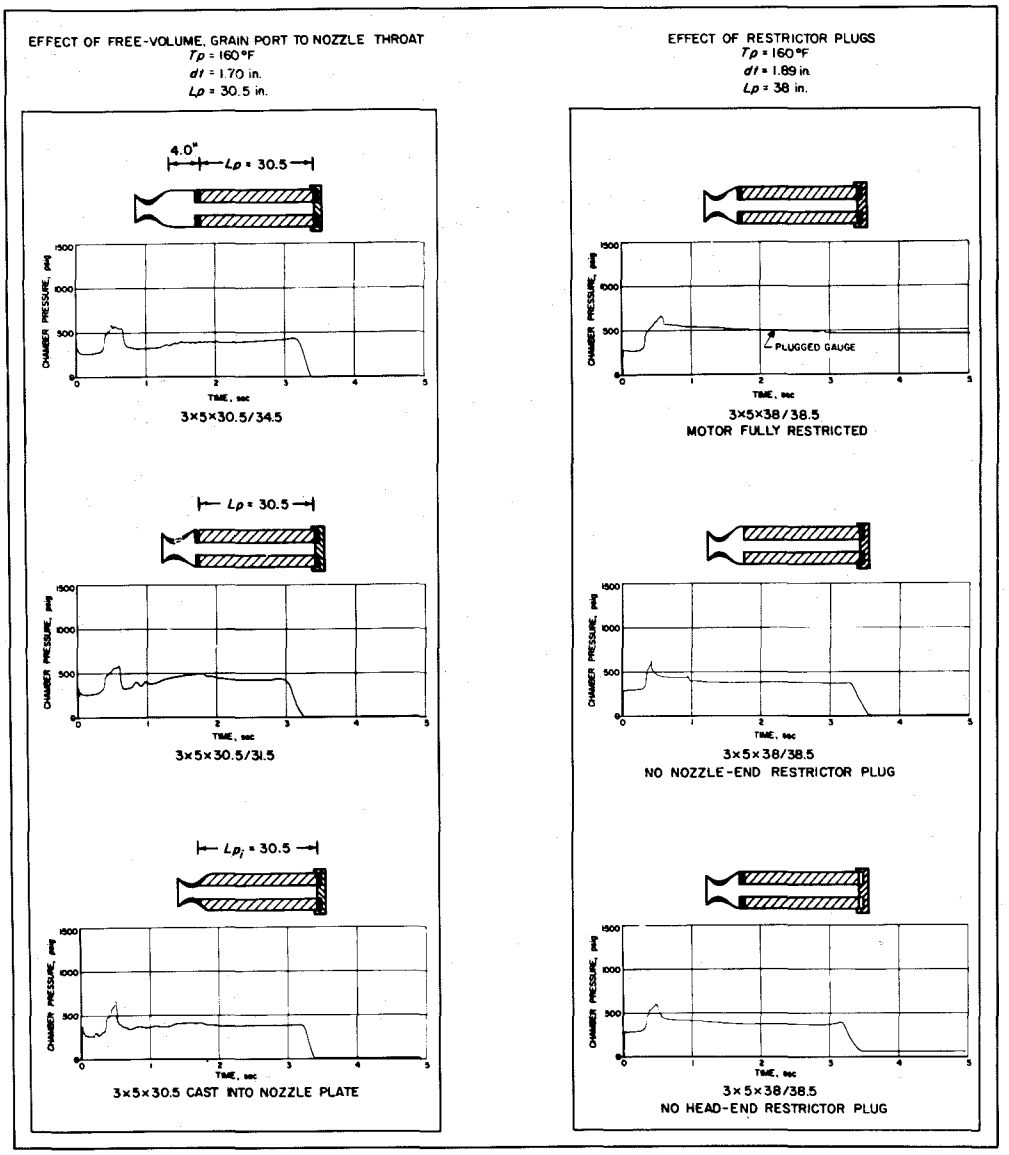

Figure 25. Effect of Varying Distance From Grain Port to Nozzle Throat; Effect of Removing Restrictor Plugs.

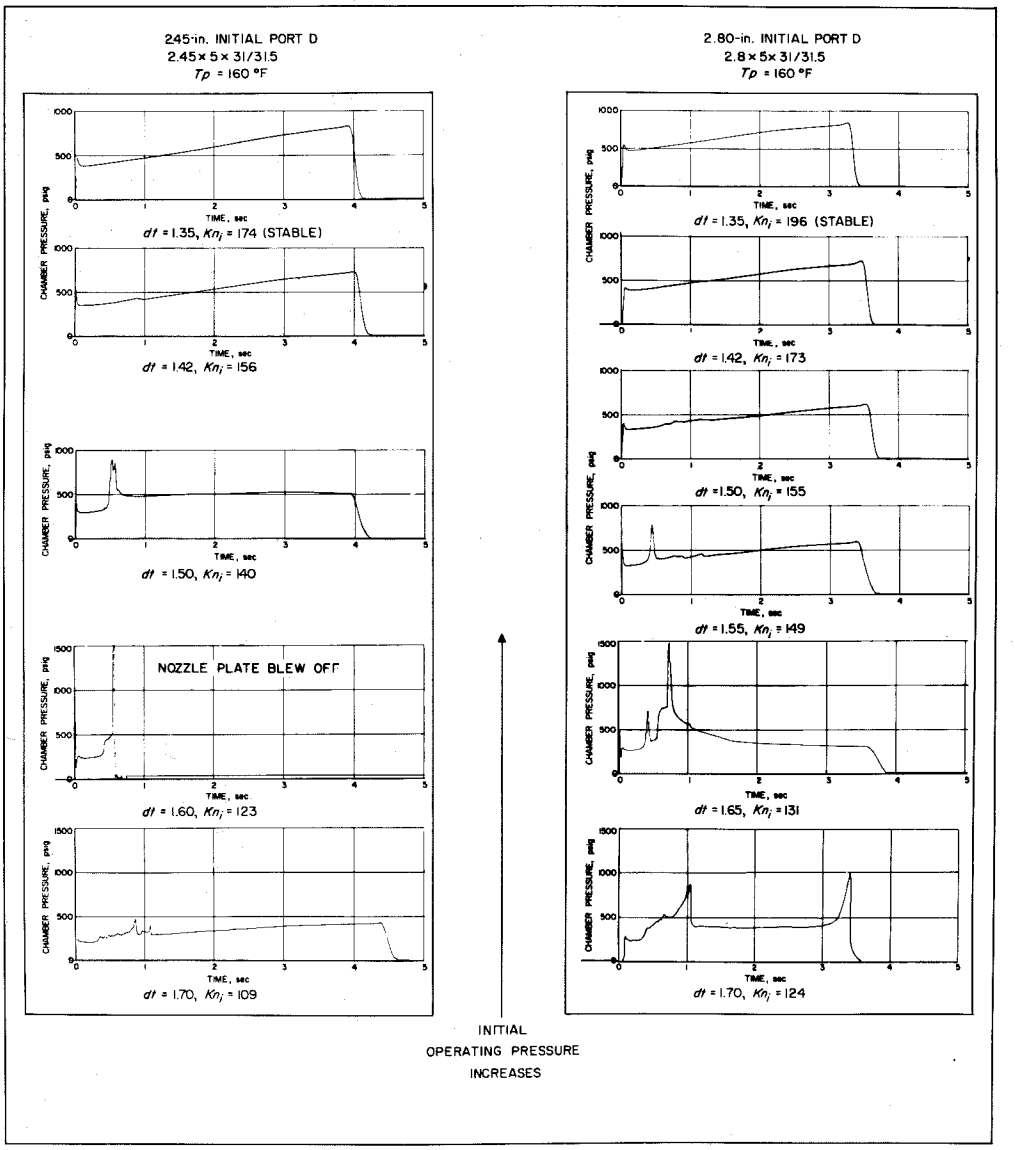

Figure 26. Effect of Varying Operating Pressure Level; 2.45 and 2.80 in. Initial Port Diameter.

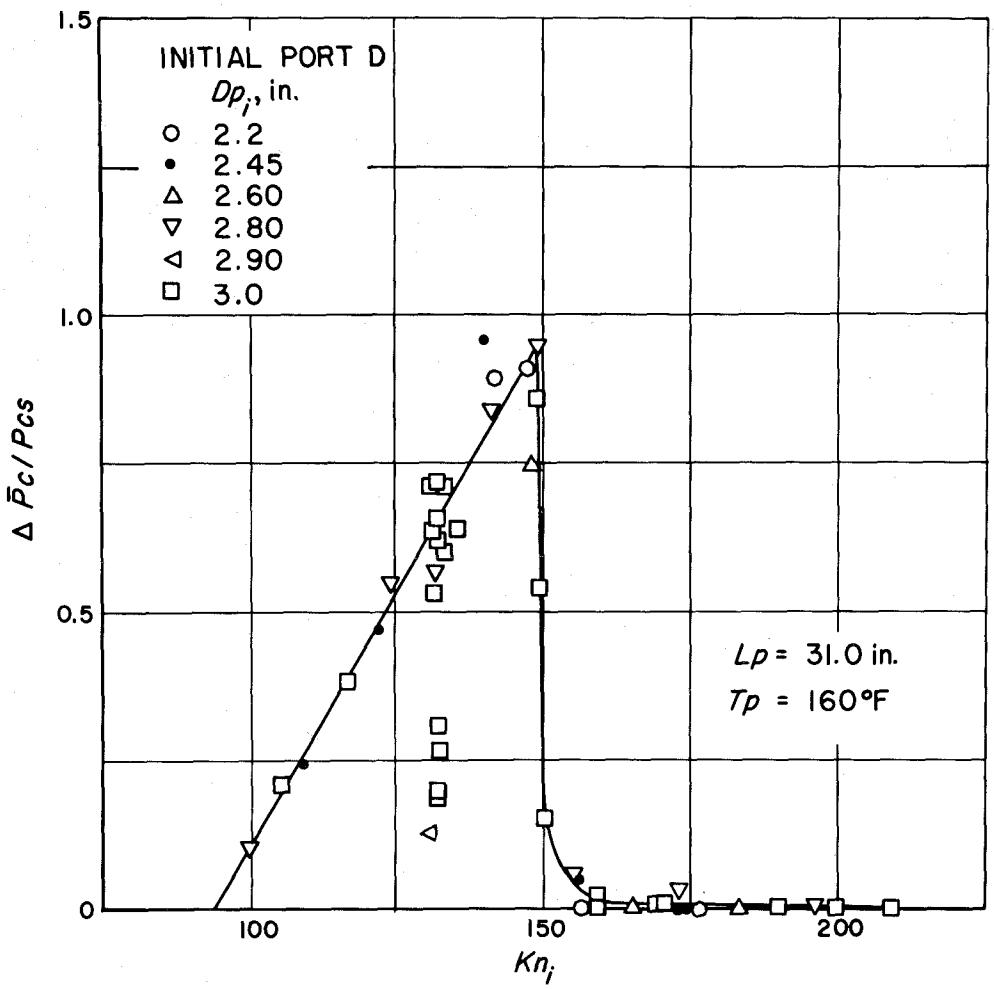

Figure 27. Unstable Increment in Chamber Pressure Versus Initial Value of Area Ratio Kn; Initial Port Diameter 2.2 to 3.0 in. Grain Length 31 in.

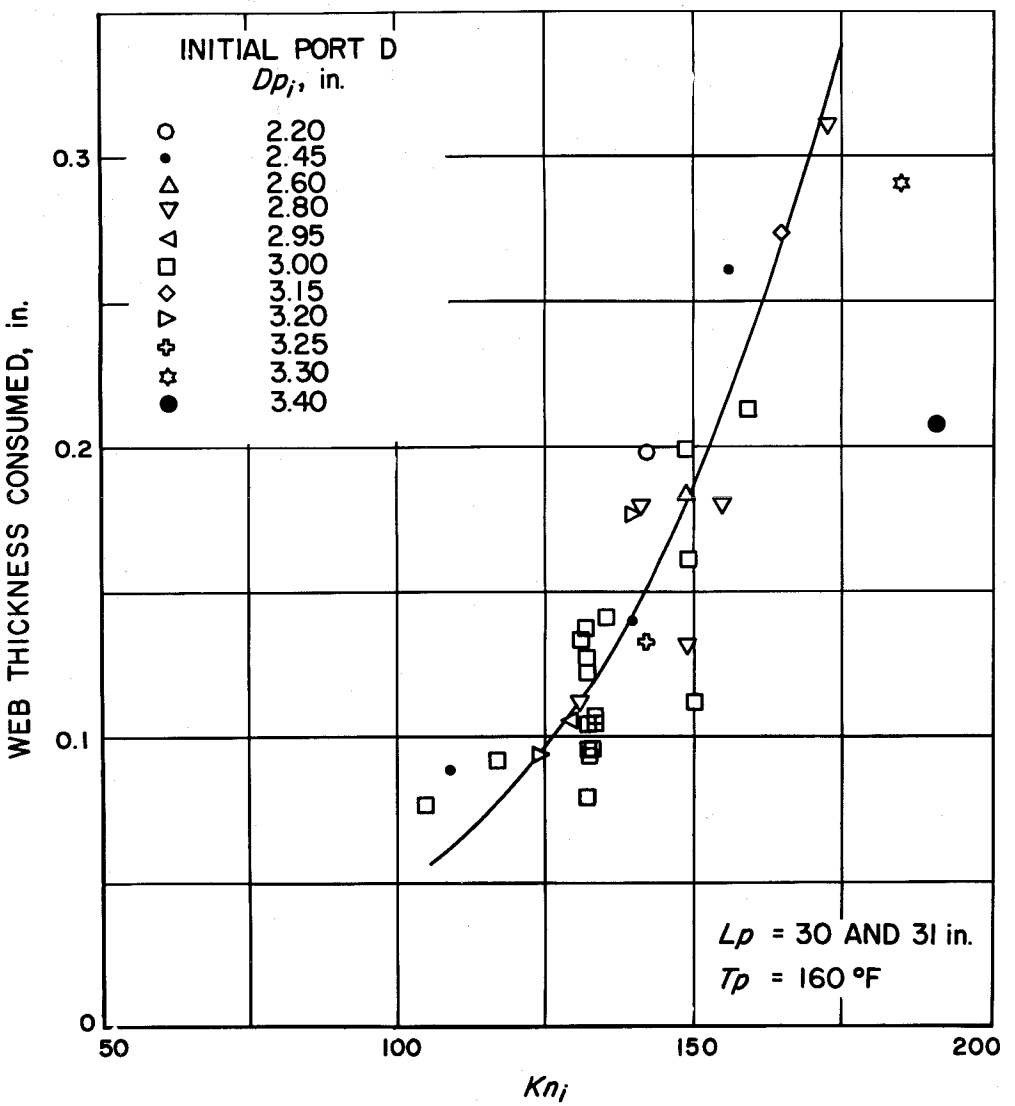

Figure 28. Grain Web Consumed From Ignition to Break in Mean Chamber Pressure Versus Initial Value of Area Ratio Kn.

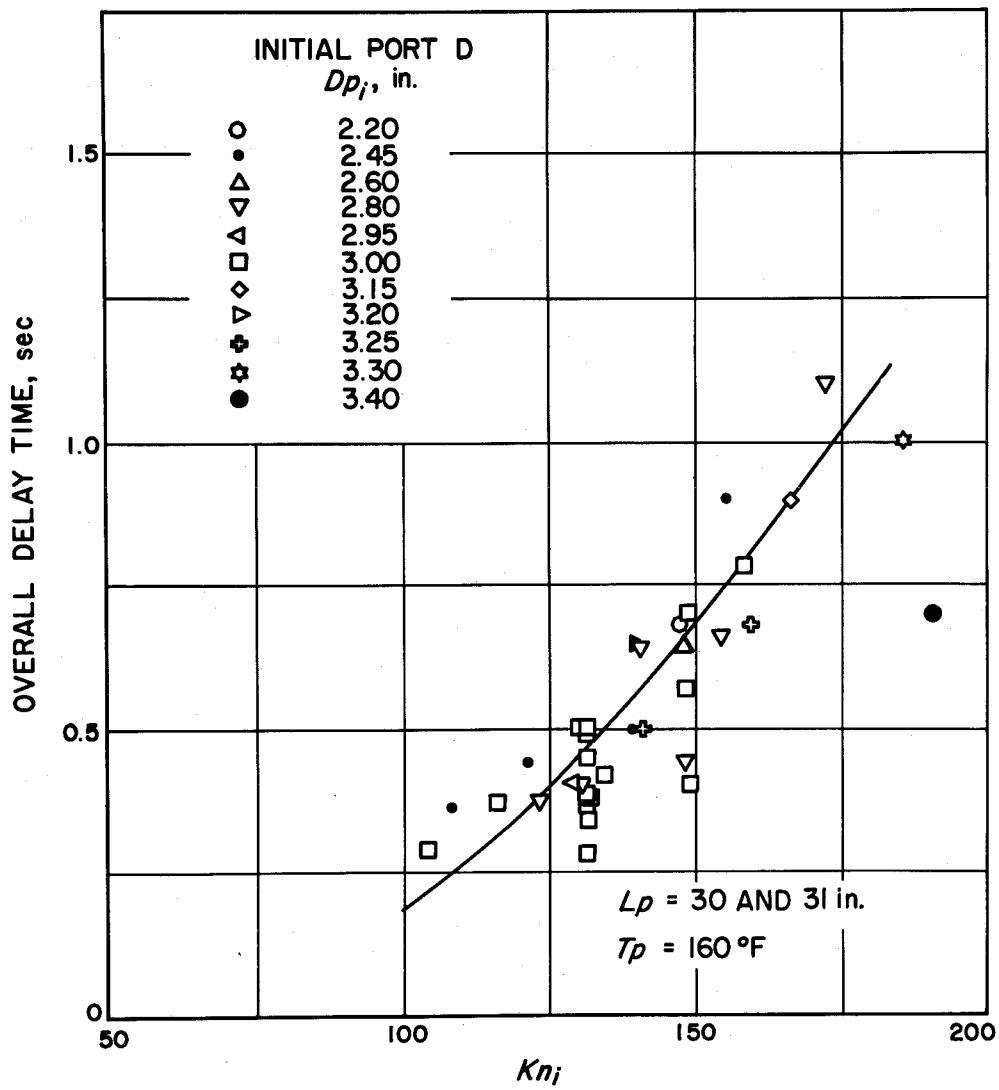

Figure 29. Delay Time From Ignition to Break In Mean Chamber Pressure Versus Initial Value of Area Ratio Kn.

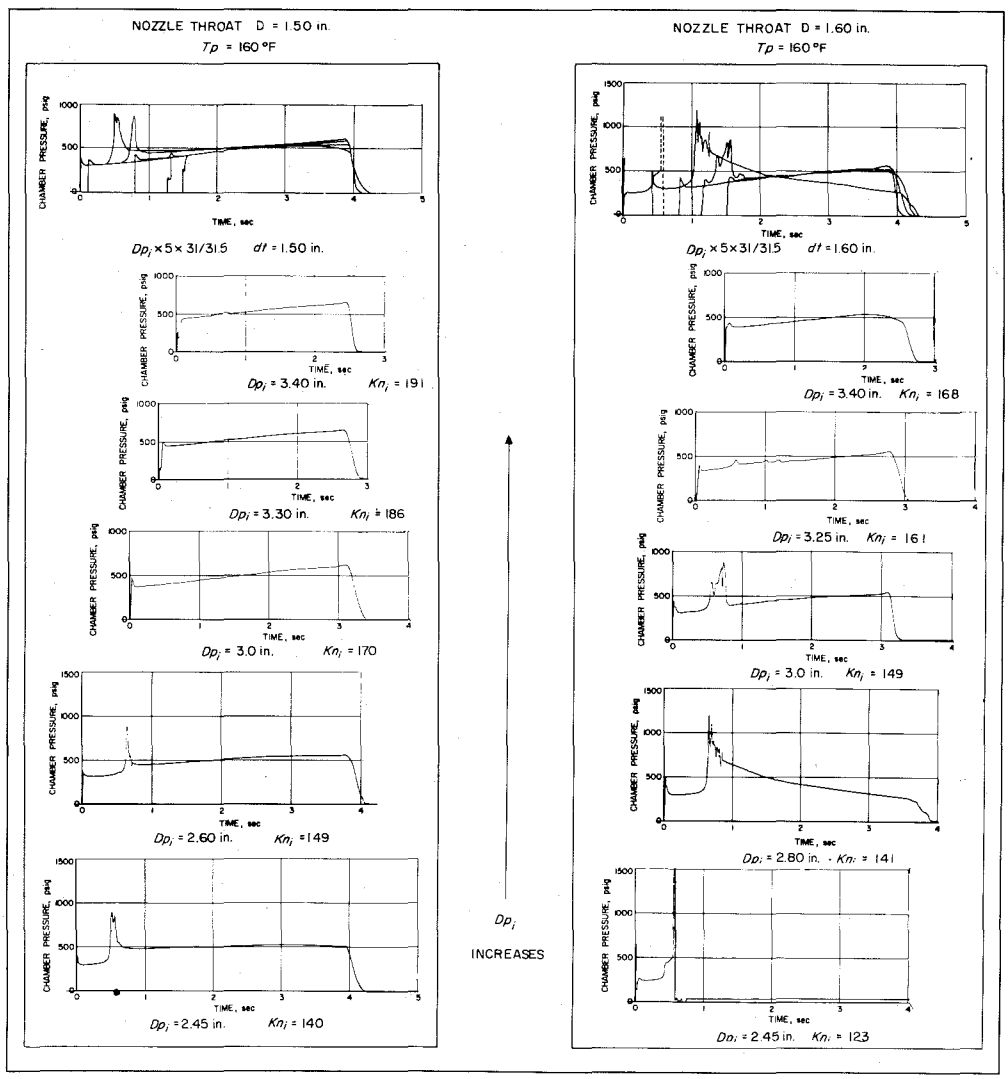

Figure 30. Effect of Varying Initial Port Diameter with Otherwise Fixed Geometry; Nozzle Throat Diameter = 1.50 and 1.60 in.

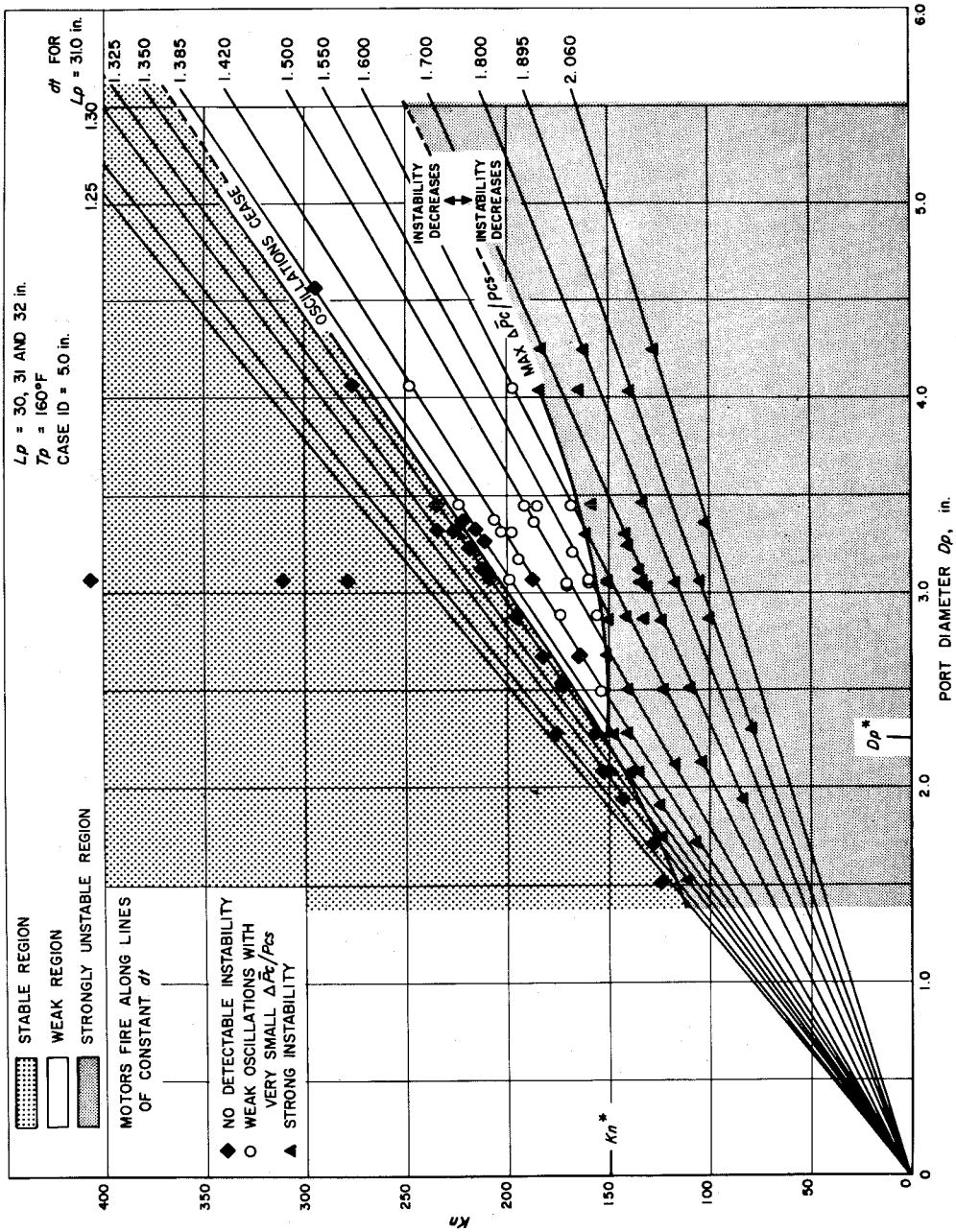

Figure 31. Instability Regions in The Area Ratio Kn, Port Diameter Dp, Plane; Grain Lengths 30, 31 and 32 in.

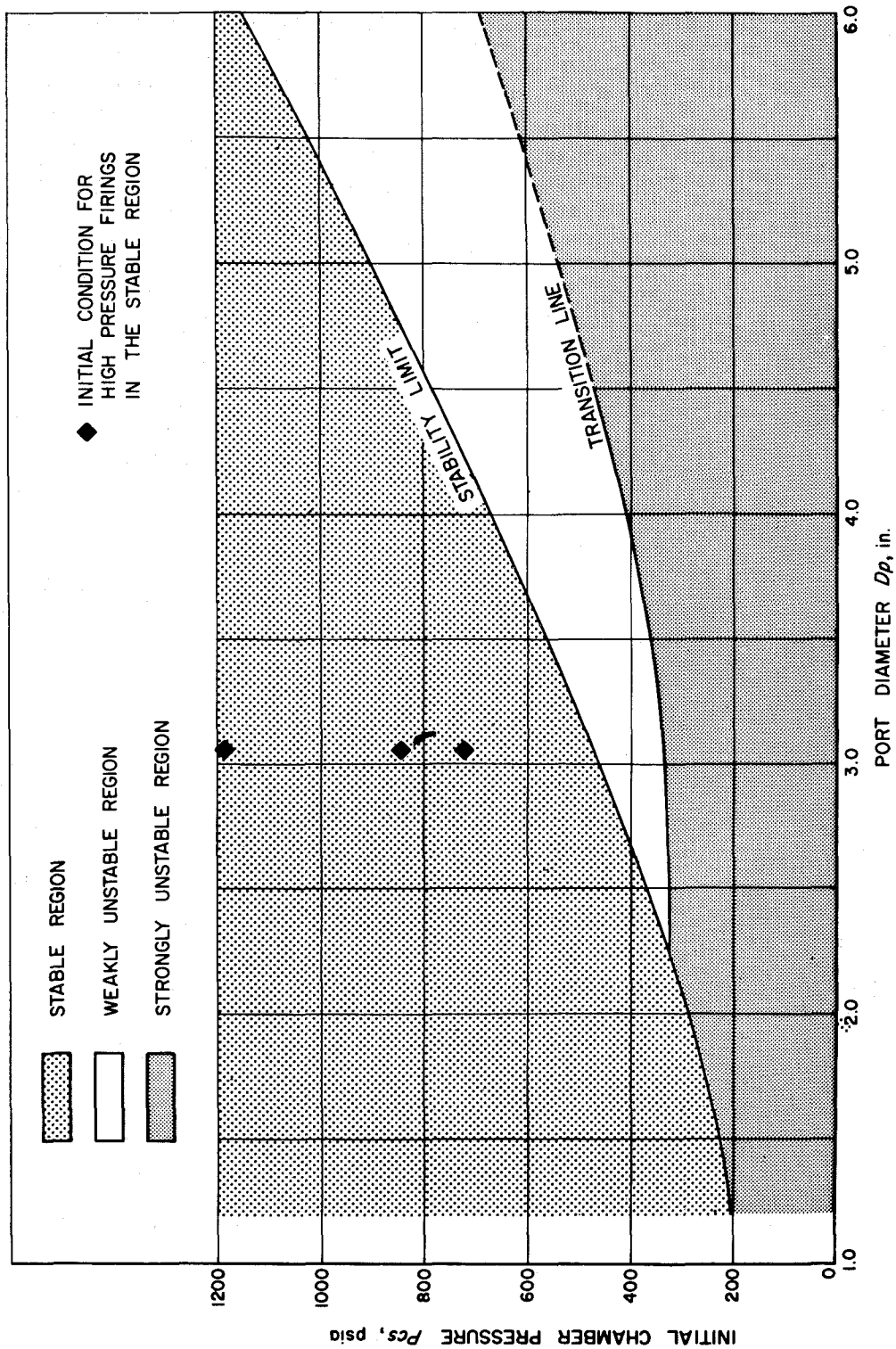

Figure 32. Instability Regions in The Chamber Pressure Pcs, Port Diameter Dp, Plane.

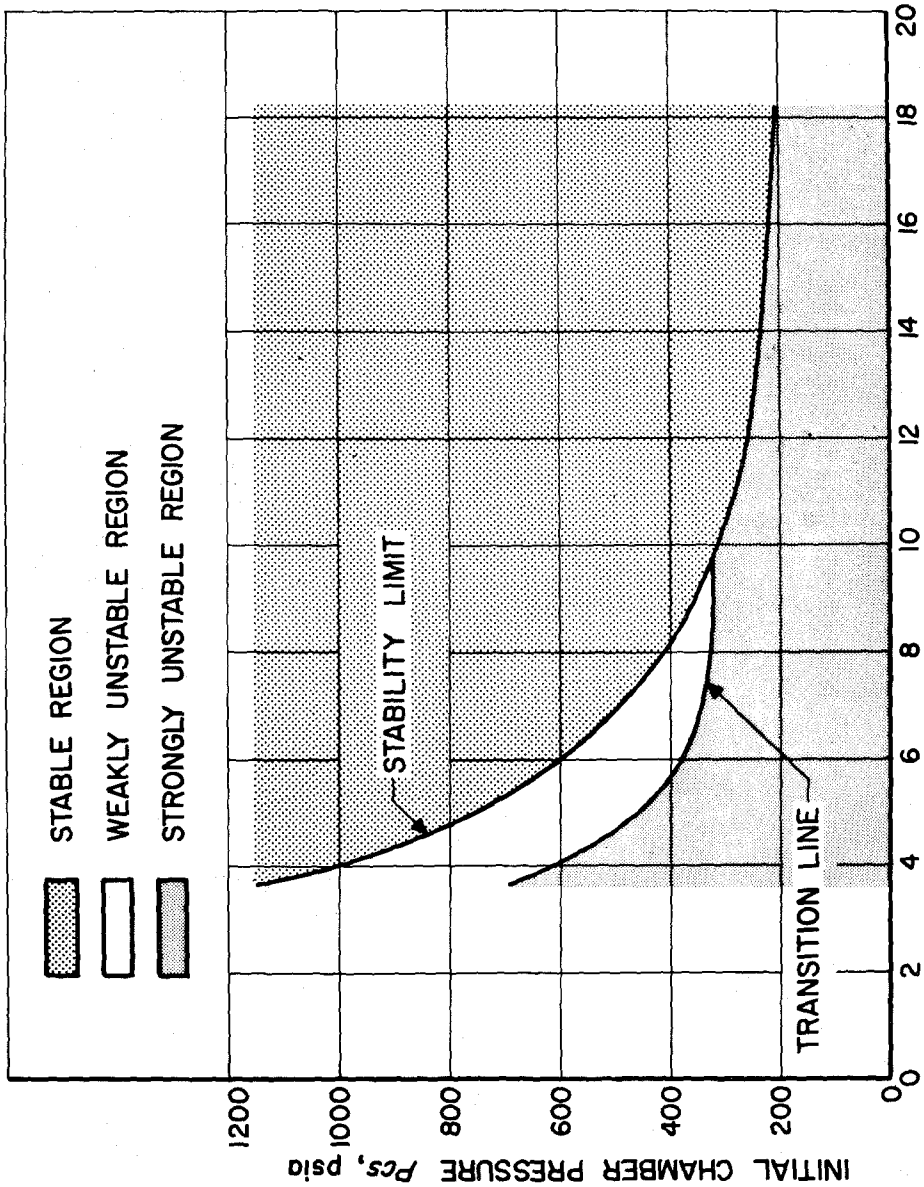

Figure 33. Instability Regions in The Chamber Pressure Pcs, Fundamental Tangential Frequency f_{100}, Plane.

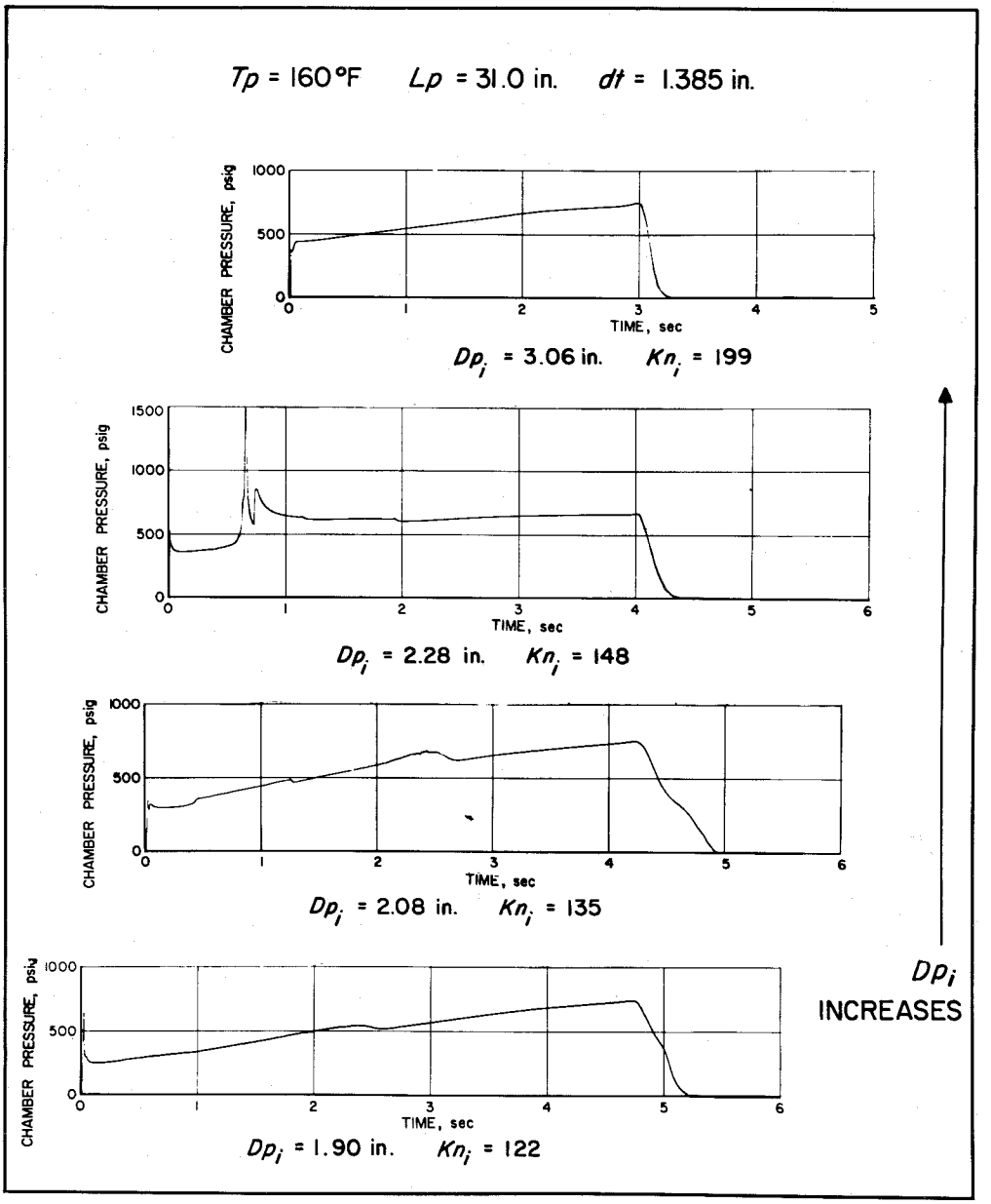

Figure 34. Effect of Varying Initial Port Diameter with Otherwise Fixed Geometry; Nozzle Throat Diameter = 1.385 in.

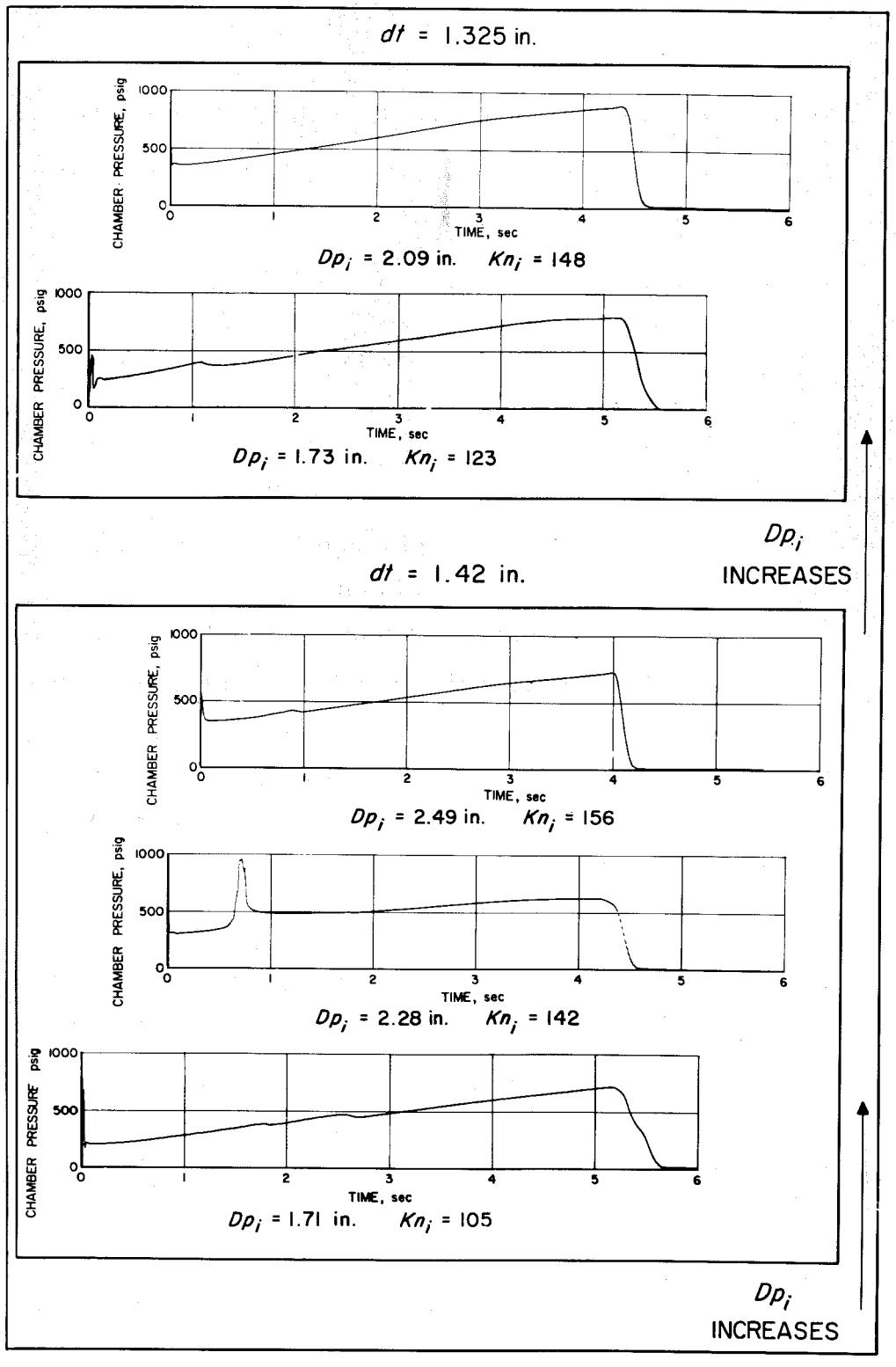

Figure 35. Effect of Varying Initial Port Diameter with Otherwise Fixed Geometry; Nozzle Throat Diameter = 1.325 and 1.42 in.

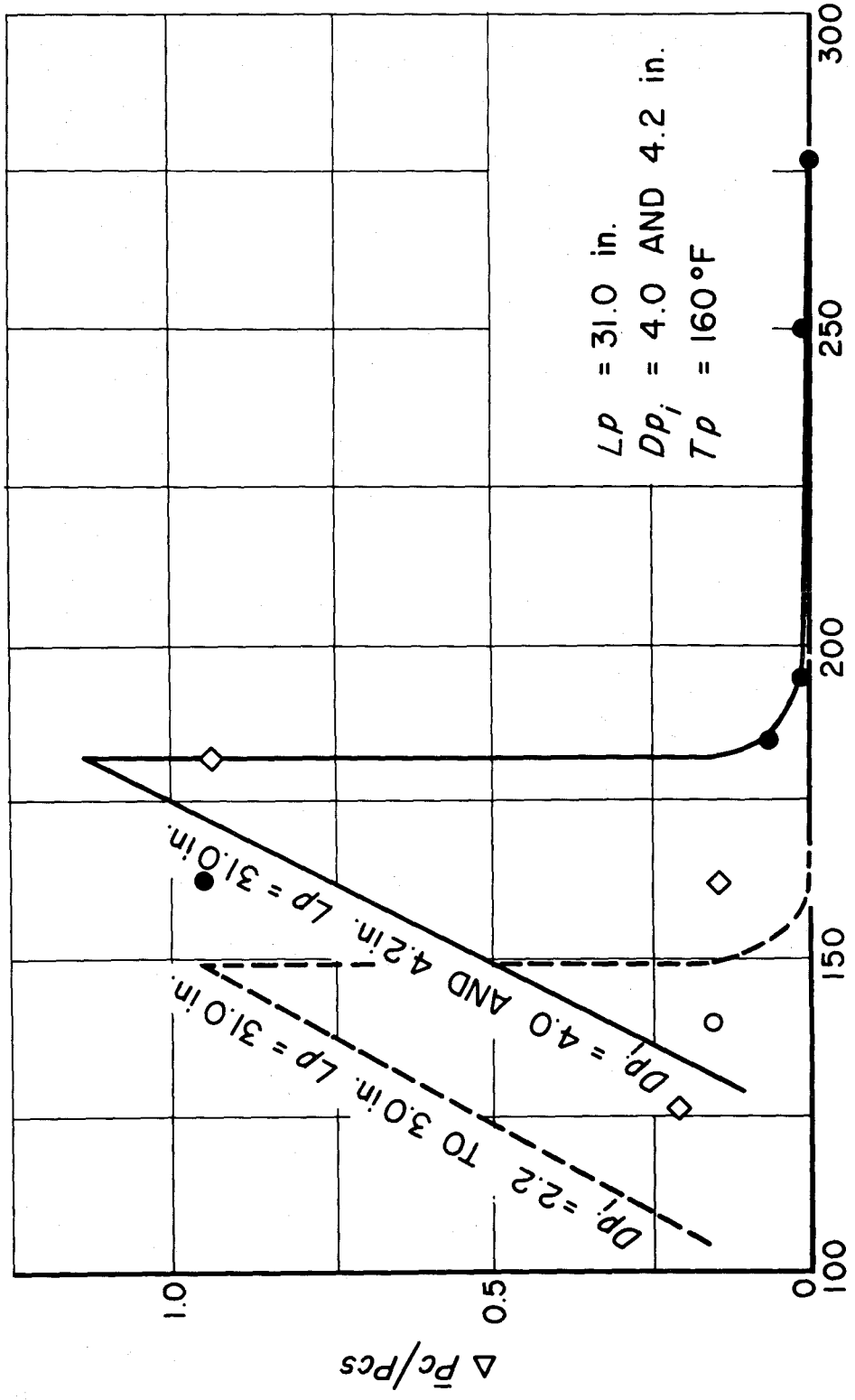

Figure 36. Unstable Increment in Chamber Pressure Versus Initial Value of Area Ratio Kn; Initial Port Diameters 4.0 and 4.2 in., Grain Length 31 in.

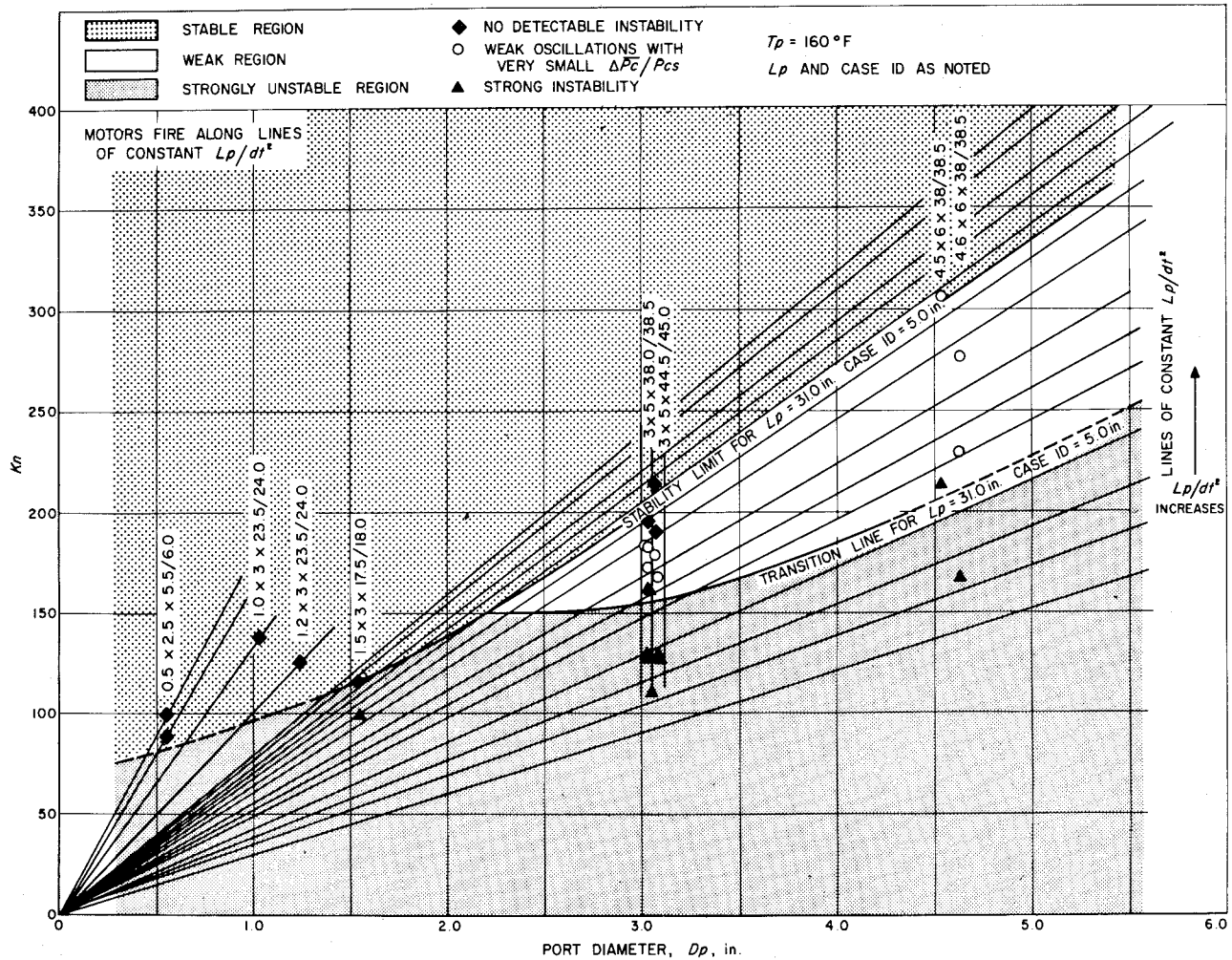

Figure 37. Instability Regions in The Area Ratio Kn, Port Diameter D_P, Plane; Odd Sized Motors.

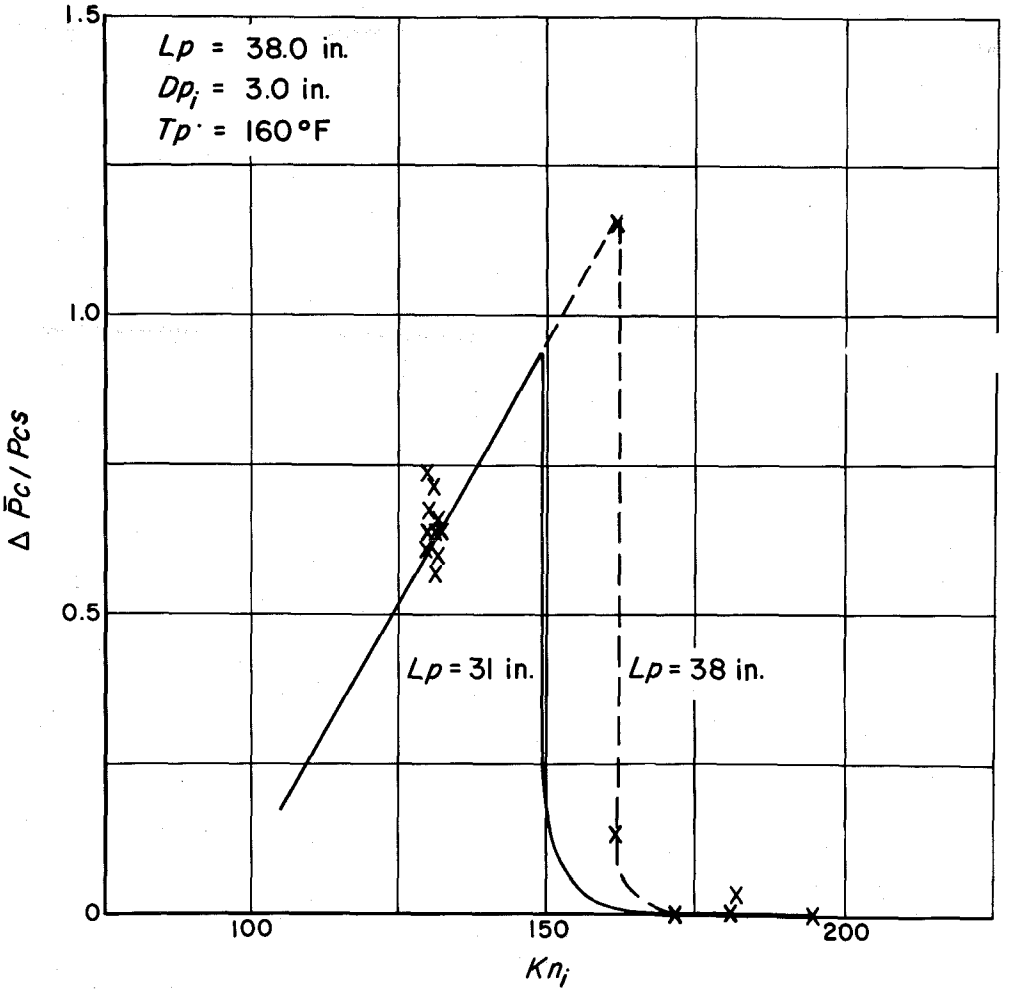

Figure 38. Unstable Increment in Chamber Pressure Versus Initial Value of Area Ratio Kn; Initial Port Diameter 3.0 in, Grain Length 38 in.

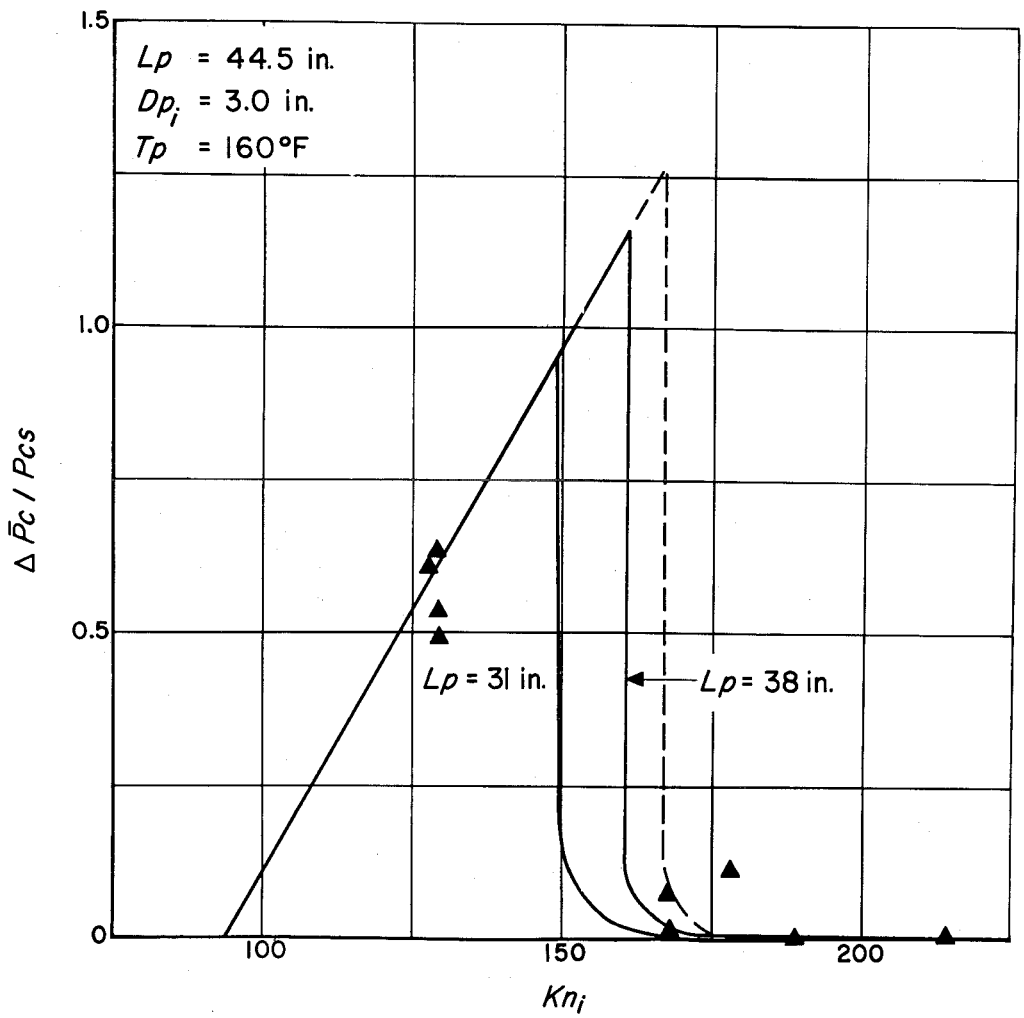

Figure 39. Unstable Increment in Chamber Pressure Versus Initial Value of Area Ratio Kn; Initial Port Diameter 3.0 in, Grain Length 44.5 in.

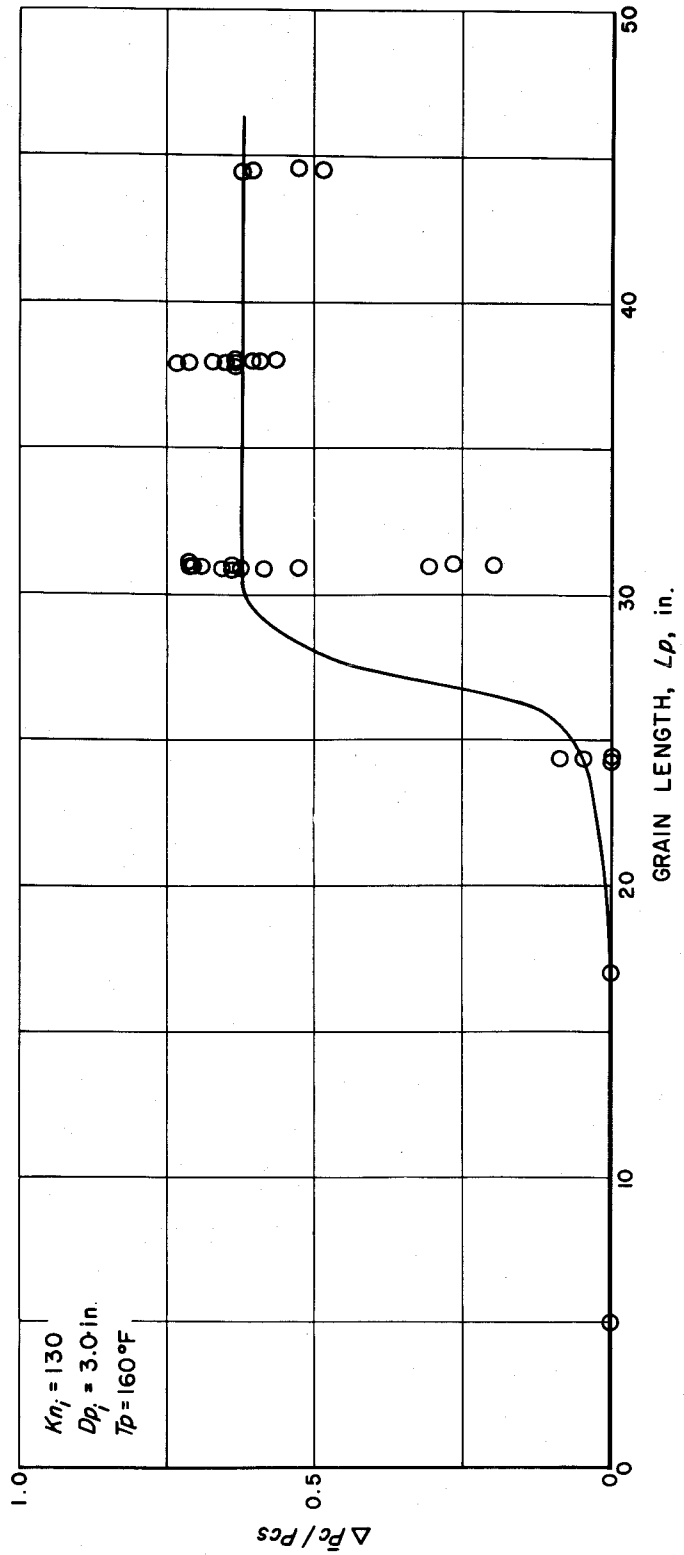

Figure 40. Unstable Increment in Chamber Pressure Versus Grain Length; Area Ratio Kn ≈ 130.

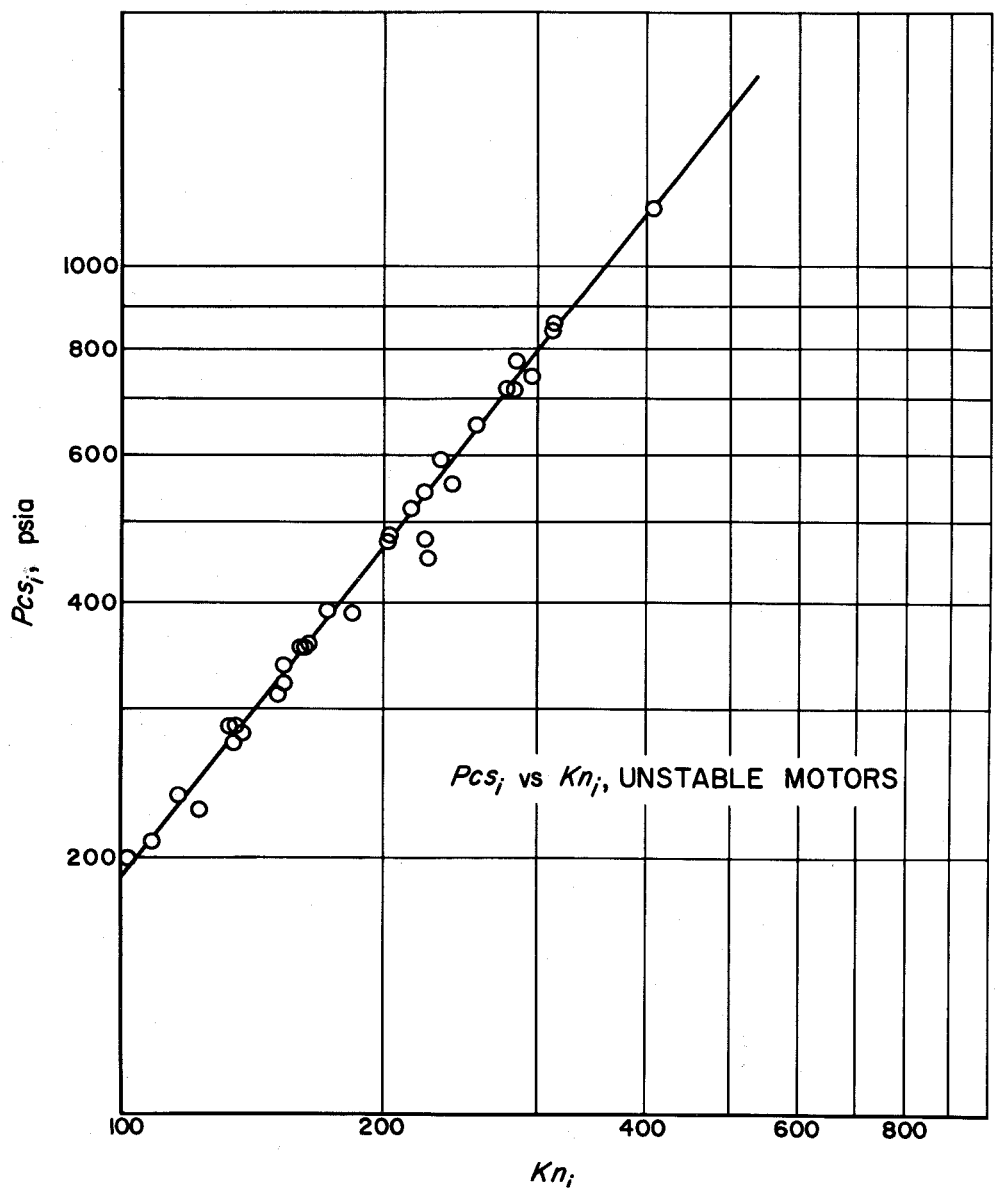

Figure 41. Initial Chamber Pressure Pcs, Versus Area Ratio Kn; Unstable Firings.

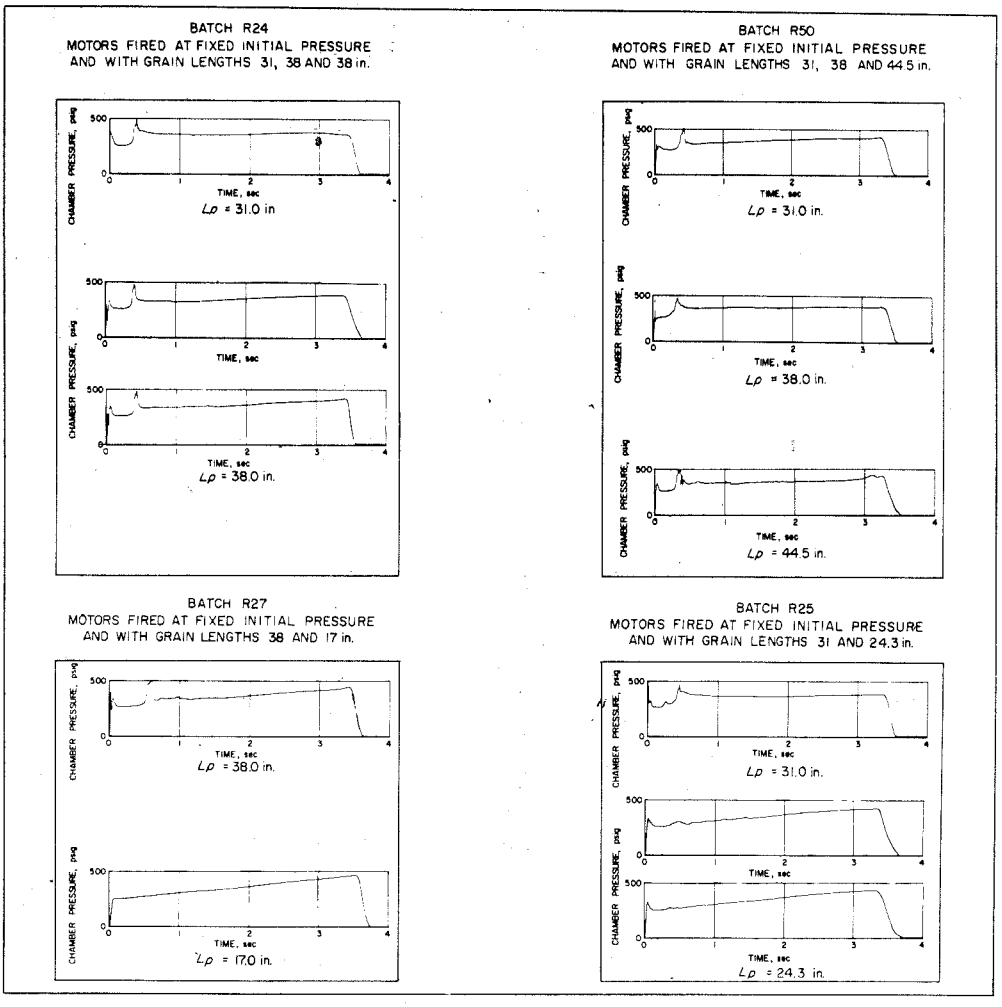

Figure 42. Effect of Grain Length; Mean Chamber Pressure Versus Time Histories of Typical Firings.

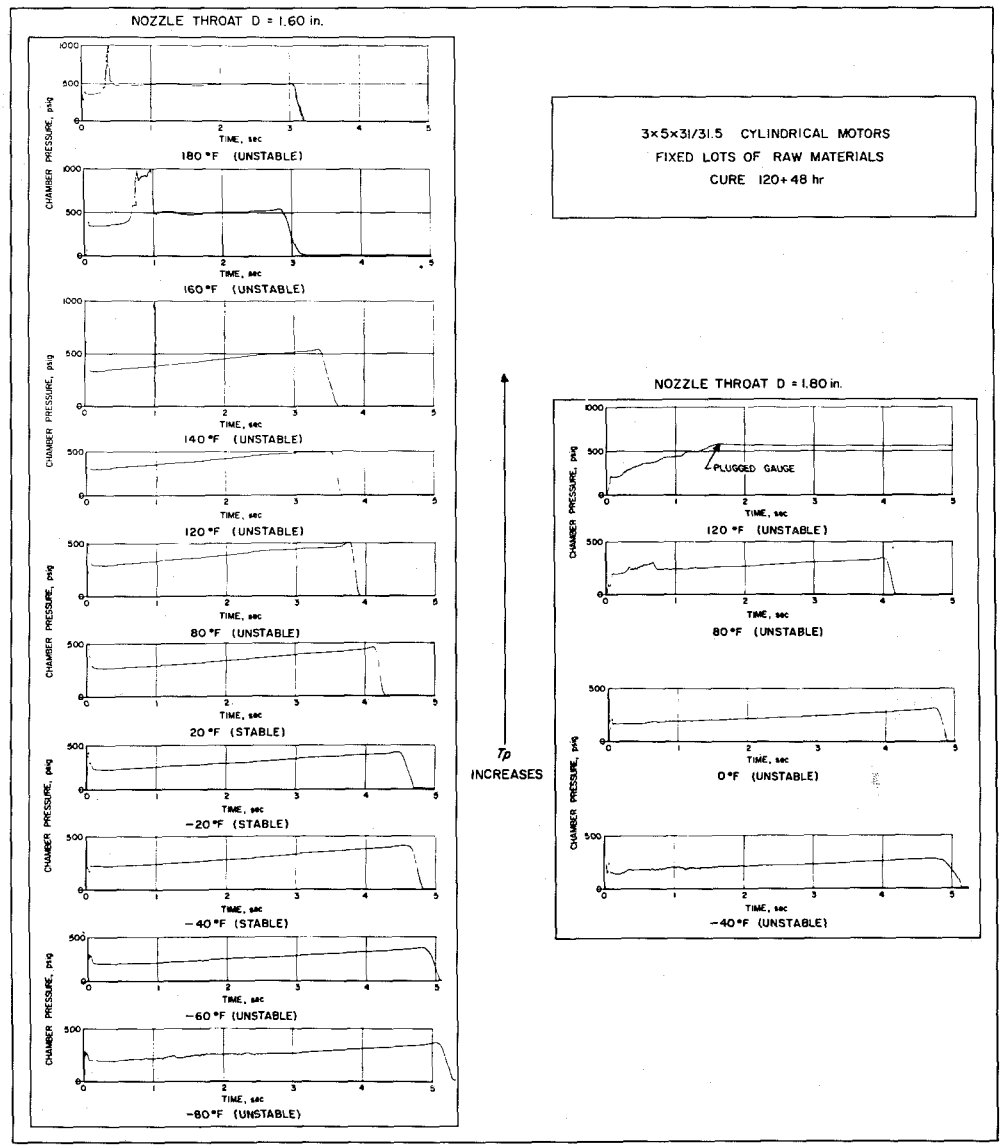

Figure 43. Effect of Varying Grain Temperature With Fixed Geometry; Nozzle Throat Diameter = 1.60 and 1.80 in.

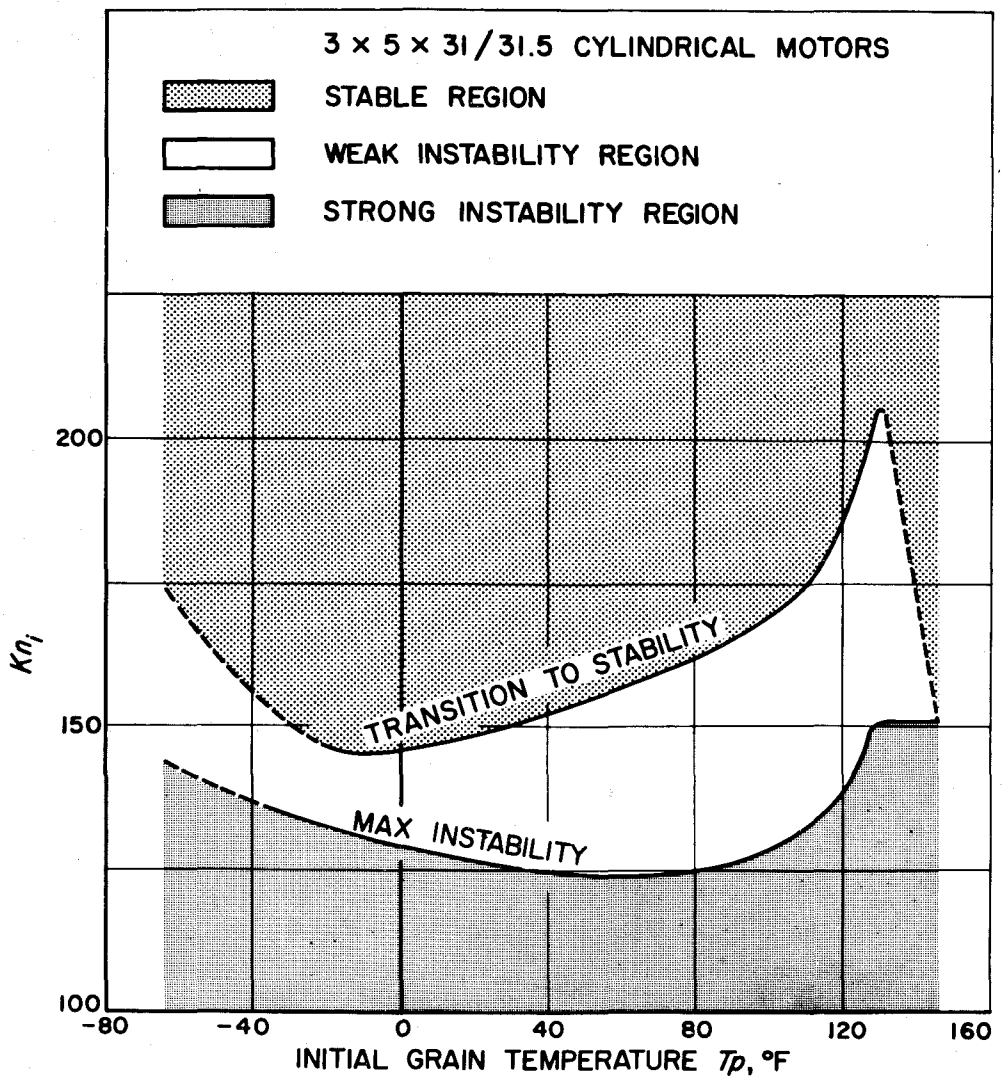

Figure 44. Instability Regions in the Initial Area Ratio Kn, Initial Grain Temperature, Plane.

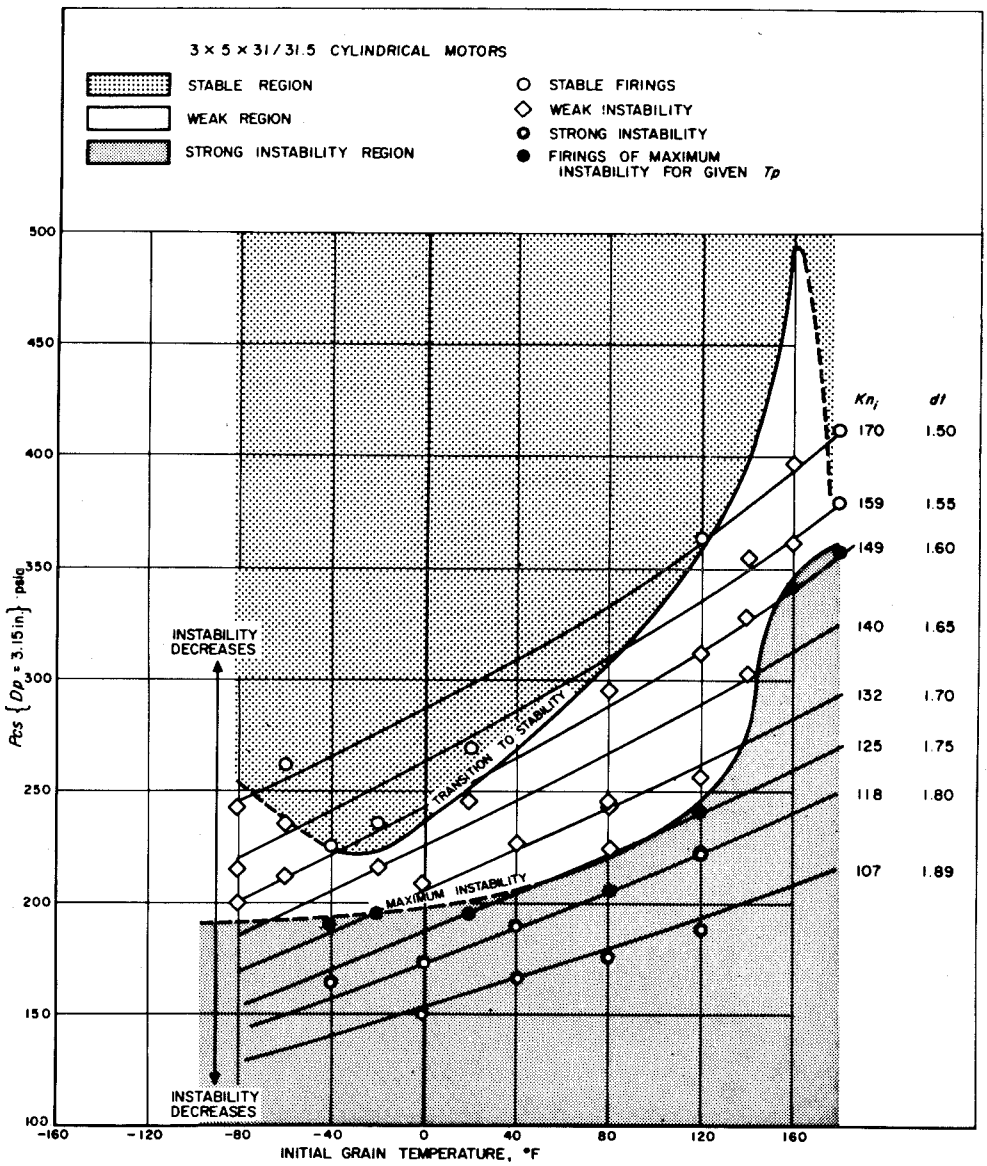

Figure 45. Instability Regions in the Initial Chamber Pressure, Initial Grain Temperature Plane.

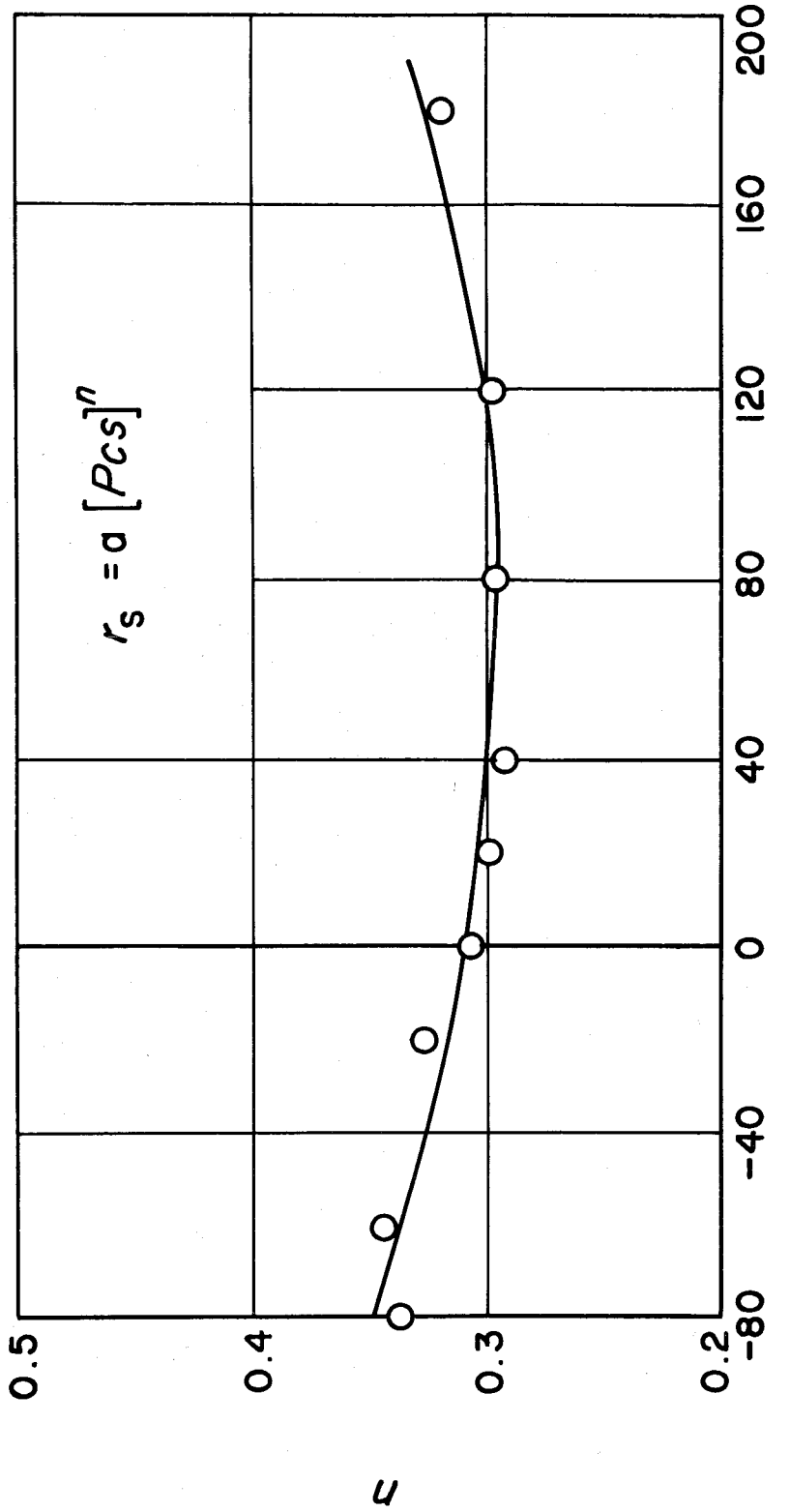

Figure 46. Burning Rate Law Parameter 'n' Versus Grain Temperature.

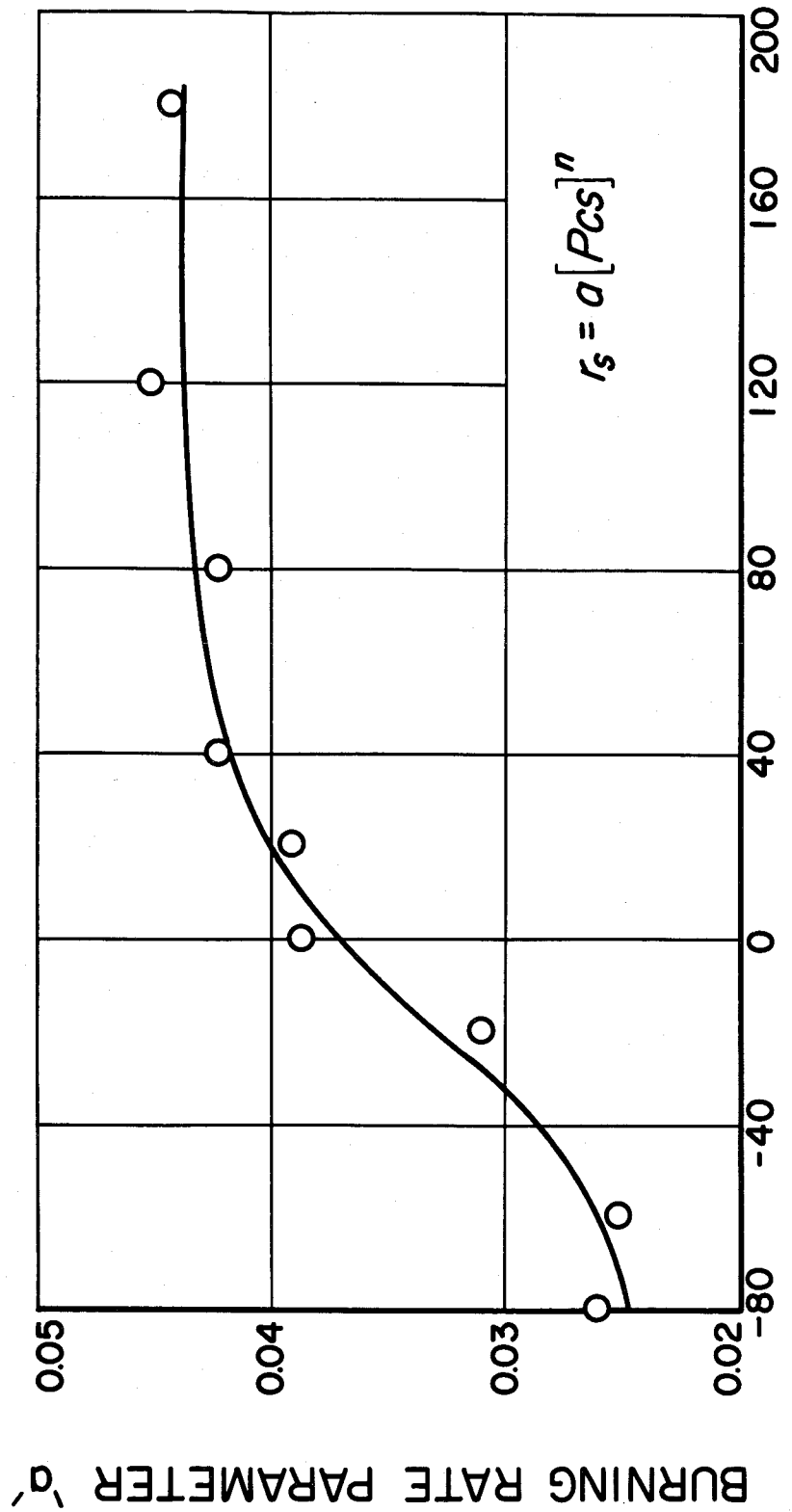

Figure 47. Burning Rate Law Parameter 'a' Versus Grain Temperature.

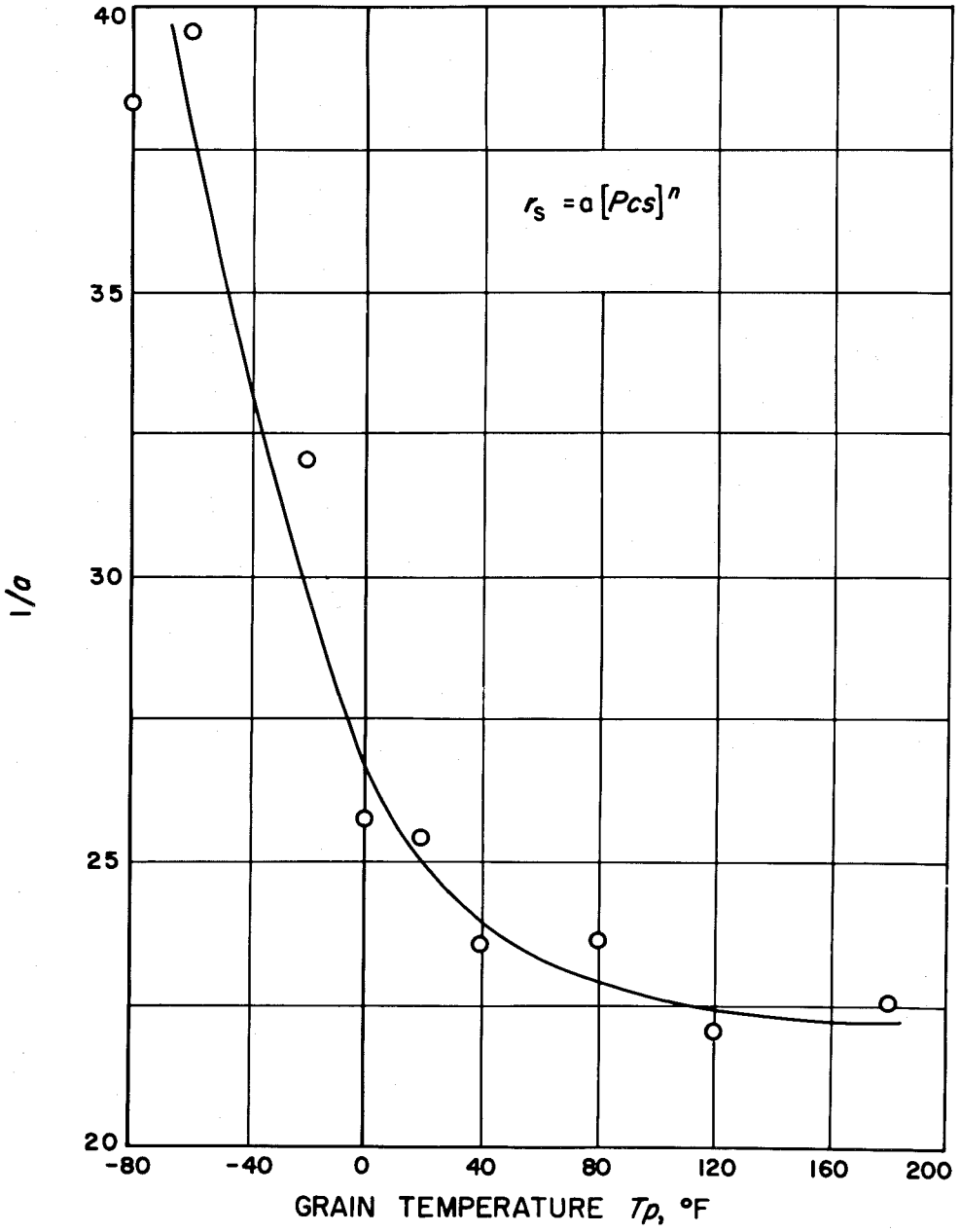

Figure 48. Reciprocal of Burning Rate Law Parameter 'a' Versus Grain Temperature.

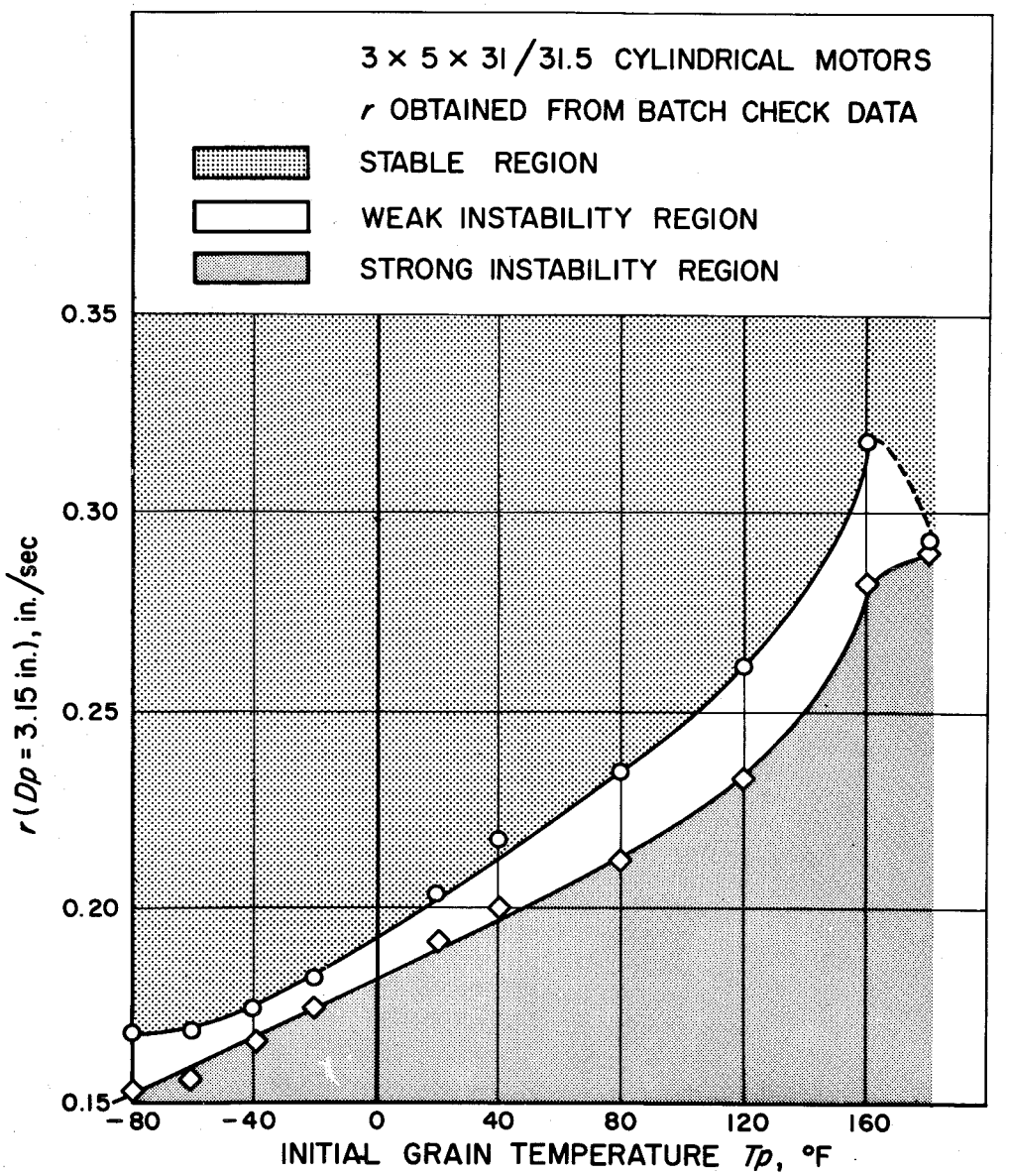

Figure 49. Instability Regions in the Initial Burning Rate, Initial Grain Temperature Plane.

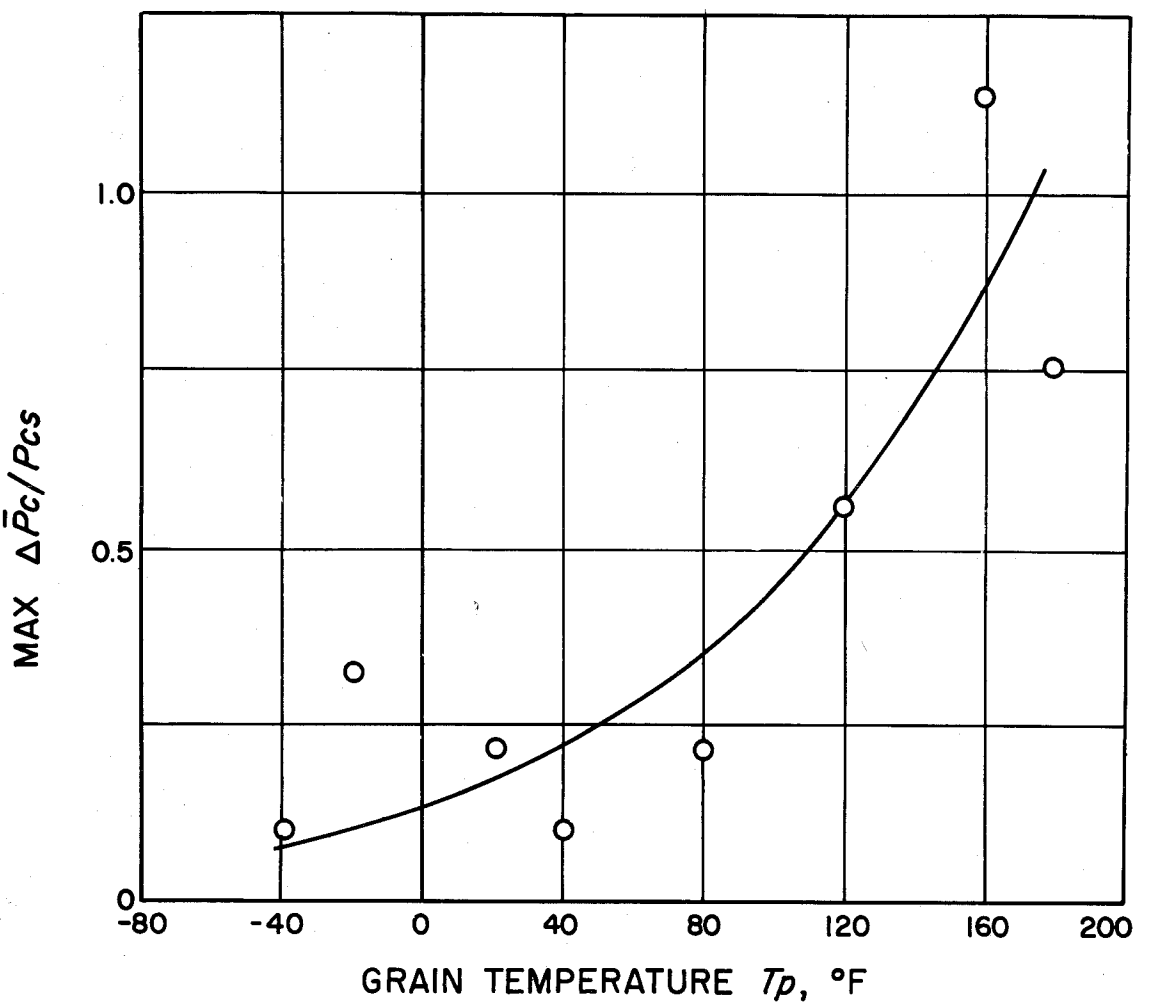

Figure 50. Maximum Unstable Increment in Mean Chamber Pressure Versus Initial Grain Temperature.

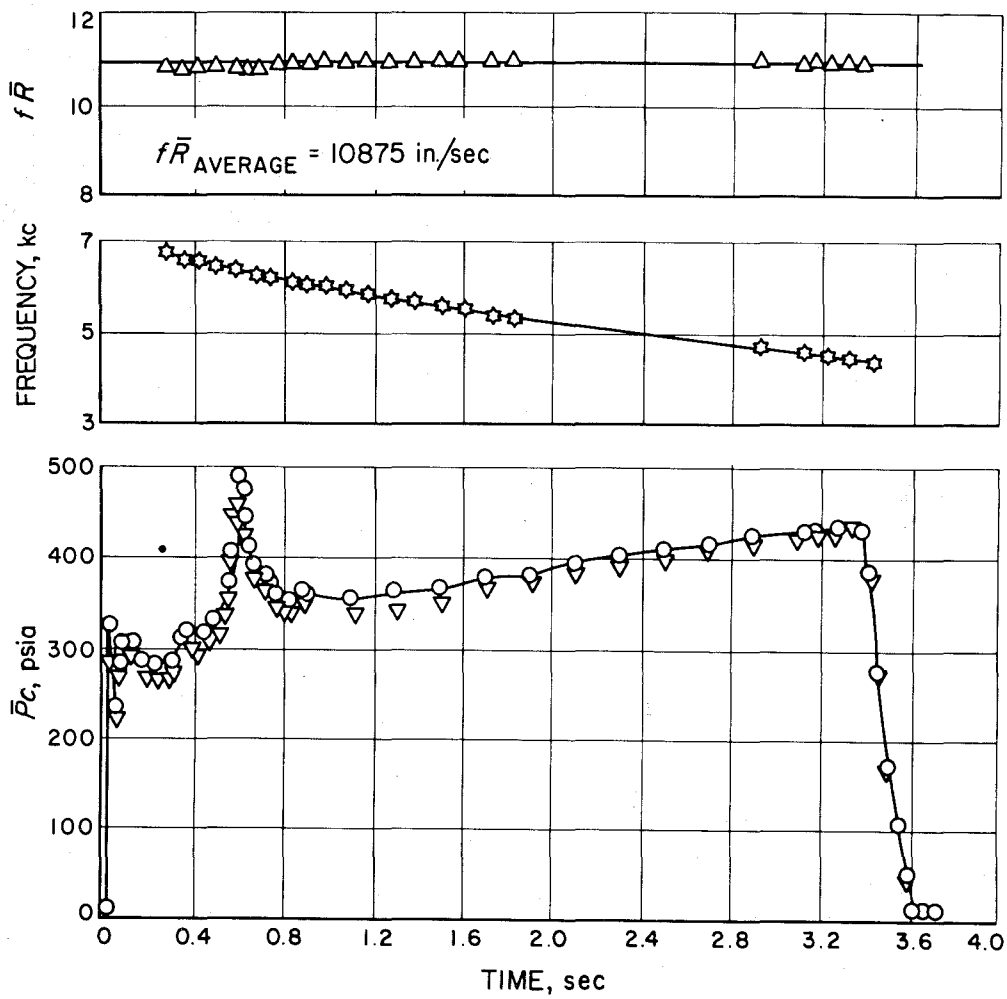

Figure 51. Typical Mean Chamber Pressure, Fundamental Frequency and Fundamental Frequency Times Instantaneous Radius, Versus Time History.

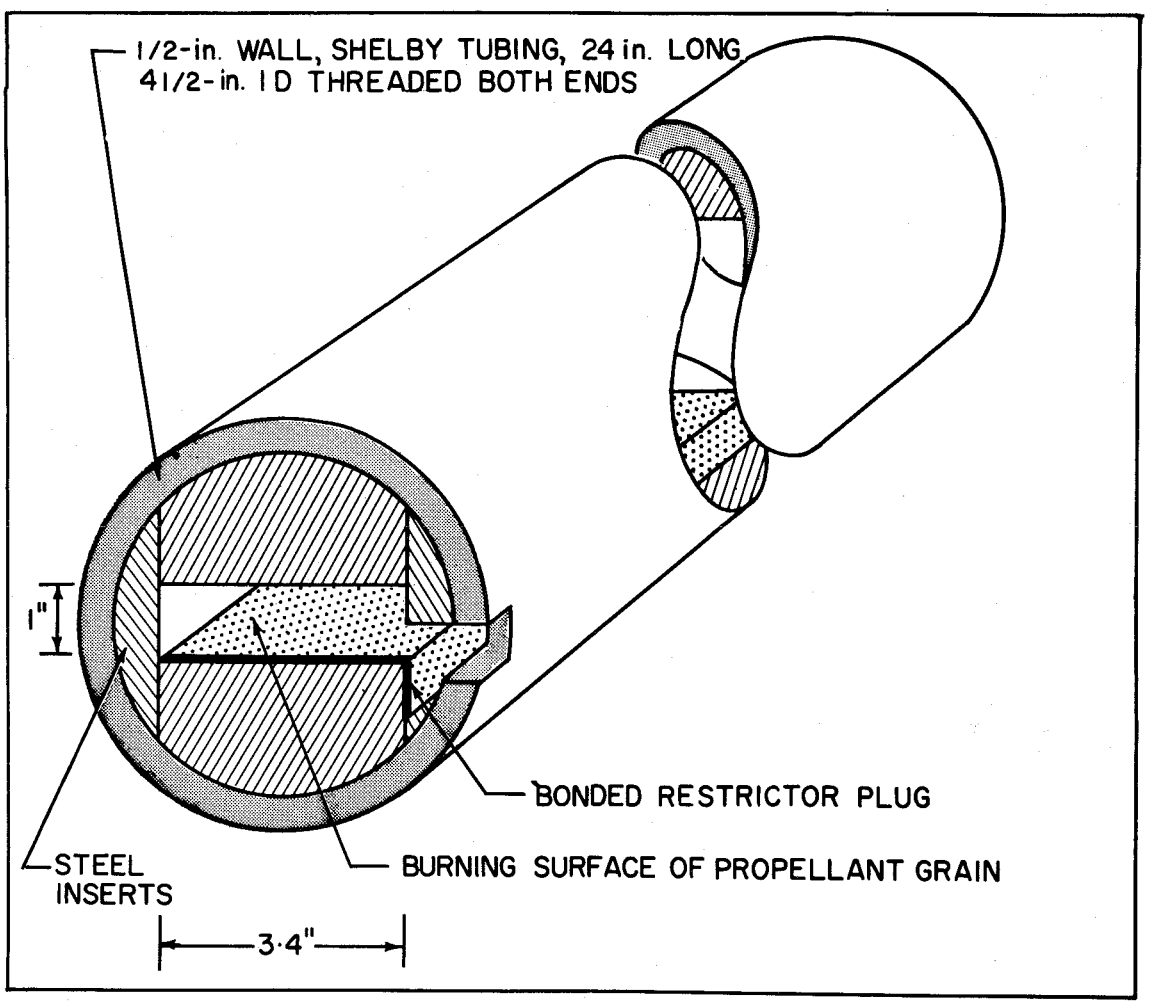

Figure 52. Type 1 Opposed Plane (Slab) Motor Configuration.

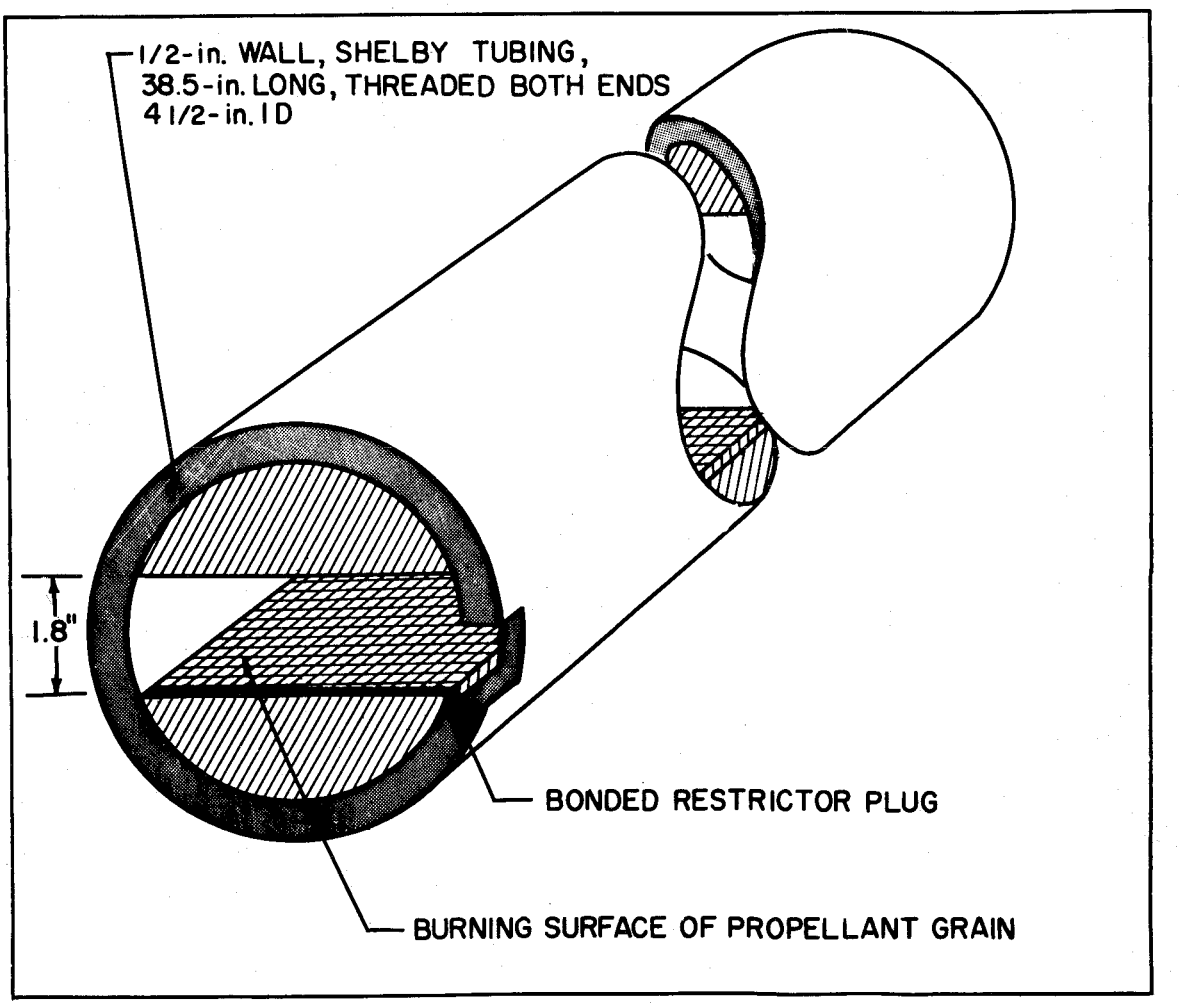

Figure 53. Type 2 Opposed Plane (Slab) Motor Configuration.

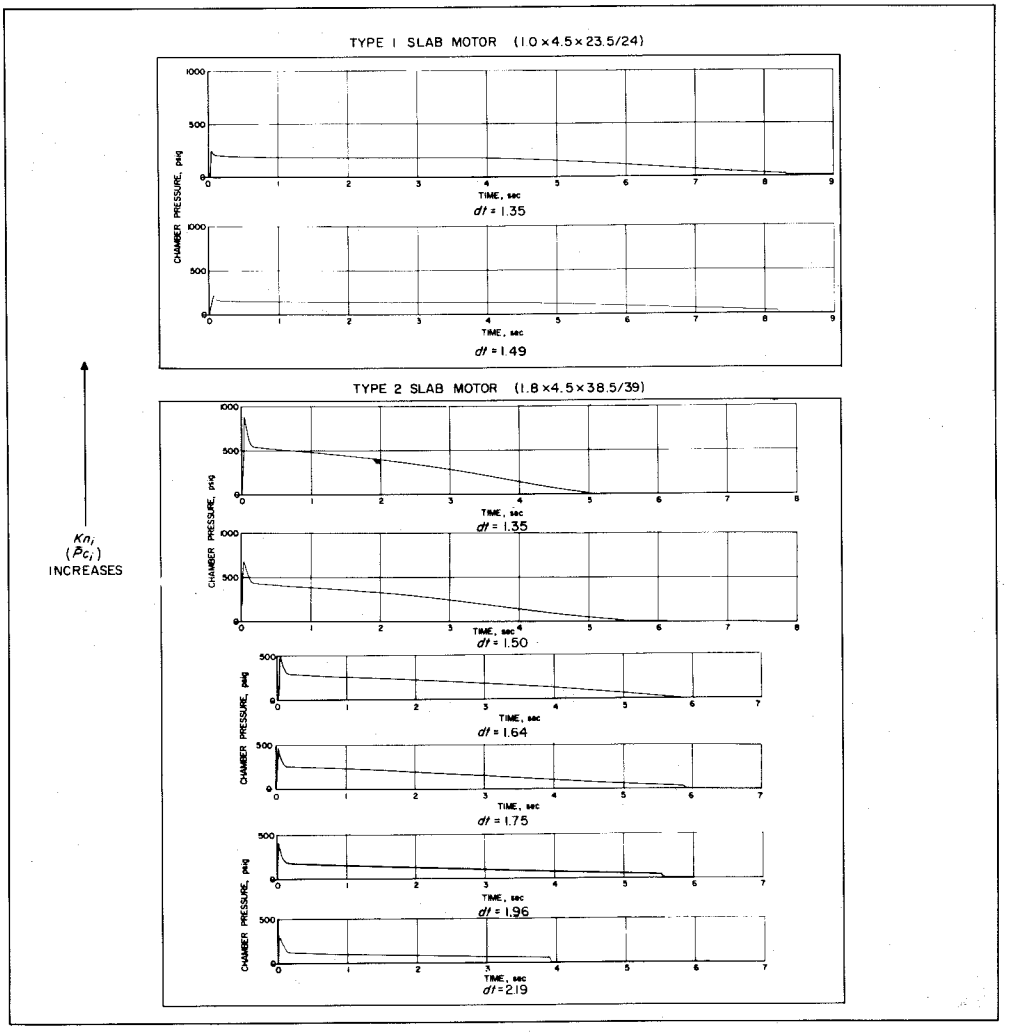

Figure 54. Mean Chamber Pressure Versus Time Histories of Type 1 and Type 2 Slab Motors.

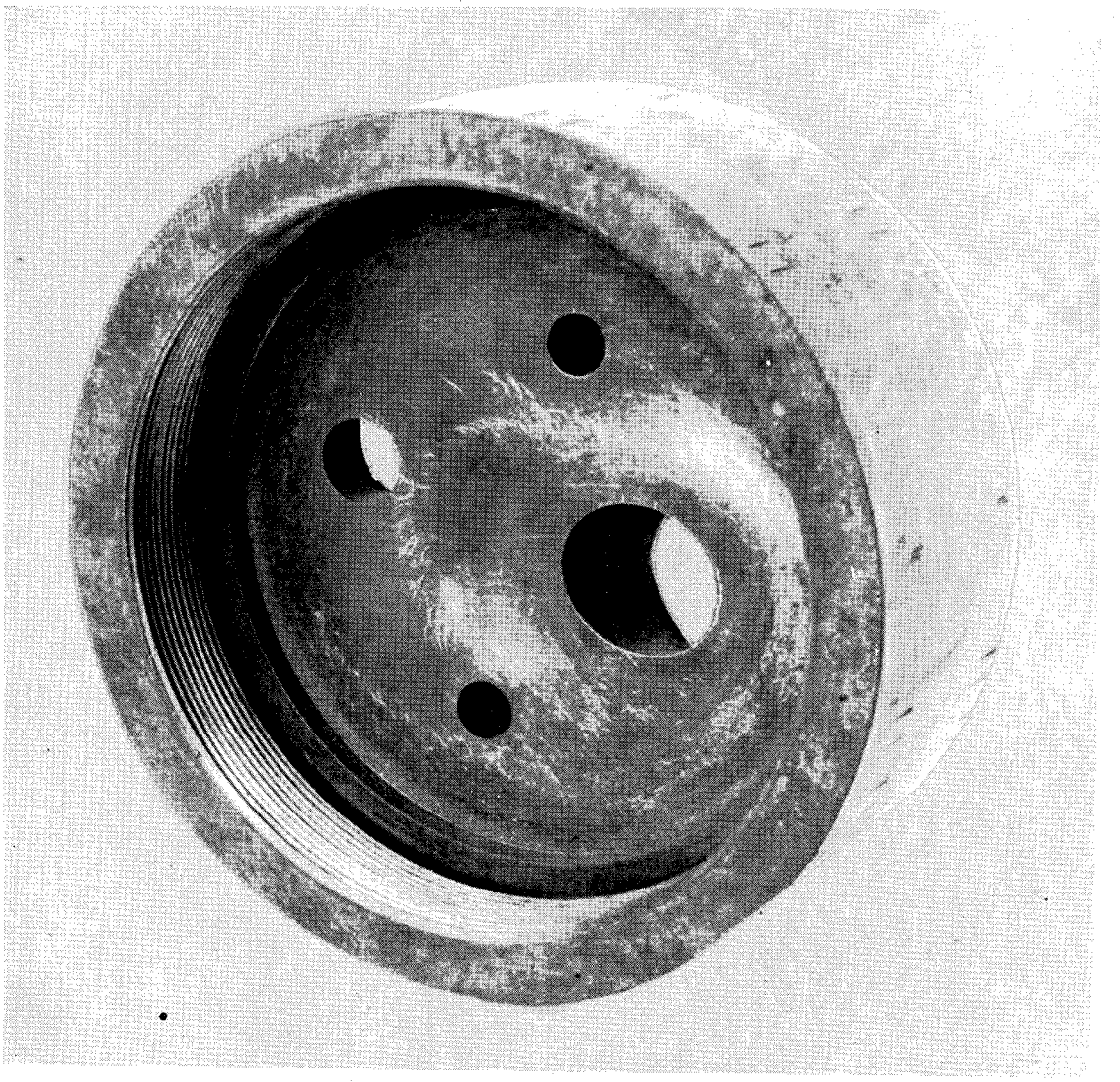

Figure 55. Internal View of Interrupt Head Plate.

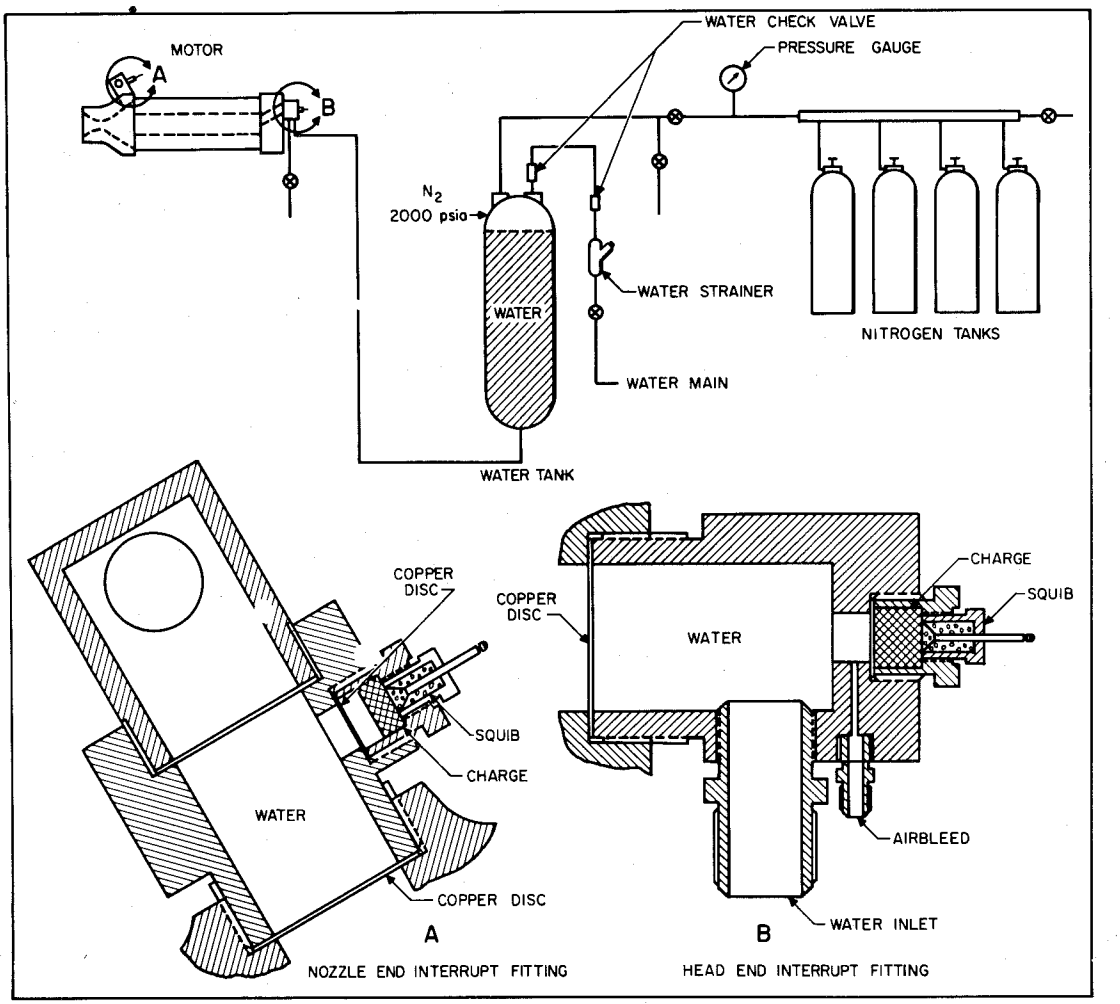

Figure 56. Schematic Drawing of Interrupt System.

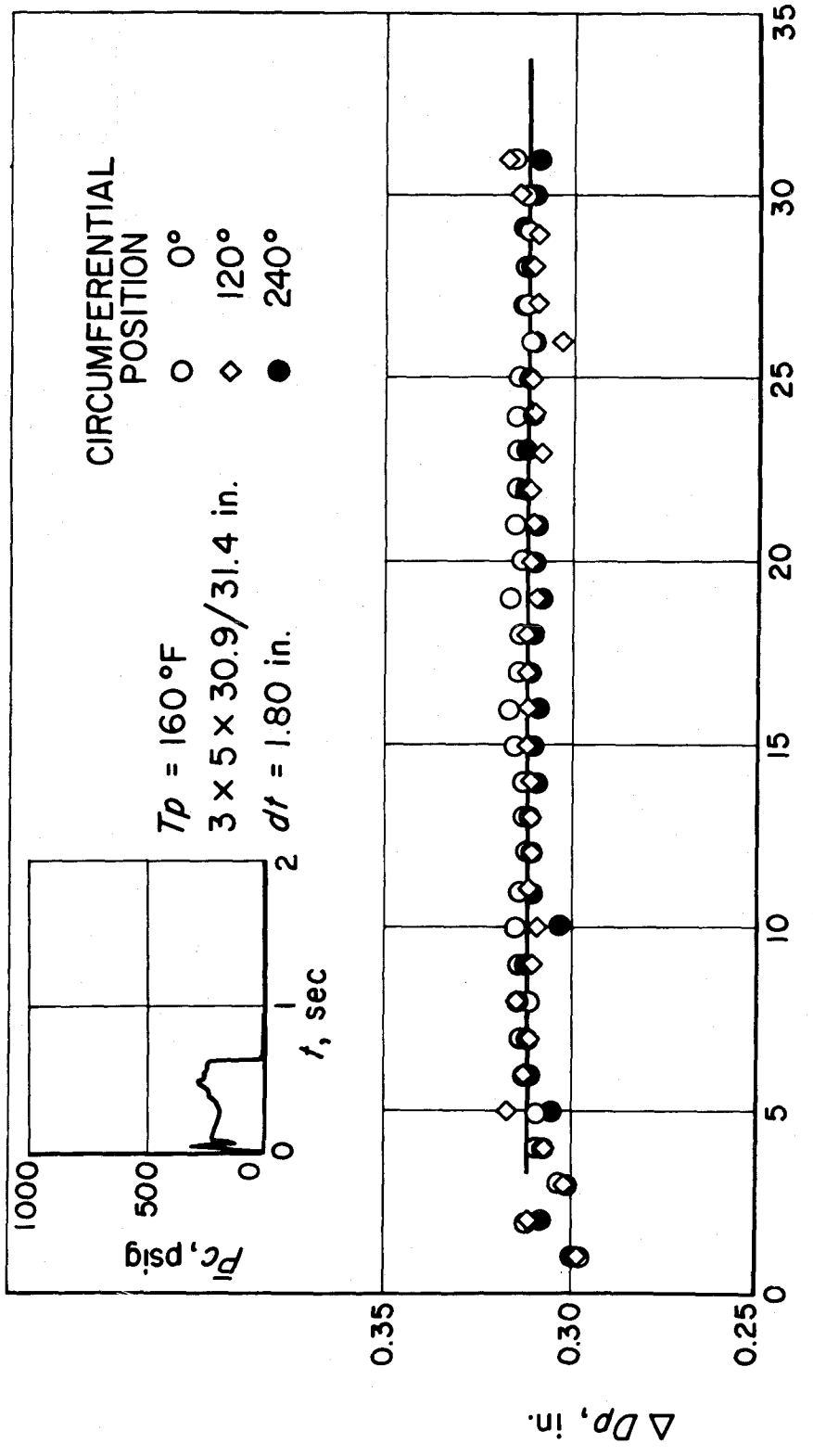

Figure 57. Change in Perforation Diameter Versus Length; Interrupted Firing R21/100.

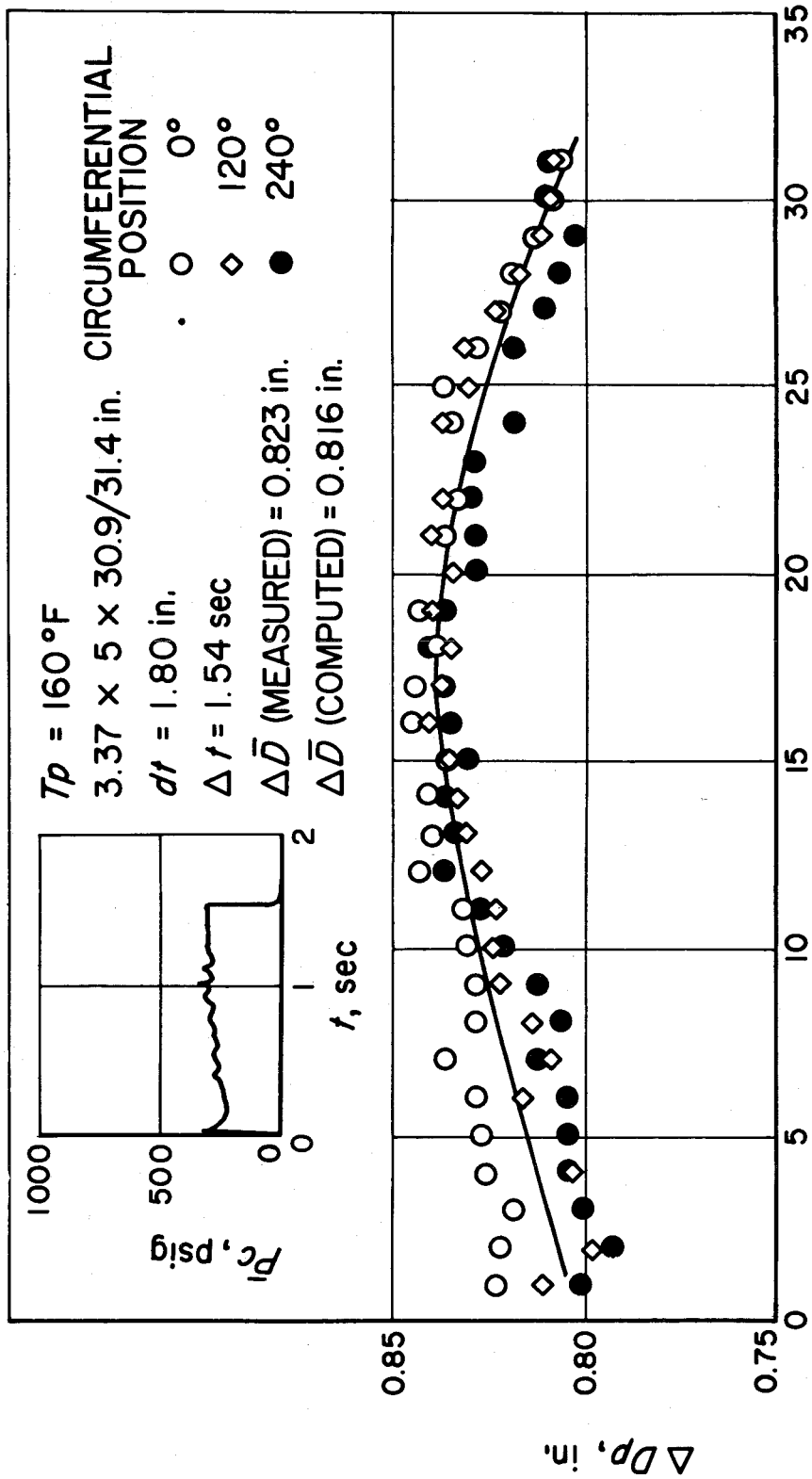

Figure 58. Change in Perforation Diameter Versus Length; Interrupted Refiring R21/100.

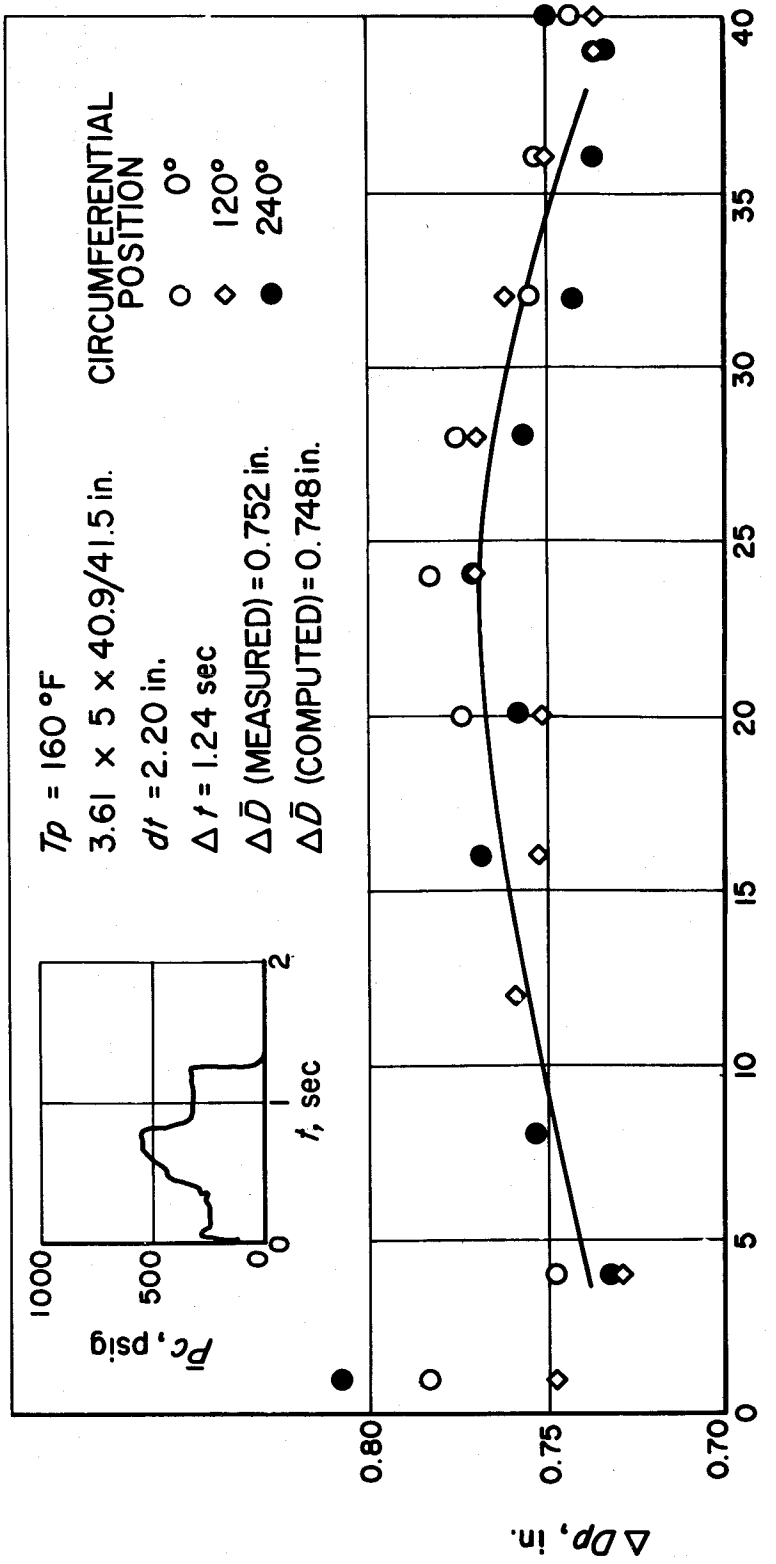

Figure 59. Change in Perforation Diameter Versus Length; Interrupted Refiring R19/92.

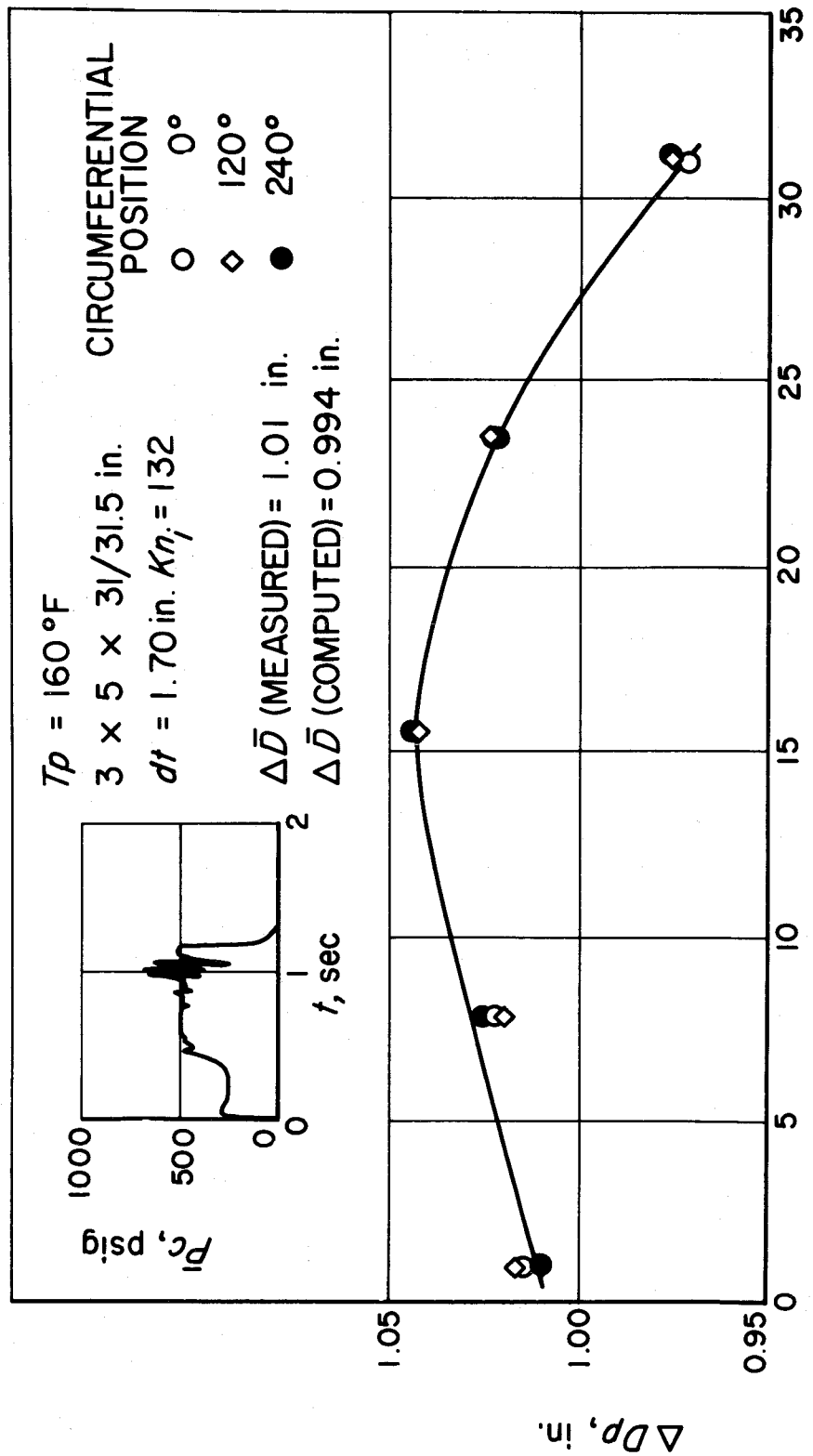

Figure 60. Change in Perforation Diameter Versus Length; Self Interrupted Firing.

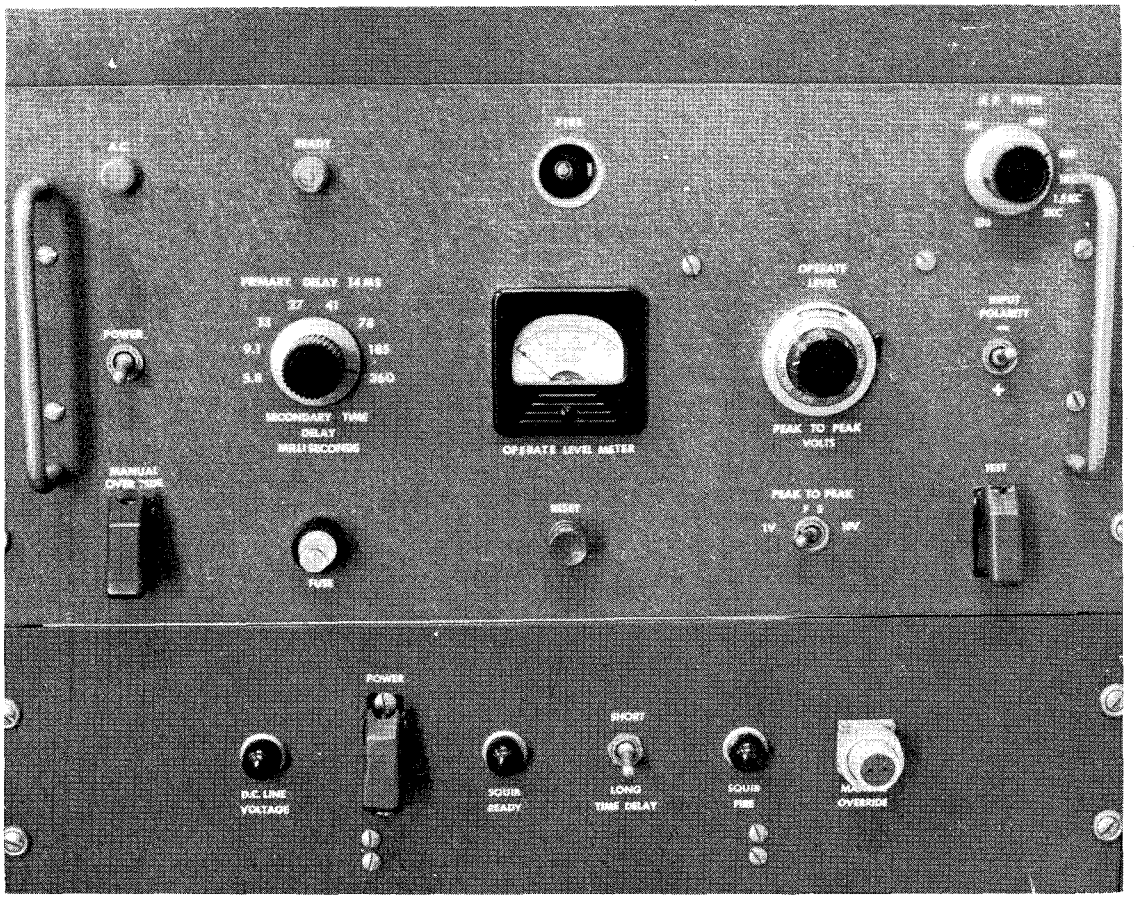

Figure 61. Automatic Electronic Interrupt Command Unit.

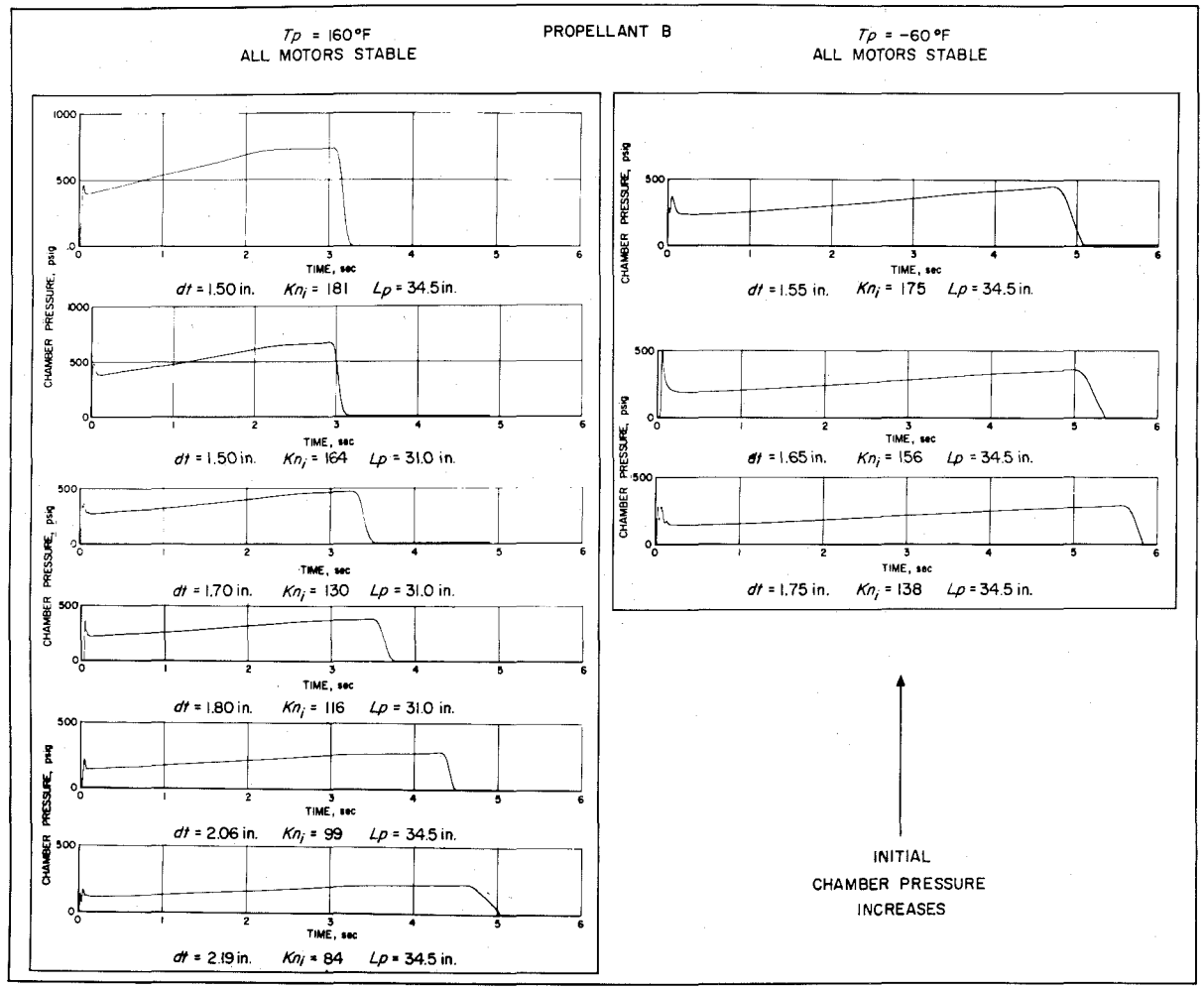

Figure 62. Effect of Varying Operating Pressure; Propellant B.